
Defining Neural Network Architecture through Polytope Structures of Dataset

Sangmin Lee¹ Abbas Mammadov¹ Jong Chul Ye²

Abstract

Current theoretical and empirical research in neural networks suggests that complex datasets require large network architectures for thorough classification, yet the precise nature of this relationship remains unclear. This paper tackles this issue by defining upper and lower bounds for neural network widths, which are informed by the polytope structure of the dataset in question. We also delve into the application of these principles to simplicial complexes and specific manifold shapes, explaining how the requirement for network width varies in accordance with the geometric complexity of the dataset. Moreover, we develop an algorithm to investigate a converse situation where the polytope structure of a dataset can be inferred from its corresponding trained neural networks. Through our algorithm, it is established that popular datasets such as MNIST, Fashion-MNIST, and CIFAR10 can be efficiently encapsulated using no more than two polytopes with a small number of faces.

1. Introduction

To comprehend the remarkable performance of deep neural networks (DNNs), extensive research has delved into their architectures and the universal approximation property (UAP). The UAP of two-layer neural networks on compact sets was initially proven by Cybenko (1989), sparking widespread exploration of the UAP in diverse settings for DNNs. Studies have focused on determining the minimal depths and widths of deep ReLU networks required for UAP (Hornik, 1991; Park et al., 2020). These foundational results contribute to unraveling the intricate relationship between approximation power and neural network architectures.

However, a converse problem to address the influence of the characteristics of training datasets necessary to attain the UAP in neural networks has received relatively less attention.

For example, when analyzing the swiss roll dataset shown in Figure 1(a), an important practical question emerges: *What are the effective depth and width required for the complete classification of this dataset?* Despite the practical relevance of this inquiry in the context of training neural networks, existing theoretical results only offer basic lower bounds (minimum depth of 2 (Hornik, 1991) and a width of $\max\{d_x + 1, d_y\}$ (Park et al., 2020)), which are often impractical for real applications. While a range of empirical evidence indicates that increasing the depth or width of networks could lead to successful outcomes, there remains an absence of theoretical assurances to foresee these results.

In this paper, we therefore tackle the challenge of identifying the optimal neural network architecture for classifying a given dataset. This task is approached through the lens of the polytope structure of deep ReLU networks, a subject that has garnered considerable attention in recent studies (Black et al., 2022; Grigsby & Lindsey, 2022; Berzins, 2023; Huchette et al., 2023). In fact, our primary theoretical goal is to address the “multiple manifold problem,” introduced by Buchanan et al. (2020): *For given two disjoint topological spaces \mathcal{X}_+ and \mathcal{X}_- , what is the optimal architecture for the neural network \mathcal{N} such that $\mathcal{N}(\mathbf{x}) > 0$ for all $\mathbf{x} \in \mathcal{X}_+$ and $\mathcal{N}(\mathbf{x}) < 0$ otherwise?*

By utilizing the geometric properties of DNNs, here we provide a comprehensive answer to this question. Our approach involves determining both upper and lower bounds for the depth and widths of networks required for dataset classification, based on the polytope covering of the datasets. Specifically, we explicitly construct a neural network with practical applicability. For example, our discovery in Theorem 3.4 reveals that the swiss roll dataset in Figure 1(a) can be efficiently classified using a three-layer ReLU network with 24 neurons, as depicted in Figure 1(c).

Another important contribution of this paper is the investigation into the converse situation, demonstrating that trained neural networks inherently capture the geometric properties of the dataset and enable the extraction of the dataset’s polytope structure. As for demonstrating practical use, we uncover and discuss simple geometric traits of real-world datasets such as MNIST, Fashion-MNIST, and CIFAR10, achieved through the training of neural networks.

¹Department of Mathematical Science, KAIST, South Korea
²Kim Jaechul Graduate School of AI, KAIST, South Korea. Correspondence to: Jong Chul Ye <jong.ye@kaist.ac.kr>.

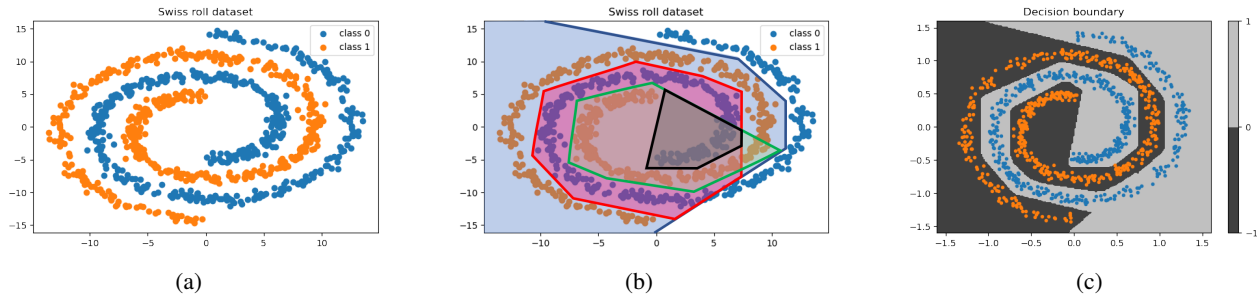


Figure 1. What type of neural network architecture is capable of effectively classifying the swiss roll dataset depicted in (a)? By establishing a collection of covering polytopes to enclose one class, as illustrated in (b), our result demonstrates that a three-layer ReLU network with the architecture $2 \xrightarrow{\sigma} 20 \xrightarrow{\sigma} 4 \rightarrow 1$ can successfully achieve this classification task, as exemplified in (c).

Importantly, our contributions can be summarized as follows:

- **Explicit construction of networks.** We introduce the novel concept of a *polytope-basis cover* (Definition 3.2), which serves to describe the geometric structure of the dataset in detail. Building on this, we propose the design of a three-layer ReLU network, specifically tailored to efficiently classify the dataset in question, using its polytope-basis cover as a guiding framework (Theorem 3.4).
- **Bounds on network widths.** We define both upper and lower bounds for the width of a neural network necessary to classify a given convex polytope region, taking into account the number of its faces (Proposition 3.1). Furthermore, we derive upper bounds on network widths when the dataset \mathcal{X} is structured as a simplicial complex or can be covered by a difference of prismatic polytopes (Theorem 3.5 and 3.6). These bounds are correlated with the number of facets or the Betti numbers of \mathcal{X} , demonstrating an interplay between the dataset’s inherent geometry and the required network architecture.
- **Investigating dataset geometry.** Building on our findings, we demonstrate that it is possible to investigate the geometric features of the dataset by training a neural network (Theorem 3.7). Specifically, we develop algorithms that are able to identify a polytope basis-cover for given datasets (Algorithm 1). Our results show that each class within the MNIST, Fashion-MNIST, and CIFAR10 datasets can be effectively distinguished using no more than two convex polytopes, each consisting of fewer than 30 faces (Table 1).

2. Preliminaries

Notation. In this paper, we focus primarily on the binary classification problem, aiming to separate two disjoint topo-

logical spaces denoted as \mathcal{X}_+ and \mathcal{X}_- , or two classes of finite points denoted as \mathcal{D}_+ and \mathcal{D}_- . The training dataset is represented as $\mathcal{D} = \mathcal{D}_+ \cup \mathcal{D}_- = \{(x_i, y_i)\}_{i=1}^n$, where $x_i \in \mathbb{R}^d$ and $y_i \in \{0, 1\}$. Throughout the paper, we denote scalars by lowercase letters and vectors by boldface lowercase letters. For a positive integer m , $[m]$ represents the set $\{1, 2, \dots, m\}$. The ReLU activation function is denoted by $\sigma(x) := \text{ReLU}(x) = \max\{0, x\}$, and it is applied to a vector coordinate-wisely. The sigmoid activation function is denoted as $\text{SIG}(x) = \frac{1}{1+e^{-x}}$. The max pooling operation is represented as $\text{MAX} : \mathbb{R}^d \rightarrow \mathbb{R}$, which returns the maximum component of the input vector. The ε neighborhood of a topological space $\mathcal{X} \subset \mathbb{R}^d$ is defined by $\mathcal{B}_\varepsilon(\mathcal{X}) := \{x \in \mathbb{R}^d : \min_{y \in \mathcal{X}} \|x - y\|_2 < \varepsilon\}$. The indicator function is denoted by

$$\mathbb{1}_{\{c\}} := \begin{cases} 1, & \text{if } c \text{ is true,} \\ 0, & \text{otherwise.} \end{cases}$$

Additionally, we define a *convex polytope* as an intersection of hyperspaces, as defined below:

Definition 2.1. A nonempty set $C \subset \mathbb{R}^d$ is called a *convex polytope with m faces* if there exist $w_k \in \mathbb{R}^d$ and $b_k \in \mathbb{R}$ for $k \in [m]$ such that $C = \bigcap_{k=1}^m \{x \in \mathbb{R}^d \mid w_k^\top x + b_k \leq 0\}$.

Network architectures. In this paper, the terminology *architecture* refers to the structure of a neural network, which means the depth and the width of hidden layers, and is often denoted by \mathcal{A} . A D -layer neural network $\mathcal{N} : \mathbb{R}^d \rightarrow \mathbb{R}$ with hidden layer widths d_1, d_2, \dots, d_{D-1} and activation functions $\text{ACT}_1, \text{ACT}_2, \dots, \text{ACT}_D$ is represented by $d \xrightarrow{\text{ACT}_1} d_1 \xrightarrow{\text{ACT}_2} d_2 \xrightarrow{\text{ACT}_3} \dots \xrightarrow{\text{ACT}_{D-1}} d_{D-1} \xrightarrow{\text{ACT}_D} 1$. When the activation function is the identity, we add nothing on the arrow. For example, $d \xrightarrow{\sigma} m \rightarrow 1$ denotes a two-layer ReLU network with m neurons, presented by

$$\mathcal{N}(x) = v_0 + \sum_{k=1}^m v_k \sigma(w_k^\top x + b_k). \quad (1)$$

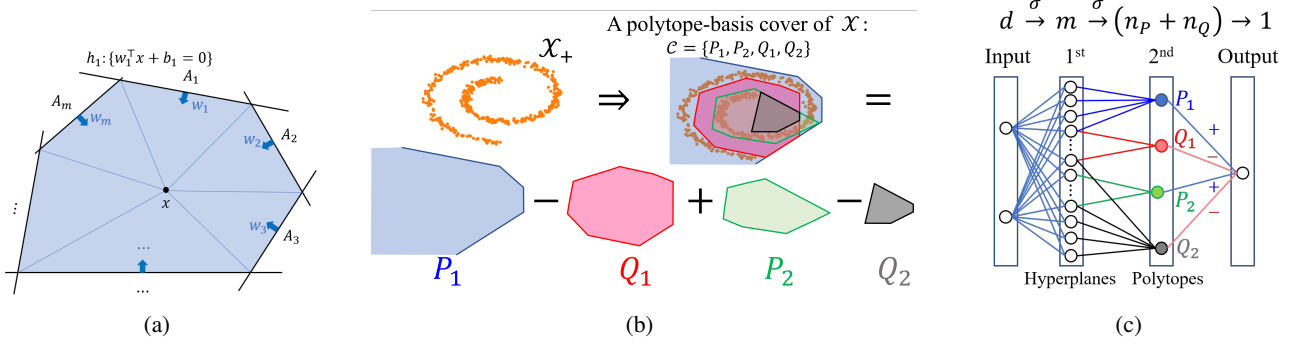


Figure 2. The fundamental ideas in our work. (a) A convex polytope enclosed by m hyperplanes can be decomposed by m small pyramids. (b) For the topological space \mathcal{X}_+ , the collection of polytopes $\mathcal{C} = \{P_1, P_2, Q_1, Q_2\}$ forms a polytope-basis cover of \mathcal{X} . (c) The constructive proof in Theorem 3.4 further exhibits the role of neurons in hidden layers: the width of first layer means the number of total faces in \mathcal{C} , and the neurons in the second layer corresponds to the polytopes in \mathcal{C} .

Definition 2.2. Let $\mathcal{X} := \mathcal{X}_+ \cup \mathcal{X}_- \subset \mathbb{R}^d$ be a union of two disjoint topological spaces. A neural network architecture \mathcal{A} is called a *feasible architecture on \mathcal{X}* if there exists a neural network with the architecture \mathcal{A} such that

$$\begin{aligned} \mathcal{N}(x) &> 0 & \text{if } x \in \mathcal{X}_+, \\ \mathcal{N}(x) &< 0 & \text{if } x \in \mathcal{X}_-. \end{aligned}$$

In other words, *feasible architecture on \mathcal{X}* refers to a network architecture capable of fully discriminating between the two specified manifolds, \mathcal{X}_+ and \mathcal{X}_- . This paper aims to explore the connection between feasible architectures and the geometrical properties of the dataset.

3. Main Contributions

In this section, we present our main findings in two forms. Firstly, we establish the upper and lower limits of network width required for classifying a specific dataset. Secondly, we illustrate how trained neural networks inherently capture the geometric characteristics of the dataset they handle.

3.1. Data geometry-dependent bounds on widths

Let $C \subset \mathbb{R}^d$ be a convex polytope with m faces. Our objective is to establish bounds on the widths of a ReLU neural network necessary for it to be feasible architecture on C . Applying piecewise linearity of ReLU networks and the volume formula of convex polytopes, the following proposition provides the answer.

Proposition 3.1. *Let $C \subset \mathbb{R}^d$ be a convex polytope enclosed by m hyperplanes, and consider $\mathcal{X} = \mathcal{X}_+ \cup \mathcal{X}_-$ where $\mathcal{X}_+ := C, \mathcal{X}_- := \mathcal{B}_\varepsilon(\mathcal{X}_+)^c$. Then, $d \xrightarrow{\sigma} m \rightarrow 1$ is a feasible architecture on \mathcal{X} with minimal depth. Conversely, if $d \xrightarrow{\sigma} d_1 \xrightarrow{\sigma} d_2 \xrightarrow{\sigma} \dots \xrightarrow{\sigma} d_k \rightarrow 1$ is a feasible*

architecture on \mathcal{X} , then

$$d_1 \cdot \prod_{j=2}^k (2d_j + 1) \geq \begin{cases} \lceil \frac{m}{2} \rceil + (d - 2), & \text{if } m \geq 2d + 1, \\ 2d - 1, & \text{if } m = 2d - 1, 2d, \\ d + 1, & \text{if } m < 2d - 1. \end{cases}$$

This lower bound is optimal when $k = 1$ and $d = 2$ (i.e., two-layer network on \mathbb{R}^2).

Proof sketch. We briefly introduce the main idea here. Let A_1, \dots, A_m be faces of C , and x be a point in C . Since C is convex, it can be decomposed to m pyramids whose common apex is x (see Figure 2(a)). Then, the volume (in Lebesgue sense) of C is equal to the sum of the volume of m pyramids. Mathematically, it is represented by

$$\text{Vol}_d(C) = \frac{1}{d} \sum_{k=1}^m \text{Vol}_{d-1}(A_k) \sigma(\mathbf{w}_k^\top x + b_k)$$

where \mathbf{w}_i is a unit vector of the hyperplane A_i , and Vol_d denotes the d -dimensional volume. From this equation, we define a two-layer ReLU network

$$\mathcal{N}(x) := 1 + M(\text{Vol}_d(C) - \frac{1}{d} \sum_{k=1}^m \text{Vol}_{d-1}(A_k) \sigma(\mathbf{w}_k^\top x + b_k))$$

for some constant M . Then $\mathcal{N}(x) = 1$ for all $x \in C$, and we can prove that $d \xrightarrow{\sigma} m \rightarrow 1$ is a feasible architecture on the polytope, by adjusting the value of M . The rest of the proof can be found in Appendix E.1. \square

In the proof of Proposition 3.1, $\sigma(\mathcal{N})$ is a two-layer ReLU network that approximates the indicator function on a convex polytope.¹ Building upon this proposition, we are interested in extending our findings to arbitrary topological

¹We also mention that the approximation of indicator functions directly induces UAP of neural networks (Theorem F.3).

spaces, specifically those that can be distinguished by a collection of polytopes. To facilitate this extension, we introduce an additional terminology.

Definition 3.2. Let $\mathcal{X} := \mathcal{X}_+ \cup \mathcal{X}_- \subset \mathbb{R}^d$ be a union of two disjoint topological spaces. A finite collection of polytopes $\mathcal{C} := \{P_1, \dots, P_{n_P}, Q_1, \dots, Q_{n_Q}\}$ is called a *polytope-basis cover* of \mathcal{X} if it satisfies

$$\begin{aligned} \sum_{k=1}^{n_P} \mathbb{1}_{\{x \in P_k\}} &> \sum_{k=1}^{n_Q} \mathbb{1}_{\{x \in Q_k\}} && \text{for all } x \in \mathcal{X}_+, \\ \sum_{k=1}^{n_P} \mathbb{1}_{\{x \in P_k\}} &\leq \sum_{k=1}^{n_Q} \mathbb{1}_{\{x \in Q_k\}} && \text{for all } x \in \mathcal{X}_-. \end{aligned}$$

Roughly speaking, a polytope-basis cover of \mathcal{X} is a polytope covering of \mathcal{X}_+ and \mathcal{X}_- that admits overlapping, where the difference number of overlapped covers is restricted to be positive or negative with respect to the label. Below, we provide an example of a polytope-basis cover for the swiss roll dataset described in Figure 1(a).

Example 3.3. Let $\mathcal{X}_+, \mathcal{X}_-$ be the orange and blue class in Figure 1(a), respectively. Figure 2(b) demonstrates a polytope-basis cover of \mathcal{X} consists of four convex polytopes: P_1, P_2, Q_1, Q_2 . It is easily checked that $\sum_{k=1}^2 \mathbb{1}_{\{x \in P_k\}} - \sum_{k=1}^2 \mathbb{1}_{\{x \in Q_k\}} = 1 > 0$ for $\forall x \in \mathcal{X}_+$, while $\sum_{k=1}^2 \mathbb{1}_{\{x \in P_k\}} - \sum_{k=1}^2 \mathbb{1}_{\{x \in Q_k\}} = 0$ for $\forall x \in \mathcal{X}_-$.

The usefulness of polytope-basis covers appears in the following theorem: we can derive an upper bound of feasible architecture on \mathcal{X} from its polytope-basis cover, by applying the constructive proof used in Proposition 3.1.

Theorem 3.4. For a given topological space $\mathcal{X} = \mathcal{X}_+ \cup \mathcal{X}_- \subset \mathbb{R}^d$, let $\mathcal{C} = \{P_1, \dots, P_{n_P}, Q_1, \dots, Q_{n_Q}\}$ be a polytope-basis cover of \mathcal{X} . Let m denote the total number of faces of the convex polytopes in \mathcal{C} . Then,

$$d \xrightarrow{\sigma} m \xrightarrow{\sigma} (n_P + n_Q) \rightarrow 1$$

is a feasible architecture on \mathcal{X} .

The proof can be found in Appendix E.2. One of the important contributions of Theorem 3.4 is that its construction exhibits the exact role of each neuron in the hidden layers. It demonstrates that for a given polytope-basis cover, a three-layer ReLU network with widths $\#(\text{hyperplanes})$ and $\#(\text{polytopes})$ in the first and second hidden layer, respectively, is a feasible architecture. For instance, we recall the polytope-basis cover represented in Figure 2(b). Each neuron in the first hidden layer represents a hyperplane in the input space, where each neuron in the second hidden layer represents a convex polytope (P_i or Q_j) in \mathcal{C} that is formed by connected neurons in the first layer as depicted in Figure 2(c).

Theorem 3.4 can be further used to derive upper bounds on width of feasible architecture in terms of topological

quantities of the given dataset. First, we investigate such bounds and feasible architecture on a simplicial complex, which is widely used in topological data analysis (TDA) to investigate the topological structure of a given point clouds.

Theorem 3.5. Let $\mathcal{X} = \mathcal{X}_+ \cup \mathcal{X}_-$ be a union of two disjoint topological spaces, where $\mathcal{X}_+ \subset \mathbb{R}^d$ is a simplicial J -complex consists of k facets. Let k_j be the number of j -dimensional facets of \mathcal{X}_+ for $j = 1, \dots, J$. Then, $d \xrightarrow{\sigma} d_1 \xrightarrow{\sigma} k \rightarrow 1$ is a feasible architecture on \mathcal{X} , where d_1 is bounded by

$$\begin{aligned} d_1 \leq \min &\left\{ k(d+1) - (d-1) \left[\sum_{j=0}^{\lfloor \frac{d-1}{2} \rfloor} \frac{k_j}{2} \right], \right. \\ &\left. (d+1) \left[\sum_{j \leq \frac{d}{2}} \left(k_j \frac{j+2}{d-j} + \frac{j+2}{j+1} \right) + \sum_{j > \frac{d}{2}} k_j \right] \right\}. \quad (2) \end{aligned}$$

The proof can be found in Appendix E.3. Theorem 3.5 reveals that the width d_1 is bounded by in terms of the number of facets k of the provided simplicial complex. From a geometric perspective, it is generally intuitive that a smaller number of facets suggests a simpler structure of the simplicial complex. This notion is mathematically expressed in (2), which suggests that the first value in (2) results in $d_1 \lesssim \frac{k}{2}(d+3)$, which magnifies as k increases. Similarly, when the maximal dimension J is smaller than $\frac{d}{2}$ and k is fixed, the summation in the second term in (2) reduces to $d_1 \lesssim (d+1) \left(k \frac{J+2}{d-J} + 2 \right)$, which rapidly diminishes as J decreases. This analysis demonstrates that a smaller dimension J demands smaller widths, which aligns with the intuition that a low-dimensional manifold could be approximated with a small number of neurons.

The result in Theorem 3.4 can be further leveraged to ascertain a neural network architecture with width bounds defined in terms of the Betti numbers. Recall that Theorem 3.4 offers an upper bound on widths when \mathcal{X} can be depicted as a difference between groups of convex sets. Expanding on this, assuming the polytope-basis cover consists of prismatic polytopes, we can derive a bound for network architecture in relation to its Betti numbers. This concept is further explained in the following theorem.

Theorem 3.6. Let $\mathcal{X} = \mathcal{X}_+ \cup \mathcal{X}_-$ be a union of two disjoint topological spaces, where \mathcal{X}_- can be separated from \mathcal{X}_+ by disjoint bounded prismatic polytope having at most m faces. Let β_k be the k -th Betti number of the polytope-basis cover. Then, the following three-layer architecture

$$\begin{aligned} d \xrightarrow{\sigma} &\left(m + 2(\beta_0 - 1) + \sum_{k=1}^d (m - 2(d - k - 1)) \beta_k \right) \\ &\xrightarrow{\sigma} \left(\sum_{k=0}^d \beta_k \right) \rightarrow 1 \end{aligned} \quad (3)$$

is a feasible architecture on \mathcal{X} . Conversely, for any such \mathcal{X} , suppose $d \xrightarrow{\sigma} d_1 \xrightarrow{\sigma} d_2 \xrightarrow{\sigma} \dots \xrightarrow{\sigma} d_D \rightarrow 1$ is a feasible architecture on \mathcal{X} . Then, the network widths must satisfy

$$\sum_{i=1}^D \prod_{j=i}^D d_j \geq 2 \sum_{k=0}^d \beta_k - 2. \quad (4)$$

The proof is in Appendix E.4. One of the important implications of Theorem 3.6 is the upper and lower bounds on network widths in terms of the Betti numbers of \mathcal{X} , which reveals the interplay between the topological characteristics of the dataset and network architectures. In Appendix, we also show in Proposition F.2 that topological property alone cannot determine the feasible architecture, highlighting the significance of prismatic polytopes assumption in Theorem 3.6. In other words, the result in Proposition F.2 implies that the geometrical assumptions in this theorem are indispensable to connecting topological features with bounds on the network widths. Furthermore, the lower bound on widths (4) shows that the sum of product of widths should be greater than the sum of Betti numbers. This finding also confirms the increased significance of widths in deeper layers as compared to earlier ones, highlighting the advantageous impact of depth in network architecture.

3.2. Polytope-basis cover search algorithm

So far, we have demonstrated how feasible architecture can be determined from the geometric characteristics of a topological space \mathcal{X} , in terms of its polytope-basis cover. In this section, we delve into the converse scenario: given a trained neural network on the dataset $\mathcal{D} = \{(x_i, y_i)\}$, can we obtain a polytope-basis cover of \mathcal{D} ? We tackle this question by leveraging the convexity of two-layer ReLU networks, which has been studied in a few previous works (Amos et al., 2017; Sivaprasad et al., 2021; Balestrierio et al., 2022) (see Appendix A for related works). Our focus also extends to the precise computation of the number of faces.

Theorem 3.7. Let \mathcal{T}_j and \mathcal{N} be two-layer and three-layer ReLU networks defined by

$$\mathcal{T}_j(\mathbf{x}) := 1 + \sum_{k=1}^{m_j} v_{jk} \sigma(\mathbf{w}_{jk}^\top \mathbf{x} + b_{jk}), \quad \forall v_{jk} < 0, \quad (5)$$

$$\mathcal{N}(\mathbf{x}) := -\frac{1}{2} + \sum_{j=1}^J a_j \sigma(\mathcal{T}_j(\mathbf{x})), \quad \forall a_j \in \{\pm 1\}. \quad (6)$$

For a given dataset $\mathcal{D} = \{(x_i, y_i)\}$, suppose \mathcal{N} satisfies

$$\sigma(\mathcal{T}_j(\mathbf{x}_i)) = 0 \text{ or } 1, \quad \forall \mathbf{x}_i \in \mathcal{D}, \forall j \in [J]. \quad (7)$$

Then, the collection of polytopes $\{C_j\}_{j \in [J]}$, defined by $C_j := \{\mathbf{x} \in \mathbb{R}^d \mid \mathcal{T}_j(\mathbf{x}) = 1\}$, becomes a polytope-basis cover of \mathcal{D} whose accuracy is same with \mathcal{N} .

Algorithm 1 Compressing algorithm.

Input: a pretrained two-layer network \mathcal{T} defined in (5), training dataset $\mathcal{D} = \{(x_i, y_i)\}_{i=1}^n$, $\lambda_{scale} > 1$
 $m \leftarrow$ the width of \mathcal{T}
 $K \leftarrow \emptyset$
for $k, l \in [m]$ **do**
 if $\mathbf{w}_l^\top \mathbf{x}_i + b_l > 0$ implies $\mathbf{w}_k^\top \mathbf{x}_i + b_k > 0$ for all $i \in [n]$ **then**
 $K \leftarrow K \cup \{k\}$
 end if
end for
if $K \neq \emptyset$ **then**
 $k \leftarrow \arg \min_{k \in K} |v_k| \cdot \|\mathbf{w}_k\|$
 remove the k -th neuron (v_k, \mathbf{w}_k, b_k) from \mathcal{T}
 $m \leftarrow m - 1$
end if
for $k \in [m]$ **do**
 if $\mathbf{w}_k^\top \mathbf{x}_i + b_k > 0$ and $0 < \mathcal{T}(\mathbf{x}_i) < 1$ for some $i \in [n]$ **then**
 $(v_k, \mathbf{w}_k, b_k) \leftarrow \lambda_{scale} \times (v_k, \mathbf{w}_k, b_k)$
 end if
end for
Output: \mathcal{T}

The proof of this theorem can be found in Appendix E.5. This theorem establishes that if a trained three-layer network \mathcal{N} , defined in (6), satisfies the condition outlined in (7), then we can derive a polytope-basis cover of the training dataset \mathcal{D} from \mathcal{N} . Below, we outline two strategies we employed to satisfy both (5) and (6) conditions.

First, to meet (5), we initialize the network weights to satisfy

$$v_{jk} < -\sqrt{\|\mathbf{w}_{jk}\|^2 + b_{jk}^2} \quad \forall j \in [J], k \in [m]. \quad (8)$$

Then, according to the implicit bias of gradient descent established by Du et al. (2018, Theorem 2.1), as stated in Proposition F.5, it is ensured that $v_{jk} < 0$ for all $j \in [J]$ and $k \in [m]$ on the gradient flow. This satisfies the first condition.

Second, to achieve (7), we introduce a novel approach called the ‘‘compressing algorithm.’’ This algorithm aims to ‘compress’ a given two-layer network \mathcal{T}_j defined in (5) to identify a minimal convex polytope representation. The process is precisely outlined in Algorithm 1.

More precisely, the algorithm operates in two main steps: 1) identifying and removing a neuron that do not significantly influence the decision boundary, and 2) amplifying the weights to delineate the faces of the decision boundary polytope. We illustrate the functionality of the algorithm in Figure 3. In Figure 3(a), the neuron indicated by the red arrow is deemed non-essential to the decision boundary and is consequently eliminated in (b). Subsequently, by scaling

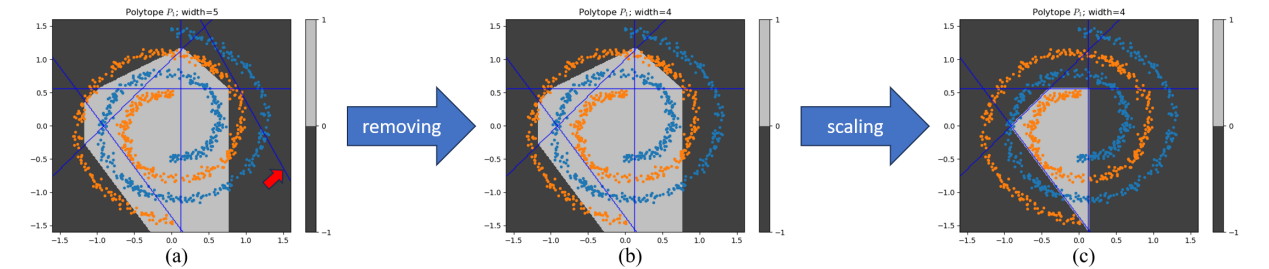


Figure 3. Visualization of Algorithm 1. For a given two-layer network \mathcal{T} defined by (5), it strategically removes and scales specific neurons of \mathcal{T} to encapsulate the characteristics of a single convex polytope. In essence, the algorithm compresses the network to reveal the minimal representation of a polytope structure.

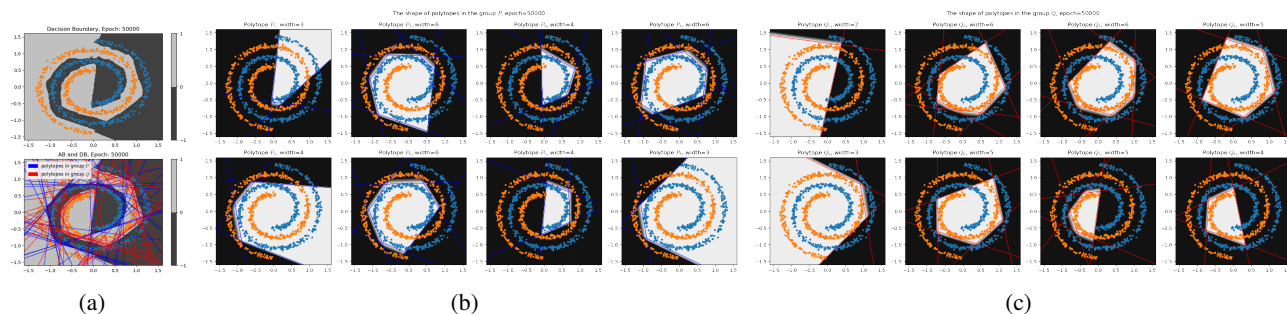


Figure 4. A polytope-basis cover derived from a trained three-layer ReLU network defined in (6), obtained from Algorithm 1. The decision boundary and activation boundaries³ of the trained network are depicted in (a). Each polytope corresponding to $a_j = +1$ and $a_j = -1$ is illustrated in (b) and (c), respectively. The result constitutes a polytope-basis cover of the swiss roll dataset.

the weights (v_k, w_k, b_k) by a factor $\lambda_{scale} > 1$, the decision boundary shrinks into a convex polytope with a number of faces equal to the width of \mathcal{T} (depicted in Figure 3(c)).

Note that a single execution of Algorithm 1 may not immediately yield the network satisfying (7). However, we prove in Proposition C.2 that by iterating this algorithm a sufficient number of times, the output of the algorithm always satisfies both (5) and (7), making it suitable for the application of Theorem 3.7. Therefore, we apply the algorithm once every thousand iterations during the gradient descent optimization process. Further details on the complete training process can be found in Appendix C.1.

Consequently, we present a polytope-basis cover of the swiss roll dataset derived from a converged three-layer network in Figure 4. The polytopes comprising the resulting cover are visualized in Figure 4 (b) and (c). This outcome demonstrates the polytope-basis cover inherent in the trained network.

Lastly, we mention that we further propose two alternative methods for obtaining a polytope-basis cover in Appendix C. Specifically, one approach involves deriving such a cover from a trained two-layer network (Algorithm 3), while the other method entails training several neural networks (Al-

gorithm 4). Further details and results of these additional algorithms are provided in Appendix C.

4. Experimental Results

In Section 3, we studied the relationship between the dataset geometry and neural network architectures. In this section, we provide two empirical results: 1) gradient descent indeed converges to the networks we unveil, and 2) we can investigate the geometric features of real-world datasets through our proposed algorithm.

4.1. Convergence on polytope-basis covers

We begin by demonstrating that gradient descent indeed converges to the networks we proposed in the preceding section, without additional regularization terms. We consider two illustrative topological spaces, \mathcal{X}_1 and \mathcal{X}_2 , as depicted in Figure 5. \mathcal{X}_1 represents a simplicial 2-complex in \mathbb{R}^2 , comprising two triangles, while \mathcal{X}_2 is a hexagon with a pentagonal hole, possessing a straightforward polytope-basis cover. The objective is to classify points within these spaces

³ For the formal definition of decision boundary (DB) and activation boundaries (ABs), see Definition C.1 in Appendix C.

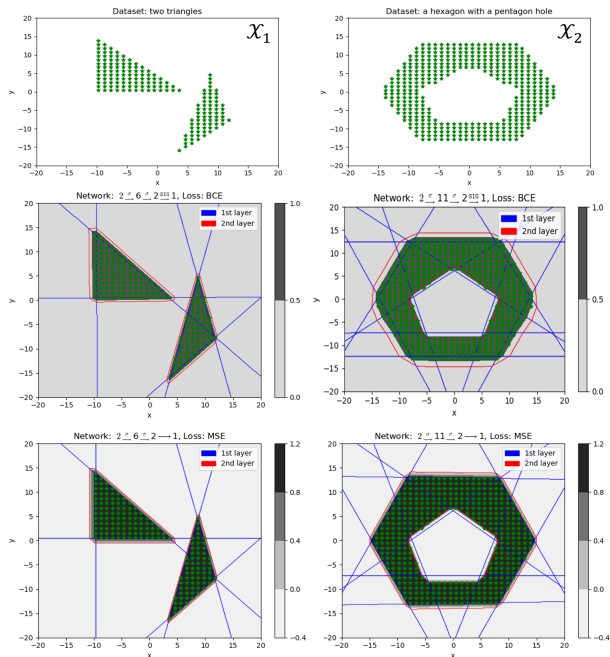


Figure 5. Experimental verification of convergence of gradient descent. Two columns exhibit the shape of two topological spaces, which are ‘two triangles’ and ‘a hexagon with a pentagon hole’. The second and third row show the converged networks by gradient descent under the BCE loss, and the MSE loss, respectively. The first layer (blue) and second layer (red) represent the hyperplane and polytopes, respectively, as discussed in Section 3.

in \mathbb{R}^2 against others. We evaluate the performance for two loss functions, which are the mean squared error (MSE) loss and the binary cross entropy (BCE) loss functions. For the BCE loss, we applied SIG on the last layer.

For the first dataset \mathcal{X}_1 , Theorem 3.5 suggests that $2 \xrightarrow{\sigma} 6 \xrightarrow{\sigma} 2 \rightarrow 1$ is a feasible architecture on \mathcal{X}_1 . To facilitate a clearer examination of weight vectors in each layer, we plot the activation boundaries³ in blue (the 1st hidden layer) and red (the 2nd hidden layer) colors, where the gray color denotes the decision boundary of the converged network. Moreover, the weight vectors in the first layer accurately enclose the two triangles, reflecting the geometrical shape of \mathcal{X}_1 . Similarly, for the second dataset \mathcal{X}_2 , Theorem 3.4 suggests that $2 \xrightarrow{\sigma} 11 \xrightarrow{\sigma} 2 \rightarrow 1$ is a feasible architecture. Specifically, the eleven hyperplanes delineating the boundaries of the outer hexagon and the inner pentagon, while two neurons in the second hidden layer align with the two polygons. These outcomes precisely correspond to our network constructions depicted in Figure 2(b, c).

We conclude this section by providing theoretical insights into the convergence behavior of gradient descent. In Appendix D, utilizing our explicit construction of neural net-

Datasets		Class number									
		0	1	2	3	4	5	6	7	8	9
MNIST	{class}	4	4	7	8	5	7	4	8	8	7
	{class} ^c	3	3	4	5	4	5	4	4	9	9
Fashion-MNIST	{class}	9+3	4	9+5	9+3	9+6	8	9+7	9+1	6	10
	{class} ^c	16	3	22	11	20	4	28	6	4	5
CIFAR10	{class}	29+3	19	23+3	24+4	19	16+3	21	21	18	21
	{class} ^c	29	7	27+3	26	26+4	17	13	10	20+4	8

Table 1. Polytope-basis covers of each class in MNIST, Fashion-MNIST, and CIFAR10 datasets. Here, $a+b$ denotes two polytopes with a and b faces. Note that each class of real-world datasets can be covered by at most two polytopes, indicating the geometric simplicity of real datasets.

works, we demonstrate that gradient descent reliably converges to global minima when the decision boundary of the network is initialized close to the target polytopes (see Theorem D.3). The specific conditions governing the initialization region are described in terms of the geometric distribution of the dataset. For a thorough understanding and precise statements, we refer readers to Appendix D.

4.2. Polytope-basis cover for real datasets

Here, we delve into the polytope-basis cover analysis of three real-world datasets: MNIST, Fashion-MNIST, and CIFAR10. We focus on binary classification tasks, specifically distinguishing one class from all other classes to obtain a polytope-basis cover of the class. For every class, we also consider its complement, denoted as $\{class\}^c$. We employed Algorithm 1 to get the minimal polytope achieving 99.99% accuracy on the union of the training and test sets.

Our empirical results are summarized in Table 1. Each column in the table corresponds to a class in the dataset, where each row presents the type of the class. The values in the table denotes the number of polytopes and their faces (we use notation $a+b$ to denote two polytopes with a and b faces, respectively). For instance, the value in the first row and the first column shows that the $\{0\}$ class images in MNIST dataset can be distinguished from other classes by a single convex polytope with four faces. On the other hand, the second row in the first column shows that the complement of the class, namely $\{0\}^c := \{1, 2, 3, 4, 5, 6, 7, 8, 9\}$, can be separated from $\{0\}$ by a convex polytope with three faces, as illustrated in Figure 6(a).

For Fashion-MNIST and CIFAR10 datasets, certain classes are covered by two polytopes instead of just one. Figure 6(b) visually illustrates the classification of the class $\{0\}$ in Fashion-MNIST, accomplished through the difference of two polytopes. In the case of the CIFAR10 dataset, the number of faces in the polytopes tends to be higher compared to other datasets, consistent with the expectation that CIFAR10 exhibits a more intricate geometric structure than MNIST or Fashion-MNIST.

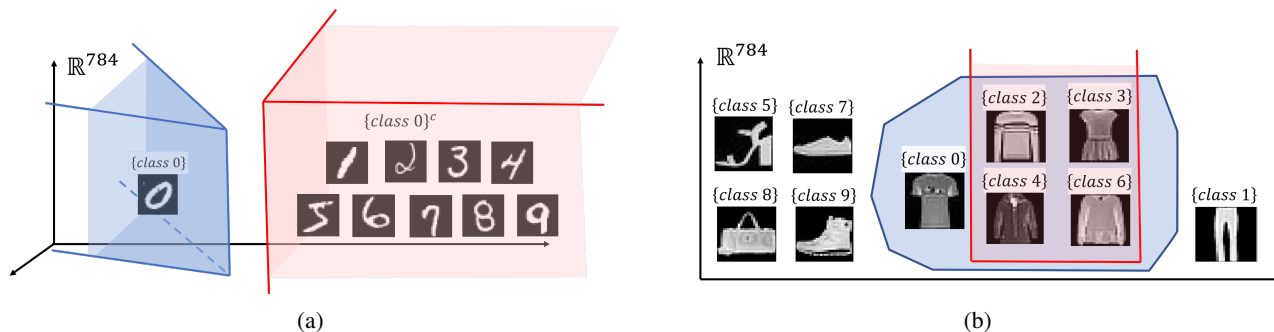


Figure 6. Illustration of a polytope-basis cover of the real datasets. (a) The class $\{0\}$ of MNIST can be separated by a single convex polytope with four faces, while the complement class $\{0\}^c$ can be separated with three faces. (b) The class $\{0\}$ of Fashion-MNIST can be separated by the difference of two polytopes, one of which contains similar images.

Furthermore, we identify the geometric complexity of each class from Table 1. In Fashion-MNIST, the complement of the class in $\{0, 2, 3, 4, 6\}$ prominently require more faces than other classes, and they all pertain to top clothes and share visual similarities (Figure 6(b)). Furthermore, it fails to find a single convex polytope cover of $\{0\}$ since the obtained polytope always contains many images in $\{2, 3, 4, 6\}$ classes, as illustrated in Figure 6(b). In contrast, the class $\{1\}$ and $\{1\}^c$ are separated by the smallest number of faces, indicating that they are less entangled with other classes. This example demonstrates *how neural networks can be utilized as a tool for quantifying the geometric complexity of datasets*. We provide further empirical examples in Appendix B.

Remark 4.1. By combining the results in Table 1 with Theorem 3.4, we can ascertain the feasible architectures of these datasets, based on their geometric characteristics. Specifically, adopting the covering polytopes with minimal number in Table 1 for each class, we deduce that

$$\begin{aligned} \text{MNIST} : & \quad 784 \xrightarrow{\sigma} 47 \xrightarrow{\sigma} 10 \rightarrow 10 \\ \text{Fashion-MNIST} : & \quad 784 \xrightarrow{\sigma} 90 \xrightarrow{\sigma} 14 \rightarrow 10 \\ \text{CIFAR10} : & \quad 3072 \xrightarrow{\sigma} 178 \xrightarrow{\sigma} 12 \rightarrow 10 \end{aligned}$$

are feasible architectures for these datasets. Note that this is the first result on the minimal architectures that can completely classify the given datasets, utilizing the geometric features of the datasets.

It is worth noting that our findings stem from Algorithm 1, which selectively removes and adjusts neurons within the network. Given the sparse connectivity observed in these networks (as demonstrated in the proof of Theorem 3.4 and illustrated in Figure 2(c)), we anticipate an inherent connection between our results and the Lottery Ticket Hypothesis (Frankle & Carbin, 2018; Malach et al., 2020). Notably, in Remark 4.1, we established the existence of the minimal network architectures for these datasets. Exploring how

these minimal architectures could be identified and pruned from trained networks represents an intriguing avenue for future investigation.

5. Conclusion

In this paper, we investigated the geometric characteristics of datasets and neural network architecture. Specifically, we established both lower and upper bounds on the necessary widths of network architectures for classifying given data manifolds, relying on its polytope-basis cover. Furthermore, we extended these insights to simplicial complexes or spaces consisting of prismatic polytopes, shedding light on how the width bound varies in response to the geometric complexity of the dataset. Conversely, we also demonstrated that the polytope structure of datasets can be inspected by training neural networks. We proposed such an algorithm, and our experimental results unveiled that each class within MNIST, Fashion-MNIST, and CIFAR10 datasets can be distinguished by at most two polytopes, with each comprising less than 30 faces. We further analyzed that the number of faces in the polytope serves as an indicator of the geometric complexity of each class. Our empirical investigations unveil that neural network indeed converges to a polytope-basis cover of dataset, and conversely, it is possible to inspect geometrical features of the dataset by training neural networks. Our findings for MNIST, Fashion-MNIST, and CIFAR10 datasets not only underscore the inherent simplicity of the geometry within these real-world datasets but also shed light on the investigating geometric complexity of individual classes.

Limitations and future work. The optimality of the polytope-basis cover obtained by Algorithm 1 has not been clarified, which remains an interesting avenue for future research.

References

- Alfarra, M., Bibi, A., Hammoud, H., Gaafar, M., and Ghanem, B. On the decision boundaries of neural networks: A tropical geometry perspective. *IEEE Transactions on Pattern Analysis and Machine Intelligence*, 45(4):5027–5037, 2022.
- Amos, B., Xu, L., and Kolter, J. Z. Input convex neural networks. In *International Conference on Machine Learning*, pp. 146–155. PMLR, 2017.
- Astorino, A. and Gaudioso, M. Polyhedral separability through successive lp. *Journal of Optimization theory and applications*, 112(2):265–293, 2002.
- Balestriero, R., Wang, Z., and Baraniuk, R. G. Deephull: Fast convex hull approximation in high dimensions. In *ICASSP 2022-2022 IEEE International Conference on Acoustics, Speech and Signal Processing (ICASSP)*, pp. 3888–3892. IEEE, 2022.
- Barannikov, S., Trofimov, I., Balabin, N., and Burnaev, E. Representation topology divergence: A method for comparing neural network representations. *arXiv preprint arXiv:2201.00058*, 2021a.
- Barannikov, S., Trofimov, I., Sotnikov, G., Trimbach, E., Korotin, A., Filippov, A., and Burnaev, E. Manifold topology divergence: a framework for comparing data manifolds. *Advances in Neural Information Processing Systems*, 34:7294–7305, 2021b.
- Beise, H.-P., Da Cruz, S. D., and Schröder, U. On decision regions of narrow deep neural networks. *Neural Networks*, 140:121–129, 2021.
- Beltran-Royo, C., Llopis-Ibor, L., Pantrigo, J. J., and Ramírez, I. Dc neural networks avoid overfitting in one-dimensional nonlinear regression. *Knowledge-Based Systems*, 283:111154, 2024.
- Berzins, A. Polyhedral complex extraction from relu networks using edge subdivision. *arXiv preprint arXiv:2306.07212*, 2023.
- Birdal, T., Lou, A., Guibas, L. J., and Simsekli, U. Intrinsic dimension, persistent homology and generalization in neural networks. *Advances in Neural Information Processing Systems*, 34:6776–6789, 2021.
- Black, S., Sharkey, L., Grinsztajn, L., Winsor, E., Braun, D., Merizian, J., Parker, K., Guevara, C. R., Millidge, B., Alfour, G., et al. Interpreting neural networks through the polytope lens. *arXiv preprint arXiv:2211.12312*, 2022.
- Buchanan, S., Gilboa, D., and Wright, J. Deep networks and the multiple manifold problem. *arXiv preprint arXiv:2008.11245*, 2020.
- Bünning, F., Schalbetter, A., Aboudonia, A., de Bady, M. H., Heer, P., and Lygeros, J. Input convex neural networks for building mpc. In *Learning for Dynamics and Control*, pp. 251–262. PMLR, 2021.
- Carlini, N., Liu, C., Erlingsson, Ú., Kos, J., and Song, D. The secret sharer: Evaluating and testing unintended memorization in neural networks. In *28th USENIX Security Symposium (USENIX Security 19)*, pp. 267–284, 2019.
- Carlini, N., Tramer, F., Wallace, E., Jagielski, M., Herbert-Voss, A., Lee, K., Roberts, A., Brown, T., Song, D., Erlingsson, U., et al. Extracting training data from large language models. In *30th USENIX Security Symposium (USENIX Security 21)*, pp. 2633–2650, 2021.
- Carlsson, S. Geometry of deep convolutional networks. *arXiv preprint arXiv:1905.08922*, 2019.
- Chen, M., Jiang, H., Liao, W., and Zhao, T. Nonparametric regression on low-dimensional manifolds using deep relu networks: Function approximation and statistical recovery. *Information and Inference: A Journal of the IMA*, 11(4):1203–1253, 2022.
- Chen, Y., Shi, Y., and Zhang, B. Input convex neural networks for optimal voltage regulation. *arXiv preprint arXiv:2002.08684*, 2020.
- Cohen, U., Chung, S., Lee, D. D., and Sompolinsky, H. Separability and geometry of object manifolds in deep neural networks. *Nature communications*, 11(1):746, 2020.
- Cybenko, G. Approximation by superpositions of a sigmoidal function. *Mathematics of control, signals and systems*, 2(4):303–314, 1989.
- Dirksen, S., Genzel, M., Jacques, L., and Stollenwerk, A. The separation capacity of random neural networks. *The Journal of Machine Learning Research*, 23(1):13924–13970, 2022.
- Du, S. S., Hu, W., and Lee, J. D. Algorithmic regularization in learning deep homogeneous models: Layers are automatically balanced. *Advances in neural information processing systems*, 31, 2018.
- Fan, F.-L., Huang, W., Zhong, X., Ruan, L., Zeng, T., Xiong, H., and Wang, F. Deep relu networks have surprisingly simple polytopes. *arXiv preprint arXiv:2305.09145*, 2023.
- Fan, J., Taghvaei, A., and Chen, Y. Scalable computations of wasserstein barycenter via input convex neural networks. *arXiv preprint arXiv:2007.04462*, 2020.

- Fawzi, A., Moosavi-Dezfooli, S.-M., Frossard, P., and Soatto, S. Empirical study of the topology and geometry of deep networks. In *Proceedings of the IEEE Conference on Computer Vision and Pattern Recognition*, pp. 3762–3770, 2018.
- Frankle, J. and Carbin, M. The lottery ticket hypothesis: Finding sparse, trainable neural networks. In *International Conference on Learning Representations*, 2018.
- Goldt, S., Mézard, M., Krzakala, F., and Zdeborová, L. Modeling the influence of data structure on learning in neural networks: The hidden manifold model. *Physical Review X*, 10(4):041044, 2020.
- Gorban, A. N. and Tyukin, I. Y. Blessing of dimensionality: mathematical foundations of the statistical physics of data. *Philosophical Transactions of the Royal Society A: Mathematical, Physical and Engineering Sciences*, 376(2118):20170237, 2018.
- Grigsby, J. E. and Lindsey, K. On transversality of bent hyperplane arrangements and the topological expressiveness of relu neural networks. *SIAM Journal on Applied Algebra and Geometry*, 6(2):216–242, 2022.
- Haase, C., Hertrich, C., and Loho, G. Lower bounds on the depth of integral relu neural networks via lattice polytopes. *arXiv preprint arXiv:2302.12553*, 2023.
- Haim, N., Vardi, G., Yehudai, G., Shamir, O., and Irani, M. Reconstructing training data from trained neural networks. *Advances in Neural Information Processing Systems*, 35: 22911–22924, 2022.
- Hajj, M. and Istvan, K. A topological framework for deep learning. *arXiv preprint arXiv:2008.13697*, 2020.
- Hajj, M. and Istvan, K. Topological deep learning: Classification neural networks. *arXiv preprint arXiv:2102.08354*, 2021.
- Hanin, B. and Rolnick, D. Deep relu networks have surprisingly few activation patterns. *Advances in neural information processing systems*, 32, 2019.
- Hannouch, K. M. and Chalup, S. Topology estimation of simulated 4d image data by combining downscaling and convolutional neural networks. *arXiv preprint arXiv:2306.14442*, 2023.
- Hornik, K. Approximation capabilities of multilayer feed-forward networks. *Neural networks*, 4(2):251–257, 1991.
- Huchette, J., Muñoz, G., Serra, T., and Tsay, C. When deep learning meets polyhedral theory: A survey. *arXiv preprint arXiv:2305.00241*, 2023.
- Kantchelian, A., Tschantz, M. C., Huang, L., Bartlett, P. L., Joseph, A. D., and Tygar, J. D. Large-margin convex polytope machine. *Advances in Neural Information Processing Systems*, 27, 2014.
- Kim, K., Kim, J., Zaheer, M., Kim, J., Chazal, F., and Wasserman, L. Pllay: Efficient topological layer based on persistent landscapes. *Advances in Neural Information Processing Systems*, 33:15965–15977, 2020.
- Liu, Y., Cole, C. M., Peterson, C., and Kirby, M. Relu neural networks, polyhedral decompositions, and persistent homology. In *Topological, Algebraic and Geometric Learning Workshops 2023*, pp. 455–468. PMLR, 2023.
- Magai, G. and Ayzenberg, A. Topology and geometry of data manifold in deep learning. *arXiv preprint arXiv:2204.08624*, 2022.
- Makkuva, A., Taghvaei, A., Oh, S., and Lee, J. Optimal transport mapping via input convex neural networks. In *International Conference on Machine Learning*, pp. 6672–6681. PMLR, 2020.
- Malach, E., Yehudai, G., Shalev-Schwartz, S., and Shamir, O. Proving the lottery ticket hypothesis: Pruning is all you need. In *International Conference on Machine Learning*, pp. 6682–6691. PMLR, 2020.
- Manwani, N. and Sastry, P. Learning polyhedral classifiers using logistic function. In *Proceedings of 2nd Asian Conference on Machine Learning*, pp. 17–30. JMLR Workshop and Conference Proceedings, 2010.
- Masden, M. Algorithmic determination of the combinatorial structure of the linear regions of relu neural networks. *arXiv preprint arXiv:2207.07696*, 2022.
- Naitzat, G., Zhitnikov, A., and Lim, L.-H. Topology of deep neural networks. *The Journal of Machine Learning Research*, 21(1):7503–7542, 2020.
- Park, S., Yun, C., Lee, J., and Shin, J. Minimum width for universal approximation. *arXiv preprint arXiv:2006.08859*, 2020.
- Paul, R. and Chalup, S. Estimating betti numbers using deep learning. In *2019 International Joint Conference on Neural Networks (IJCNN)*, pp. 1–7. IEEE, 2019.
- Pestov, V. Is the k-nn classifier in high dimensions affected by the curse of dimensionality? *Computers & Mathematics with Applications*, 65(10):1427–1437, 2013.
- Piwiek, P., Klukowski, A., and Hu, T. Exact count of boundary pieces of relu classifiers: Towards the proper complexity measure for classification. *arXiv preprint arXiv:2306.08805*, 2023.

- Rolnick, D. and Kording, K. Reverse-engineering deep relu networks. In *International Conference on Machine Learning*, pp. 8178–8187. PMLR, 2020.
- Rudin, W. et al. *Principles of mathematical analysis*, volume 3. McGraw-hill New York, 1976.
- Sankaranarayanan, P. and Rengaswamy, R. Cdinn–convex difference neural networks. *Neurocomputing*, 495:153–168, 2022.
- Sivaprasad, S., Singh, A., Manwani, N., and Gandhi, V. The curious case of convex neural networks. In *Machine Learning and Knowledge Discovery in Databases. Research Track: European Conference, ECML PKDD 2021, Bilbao, Spain, September 13–17, 2021, Proceedings, Part I 21*, pp. 738–754. Springer, 2021.
- Telgarsky, M. Representation benefits of deep feedforward networks. *arXiv preprint arXiv:1509.08101*, 2015.
- Tiwari, S. and Konidaris, G. Effects of data geometry in early deep learning. *arXiv preprint arXiv:2301.00008*, 2022.
- Vallin, J., Larsson, K., and Larson, M. G. The geometric structure of fully-connected relu-layers. *arXiv preprint arXiv:2310.03482*, 2023.
- Vincent, J. A. and Schwager, M. Reachable polyhedral marching (rpm): An exact analysis tool for deep-learned control systems. *arXiv preprint arXiv:2210.08339*, 2022.
- Wang, T., Buchanan, S., Gilboa, D., and Wright, J. Deep networks provably classify data on curves. *Advances in neural information processing systems*, 34:28940–28953, 2021.
- Xu, S., Vaughan, J., Chen, J., Zhang, A., and Sudjianto, A. Traversing the local polytopes of relu neural networks. In *The AAAI-22 Workshop on Adversarial Machine Learning and Beyond*, 2021.

Appendix

Appendix A. Related works

Appendix B. Geometric analysis on the manifold of real-world datasets

Appendix C. Algorithms for finding polytope-basis covers

C.1 A polytope-basis cover derived from a trained three-layer ReLU network

C.2 A polytope-basis cover derived from a trained two-layer ReLU network

C.3 The efficient algorithm to find real-world datasets

C.4 Comparison of proposed algorithms.

Appendix D. Convergence on the proposed networks

Appendix E. Proofs

E.1 Proof of Proposition 3.1

E.2 Proof of Theorem 3.4

E.3 Proof of Theorem 3.5

E.4 Proof of Theorem 3.6

E.5 Proof of Theorem 3.7

E.6 Proof of Proposition C.2

E.7 Proof of Theorem D.3

Appendix F. Additional propositions and lemmas

A. Related Works

Geometric approaches to ReLU networks. Various geometric methodologies have been employed to explore the approximation capabilities of deep ReLU networks. Hanin & Rolnick (2019), for instance, introduced the concept of bent hyperplanes in the input space, assessing its theoretical and empirical complexities. The methodology known as the ‘bent hyperplane arrangement’ has been applied across various research domains. Notably, it has been utilized in the analysis of decision regions (Beise et al., 2021; Grigsby & Lindsey, 2022; Black et al., 2022) or characterizing linear regions within ReLU networks (Rolnick & Kording, 2020), which is also intricately connected to our proofs in Theorem 3.1 and 3.6.

On the other hand, there has been a burgeoning interest in investigating polytope structures induced by deep ReLU networks (Fawzi et al., 2018; Xu et al., 2021; Alfarra et al., 2022; Vincent & Schwager, 2022; Black et al., 2022; Haase et al., 2023; Liu et al., 2023; Fan et al., 2023; Huchette et al., 2023; Vallin et al., 2023; Piwek et al., 2023). Masden (2022) introduced algorithms capable of extracting the polytope structure inherent in networks and deriving topological properties of the decision boundary. Carlsson (2019) and Vallin et al. (2023) considered the pre-image of ReLU networks, characterizing the geometric shapes of the decision boundary to gain an understanding of the polytope partitions of deep ReLU networks.

Nonetheless, there has been a scarcity of exploration into the explicit construction of neural networks for the purpose of classifying a given dataset, as illustrated in Figure 1. In this study, we address the practical challenge of distinguishing between the two data manifolds, and we introduce practical algorithms for constructing covering polytopes based on the properties of ReLU networks. This approach can be considered a complementary method for investigating the approximation capabilities of neural networks in terms of polytopes - a geometric aspect that has not been extensively explored.

Exploring input convexity in neural networks. Recent years have witnessed a surge in research dedicated to unraveling the convexity of ReLU networks concerning their input. Crucially, it has been established that the ReLU activation function demonstrates convexity concerning its input when composited weights are all positive (Proposition 1 in (Amos et al., 2017), cf. Lemma F.4). This discovery led to the inception of Input Convex Neural Networks (ICNNs) by Amos et al. (2017),

a characteristic that has been effectively leveraged in various applications (Makkuva et al., 2020; Chen et al., 2020; Fan et al., 2020; Büning et al., 2021; Balestrierio et al., 2022). Notably, Balestrierio et al. (2022) applied this idea and proposed *DeepHull*, the algorithm to approximate the convex hull by convex deep networks. On the other hand, Sivaprasad et al. (2021) asserted that these convex neural networks exhibit self-regularization effects, demonstrating superior generalization performance in specific tasks. Additionally, research has delved into representing neural networks as the difference of convex (DC) functions (Sankaranarayanan & Rengaswamy, 2022; Piwek et al., 2023; Beltran-Royo et al., 2024). Sankaranarayanan & Rengaswamy (2022) employed Linear Programming to optimize polyhedral DC functions, capitalizing on the piecewise linearity induced by the ReLU activation function.

In this study, we decompose a trained ReLU network into the difference of several convex functions and leverage this decomposition to induce a polytope-basis cover for a given dataset. Specifically, we employ the ICNN architectures to derive a convex polytope cover, revealing how trained neural networks capture the geometric characteristics of the training dataset. While Balestrierio et al. (2022) explored a similar approach by minimizing the volume of the polytope as a regularizer, our main focus is on minimizing the number of neurons to reduce a polytope with a small number of faces. Consequently, our empirical results can be considered as an application of ICNNs to extract geometric features of datasets in terms of polytopes.

Moreover, it is noteworthy that previous studies imposed restrictions on the weights, either by enforcing $W_k \geq 0$ (Amos et al., 2017; Sivaprasad et al., 2021) or by substituting them with squared values $W_k^2 \geq 0$ (Sankaranarayanan & Rengaswamy, 2022), to maintain network convexity. In contrast, we achieve this solely by adjusting the initialization conditions, leveraging the implicit bias of gradient descent (Du et al., 2018).

Complexity of datasets and neural network architectures. Several studies have delved into the intricate relationship between the geometric features of datasets and neural network training, often referred to as the *multiple manifold problem* (Goldt et al., 2020; Buchanan et al., 2020; Wang et al., 2021; Chen et al., 2022; Tiwari & Konidaris, 2022). This problem typically involves the binary classification of two low-dimensional manifolds by neural networks. For instance, Buchanan et al. (2020) and Wang et al. (2021) focused on the task of distinguishing between two curves (i.e., one-dimensional manifolds), investigating the convergence speed and generalization concerning the geometric features of the dataset. Similarly, in the context of low-dimensional data manifolds, Tiwari & Konidaris (2022) examined the effects of data geometry on the complexity of trained neural networks, measuring the distance to the manifold. In a related vein, Dirksen et al. (2022) considered the separation problem with randomly initialized ReLU networks, explicitly linking required widths to weight initialization. Additionally, numerous empirical studies have supported the implicit relationship between network architecture and the geometric complexity or topological structure of the data manifold (Fawzi et al., 2018; Kim et al., 2020; Cohen et al., 2020; Birdal et al., 2021; Barannikov et al., 2021a;b; Naitzat et al., 2020; Hajj & Istvan, 2020, 2021; Magai & Ayzenberg, 2022). These theoretical and empirical findings suggest a high correlation between neural network architecture and the training dataset: *a more complicated dataset requires a more complex architecture*.

However, a notable gap still exists in the literature when it comes to explicitly constructing a neural network in practice. For example, as introduced in Section 1, it remains unknown which architecture of neural networks can or cannot completely classify a given dataset with explicit construction of neural networks.

Estimating dataset characteristics from a trained network. Once a neural network is trained, it is well-established that the trained network encapsulates information or characteristics of the training dataset (Carlini et al., 2019, 2021; Haim et al., 2022). This phenomenon, implies that neural networks can be employed to extract information about the dataset through the training process. From a topological perspective, Paul & Chalup (2019) introduced a method for estimating the Betti numbers of 2D or 3D datasets using convolutional neural networks, later extended to 4D datasets by (Hannouch & Chalup, 2023). In the geometric realm, Kantchelian et al. (2014) proposed the large-margin convex polytope machine with a training algorithm to find a convex polytope that encloses one class with a large margin. Their empirical results demonstrated that the digit '2' class of MNIST has a simple convex polytope cover that generalizes well.

However, there are still opportunities for more precise investigations into the dataset geometry in terms of polytopes, which are induced from ReLU networks. In this paper, we propose an algorithm that derives a polytope-basis cover of a given dataset by learning neural networks, building upon our theoretical analysis. Moreover, it reveals the number of faces of the polytopes, which can describe the geometric complexity of dataset.

Our contributions. In this paper, we harmonize diverse perspectives on neural networks, offering insights into the intrinsic relationship between the geometric complexity of datasets and network architectures. Our focus centers on the polytope structure induced by ReLU networks (Theorems 3.4, 3.5, 3.6). The principal contribution of our work lies in delineating lower and upper bounds on widths within deep ReLU networks for the classification of a given dataset, drawing from the polytope structure inherent in the data. Our theoretical results not only elucidate how the geometric complexity of a dataset influences the required widths of neural networks but also illuminate the nuanced role of neurons in deep layers.

Furthermore, we present algorithms aimed at deriving a polytope-basis cover for given datasets, thereby highlighting the inherent link between trained neural networks and the polytope structure of the training datasets. While prior research (Kantchelian et al., 2014; Sivaprasad et al., 2021) merely showcased the polyhedral separability of certain classes in MNIST or CIFAR10, we determine the exact number of faces required for covering polytopes of each class. Essentially, our work introduces a novel methodology for exploring the intricate relationship between dataset geometry and neural networks.

B. Geometric simplicity of real-world datasets

In this section, we present empirical results illustrating how the number of faces of covering polytopes reflects the geometric characteristics of a class. Specifically, we examine a classification task under varying levels of noisy labels. We focus on the class $\{1\}$ in each dataset and manipulate the noise levels (r) across values of 0, 0.01, 0.1, 0.25, 0.5, and 0.90 while maintaining the total number of data points in the class. The noisy class with noise level r is denoted by $\{1\}_r^{noise}$.

Here we give an example: When $r = 0.00$, the $\{1\}_{r=0.00}^{noise}$ class is identical to the $\{1\}$ class in Fashion-MNIST, comprising 6000 T-shirt images. As r increases, such as $r = 0.01$, the noised class $\{1\}_{r=0.01}^{noise}$ still consists of 6000 images, but only 99% of them are T-shirt images, with the remaining 1% randomly selected from other classes. Consequently, when $r = 0.9$, $\{1\}_{r=0.9}^{noise}$ contains 600 T-shirt images and 5400 randomly selected images from other classes, i.e., totally randomly selected images in the Fashion-MNIST dataset. The task is finding a single converging polytope that contains $\{1\}_{r=0.9}^{noise}$ against the other data.

We utilize Algorithm 1 to identify a single polytope with minimal width, achieving an accuracy greater than 99.9% on the noised dataset. To mitigate the randomness inherent in image selection, we compute the average value over five repetitions. The results are presented in Table 2.

Dataset \ noise level r	0.00	0.01	0.10	0.25	0.50	0.90
MNIST class $\{1\}$	3	5.2	29.2	46.6	64.0	52.4
F-MNIST class $\{1\}$	3	4.6	39.0	57.4	77.0	65.6
CIFAR10 class $\{1\}$	12	12.8	16.2	19.6	28.4	35.6

Table 2. The average number of faces required for a convex polytope to cover the class $\{1\}_r^{noise}$, with varying levels of random labels (r). As the proportion of random labels in the class rises, there is a noticeable corresponding increase in the requisite number of faces.

The results illustrate a positive correlation between the prevalence of noisy labels and the increasing complexity of covering polytopes: as the level of noise rises, the requisite number of faces also increases accordingly. Specifically, Table 2 demonstrates that images within the same class can be effectively distinguished by a convex polytope with a smaller number of faces, highlighting the inherent geometric complexity of real-world datasets.

Moreover, our result can demonstrate some previous works that classified these datasets using convex polytopes. Notably, for MNIST (Kantchelian et al., 2014) and CIFAR10 (Sivaprasad et al., 2021), it has been observed that convex polytope classifiers exhibit self-regularization effects and robustness to label noise. Our results presented in Table 2 validate this observation based on the geometric features of the datasets: each class in the datasets inherently possesses simple geometry, enabling convex classifiers to generalize effectively.

A particularly intriguing finding emerges when comparing the results with 50% corrupted labels ($r = 0.5$) to those with fully-mixed labels ($r = 0.9$). Notably, for MNIST and Fashion-MNIST datasets, Table 2 suggests that the 50% corrupted dataset is even more challenging to segregate than the fully-mixed counterpart. In other words, a convex polytope with fewer faces must encompass the original images from the uncorrupted class $\{1\}$ - the 'digit 1 images' in MNIST or the 'T-shirts images' in FashionMNIST-, necessitating a larger number of faces

for the polytope to effectively segregate them. This observation emphasizes the geometric simplicity of MNIST and Fashion-MNIST datasets, contrasting with the behavior observed in CIFAR10, which does not exhibit this trend.

Remark B.1. To prevent potential misunderstandings regarding the results in Table 2, we offer two insights. Firstly, in the case of the fully-mixed class ($r = 0.9$), it is not surprising that an arbitrary set of points in high-dimensional space can be separated by a single convex polytope. This phenomenon is rooted in the curse of dimensionality, where in higher dimensions, points are inherently easier to separate (Pestov, 2013; Gorban & Tyukin, 2018). Indeed, Table 2 illustrates that random images in CIFAR10 are separated with fewer faces compared to other datasets. Secondly, it’s worth noting that although two manifolds may be polyhedrally separable, this does not necessarily imply that each manifold is convex, as depicted in Figure 7.

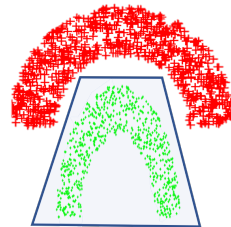


Figure 7. Although two manifolds are polyhedrally separable, both manifolds may not exhibit convexity.

C. Algorithms for finding polytope-basis covers

In this section, we provide detailed explanations of our algorithms, including each step, motivation, and theoretical results. Moreover, we further introduce two algorithms that reduce polytope-basis covers. The section is structured into four subsections.

In Section C.1, we delve into the motivation behind Algorithm 1 and provide a comprehensive explanation of its implementation. In Section C.2, we introduce Algorithm 3, which extracts a polytope-basis cover from a trained two-layer ReLU network. In Section C.3, we unveil Algorithm 4, an efficient algorithm designed to produce a polytope-basis cover for a given dataset using a minimal number of polytopes. Lastly, in Section C.4, we conduct a comparative analysis of our proposed algorithms.

C.1. A polytope-basis cover derived from a three-layer ReLU network

In Section 3.2, we introduced the compressing algorithm (Algorithm 1) that deforms two-layer network to represent a simple convex polytope. Before we provide detail descriptions, we introduce some terminologies.

Definition C.1. Let $\mathcal{N}(\mathbf{x}) := v_0 + \sum_{k=1}^m v_k \sigma(\mathbf{w}_k^\top \mathbf{x} + b_k)$ be a two-layer ReLU network. For each $k \in [m]$, we refer a pair (v_k, \mathbf{w}_k, b_k) as a *neuron* of \mathcal{N} . We say a neuron $\sigma(\mathbf{w}_k^\top \mathbf{x} + b_k)$ *activates* (or *deactivates*) \mathbf{x} if $\mathbf{w}_k^\top \mathbf{x} + b_k > 0$ (or $\mathbf{w}_k^\top \mathbf{x} + b_k < 0$, respectively). The *activation boundary* (AB) of a neuron (v_k, \mathbf{w}_k, b_k) is defined by $\{\mathbf{x} \in \mathbb{R}^d \mid \mathbf{w}_k^\top \mathbf{x} + b_k = 0\}$. Similarly, the *decision boundary* (DB) of \mathcal{N} is defined by the set $\{\mathbf{x} \in \mathbb{R}^d \mid \mathcal{N}(\mathbf{x}) = 0\}$.

Roughly speaking, the activation boundaries of \mathcal{T} are non-differentiable points of \mathcal{T} . For example, the leftmost column in Figure 4 or 8 shows the decision boundary and activation boundaries of a trained two-layer ReLU network.

Let \mathcal{T} be a two-layer ReLU network defined in (5), thus $v_k < 0$ for all $k \in [m]$. Let S be the region defined by $S := \{\mathbf{x} \mid \mathcal{T}(\mathbf{x}) = 1\}$. If it is nonempty, then it is a convex polytope with m faces by Definition 2.1). However, its decision boundary $R := \{\mathbf{x} \mid \mathcal{T}(\mathbf{x}) > 0\} \supset S$ may contain more data points than S . For the given dataset \mathcal{D} , to achieve (7), the objective of the compressing algorithm is to achieve

$$R \cap \mathcal{D} = S \cap \mathcal{D}. \quad (9)$$

Note that (9) directly implies (7). Below, we demonstrate a detailed examination of the compressing algorithm, which was briefly introduced in Section 3. The algorithm comprises two parts: **1.** eliminating a redundant neuron, and **2.** scaling some neurons.

- **PART 1. Eliminating a redundant neuron.** The first part involves the removal of remaining redundant neurons that may activate some data points but do not contribute significantly to the network output. Specifically, in Figure 3(a), the neuron indicated by the red arrow does not contribute to the change of the decision boundary since the training data points activated by this neuron already exhibit negative outputs, i.e., $\mathcal{T}(\mathbf{x}) < 0$ already. In essence, eliminating such neurons does not significantly alter the decision boundary of \mathcal{T} . However, although the removal of this neuron maintains the decision boundary of \mathcal{T} , it does affect the output value of \mathcal{T} , consequently influencing other subnetworks

in the three-layer network \mathcal{N} . To address this, the algorithm removes only one neuron at once, which has the smallest value of $|v_k| \cdot \|\mathbf{w}_k\|$.

- **PART 2. Scaling neurons.** The second part is deforming the given network to satisfy (9) by magnifying neurons. From the definition of $\mathcal{T}(\mathbf{x}) = 1 + \sum_k v_k \sigma(\mathbf{w}_k^\top \mathbf{x} + b_k)$, recall that all $v_k < 0$. If we take $v_k \rightarrow -\infty$ for all k , then the region $R = \{\mathbf{x} \in \mathbb{R}^d \mid 0 < \mathcal{T}(\mathbf{x})\}$ shrinks to the region $S = \{\mathbf{x} \in \mathbb{R}^d \mid \mathcal{T}(\mathbf{x}) = 1\}$ (cf. Figure 14(b) may help understanding this sentence.) This is the trick we used to figure out the minimal polytope representation of the decision region.

In this step, we just increase the magnitude of a neuron (v_k, \mathbf{w}_k, b_k) for $k \in [m]$ if it has an activated data \mathbf{x}_i such that $\mathcal{T}_j(\mathbf{x}) \neq 1$. The multiplication constant is referred to λ_{scale} to (v_k, \mathbf{w}_k, b_k) in the algorithm. Furthermore, note also that the updated neuron still satisfies (8), thus gradient descent algorithm can be parallelized with keeping $v_k < 0$. In the example in Figure 3, check that the decision boundary in Figure 3(b) is indeed shrunk in (c).

However, removing a neuron (part 1) and adjusting the scaling of some neurons (part 2) will inevitably alter the network’s output, which could potentially decrease its classification accuracy. Therefore, as highlighted in Section 3, it is advisable to apply the compressing algorithm in conjunction with an optimization process, as outlined in Algorithm 2.

Algorithm 2 Extracting a polytope-basis cover from a three-layer ReLU network

Require: a pretrained three-layer network $\mathcal{N}(\mathbf{x})$ defined in (6), the training dataset $\mathcal{D} = \{(x_i, y_i)\}_{i=1}^n$, Epochs
for $epoch = 1, \dots, Epochs$ **do**
 for $iteration = 1, 2, \dots, 1000$ **do**
 one-step gradient descent for \mathcal{N} under the BCE loss (14)
 end for
 for $j = 1, \dots, J$ **do**
 $\mathcal{T}_j \leftarrow \text{COMP}(\mathcal{T}_j)$ ▷ the compressing algorithm (Algorithm 1)
 end for
 end for
 if there exists $i \in [n]$ and $j \in [J]$ such that $0 < \mathcal{T}_j(\mathbf{x}_i) < 1$ **then**
 repeat
 $\mathcal{T}_j \leftarrow \text{COMP}(\mathcal{T}_j)$ ▷ the compressing algorithm (Algorithm 1)
 until $\sigma(\mathcal{T}_j(\mathbf{x}_i))$ is either 0 or 1 for all $i \in [n]$ and $j \in [J]$
 end if
 Output: \mathcal{N}

Figure 4 illustrates the results obtained by applying Algorithm 2. A three-layer network \mathcal{N} defined in (6) with $J = 16$ polytopes, each consisting of 20 neurons (architecture $2 \xrightarrow{\sigma} 320 \xrightarrow{\sigma} 16 \rightarrow 1$), was pre-trained on the swiss-roll dataset. Subsequently, Algorithm 1 was applied to compress each \mathcal{T}_j with fine tuning, resulting in a compressed three-layer network with architecture $2 \xrightarrow{\sigma} 72 \xrightarrow{\sigma} 16 \rightarrow 1$. Then, for the polytopes defined by $C_j := \{\mathbf{x} \in \mathbb{R}^d \mid \mathcal{T}_j(\mathbf{x}) = 1\}$, the collection of polytopes $\mathcal{C} = \{C_j\}_{j \in [J]}$ becomes a polytope-basis cover of the dataset, comprising these 16 polytopes of \mathcal{N} . The obtained polytopes are illustrated in Figure 4(b, c).

Furthermore, it is noteworthy to mention the time efficiency of both Algorithm 1 and 2. Despite the presence of multiple for loops, these algorithms are implemented efficiently using parallel computing in PyTorch. Empirically, they demonstrate quick performance with practical neural network widths. On a theoretical level, Proposition C.2 ensures that Algorithm 2 terminates within a finite timeframe and provides a polytope-basis cover that achieved the same accuracy with the converged neural network \mathcal{N} .

C.2. A polytope-basis cover derived from a two-layer ReLU network

In this section, we propose another algorithm that extracts a polytope-basis cover from a trained two-layer ReLU network \mathcal{N} defined in (1). First, we decompose \mathcal{N} as the difference of two convex functions:

$$\mathcal{N}(\mathbf{x}) = v_0 + \sum_{k=1}^m v_k \sigma(\mathbf{w}_k^\top \mathbf{x}_k + b_k)$$

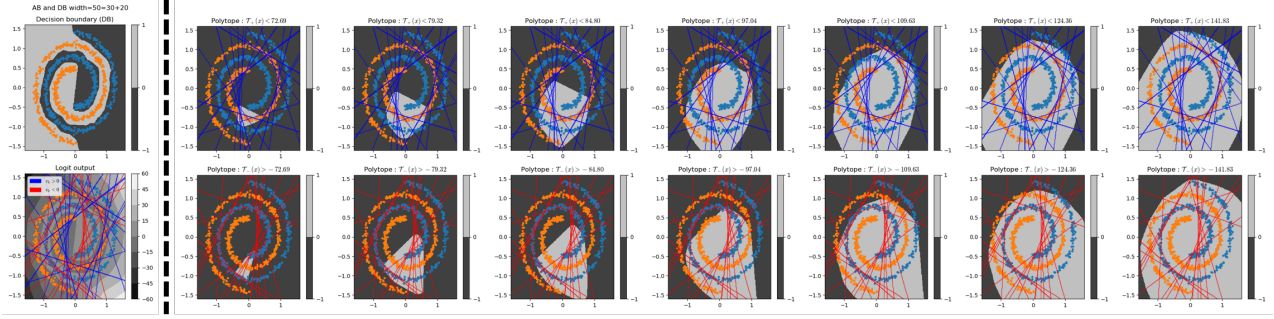


Figure 8. A polytope-basis cover derived by Algorithm 3 from a trained two-layer ReLU network with architecture $2 \xrightarrow{\sigma} 50 \rightarrow 1$. The decision boundary and all activation boundaries of the converged network are described in the leftmost column. The algorithm provides a polytope-basis cover consists of 68 polytopes, and some of them are illustrated in other columns.

$$\begin{aligned}
 &= \left(\frac{1}{2}v_0 + \sum_{v_k > 0} v_k \sigma(\mathbf{w}_k^\top \mathbf{x}_k + b_k) \right) + \left(\frac{1}{2}v_0 + \sum_{v_k < 0} v_k \sigma(\mathbf{w}_k^\top \mathbf{x}_k + b_k) \right) \\
 &=: \mathcal{N}_+(\mathbf{x}) + \mathcal{N}_-(\mathbf{x}).
 \end{aligned}$$

Note that both \mathcal{N}_+ and \mathcal{N}_- are convex and concave functions, respectively, by Lemma F.4. Now, we consider the network output of each data. For any $\mathbf{x}_i \in \mathcal{D}$, we have

$$\begin{aligned}
 \mathcal{N}(\mathbf{x}_i) > 0 &\Leftrightarrow \mathcal{N}_+(\mathbf{x}_i) > -\mathcal{N}_-(\mathbf{x}_i), \\
 \mathcal{N}(\mathbf{x}_i) < 0 &\Leftrightarrow \mathcal{N}_+(\mathbf{x}_i) < -\mathcal{N}_-(\mathbf{x}_i).
 \end{aligned}$$

Now, we quantize these functions. With the similar idea of Lebesgue integration, we can approximate the convex function $\mathcal{N}_+(\mathbf{x})$ by a simple function. Here, the *simple function* means a linear combination of indicator functions, importantly considered in mathematical field like Lebesgue theory (Rudin et al., 1976). Let $M := \max_{\mathbf{x} \in \mathcal{D}} \mathcal{N}_+(\mathbf{x})$. Then, for a given $\varepsilon > 0$, we can approximate $\mathcal{N}_+(\mathbf{x})$ by

$$\begin{aligned}
 \mathcal{N}_+(\mathbf{x}) &\approx M - \sum_{l=0}^{\infty} l\varepsilon \cdot \mathbb{1}_{\{M-(l+1)\varepsilon < \mathcal{N}_+(\mathbf{x}) < M-l\varepsilon\}}(\mathbf{x}) \\
 &= M - \varepsilon \sum_{C \in \mathcal{C}_Q} \mathbb{1}_{\{\mathbf{x} \in C\}}
 \end{aligned}$$

where \mathcal{C}_Q is collection of polytopes defined by $C := \{\mathbf{x} \mid \mathcal{N}_+(\mathbf{x}) < M - l\varepsilon\}$ for $l = 0, 1, \dots$. This decomposition can be understood as quantization of $\mathcal{N}_+(\mathbf{x})$ by slices with height ε . Moreover, the above approximation would be accurate as $\varepsilon \rightarrow 0$. Similarly, $\mathcal{N}_-(\mathbf{x})$ can be approximated in the similar manner. The main idea to obtain a polytope-basis cover \mathcal{C} from \mathcal{N} is selecting sufficiently many ε 's to quantize \mathcal{N}_+ and \mathcal{N}_- .

More precisely, we construct a polytope-basis cover from the values of \mathcal{N} . If \mathcal{C} is not a polytope-basis cover yet, we select an incorrectly classified data point $\hat{\mathbf{x}}$ with the smallest confidence value, i.e., $\hat{\mathbf{x}} := \arg \min_{\mathbf{x}_i \in \mathcal{D}} |\mathcal{N}(\mathbf{x}_i)|$. Subsequently, we choose an intermediate value c between $\mathcal{N}_+(\hat{\mathbf{x}})$ and $\mathcal{N}_-(\hat{\mathbf{x}})$ and add two polytopes $C_+ := \mathcal{N}_+ < c$ and $C_- := \mathcal{N}_- > -c$ to the cover \mathcal{C} . Then, the value

$$\left| \sum_{C \in \mathcal{C}_P} \mathbb{1}_{\{\mathbf{x} \in C\}}(\hat{\mathbf{x}}) - \sum_{C \in \mathcal{C}_Q} \mathbb{1}_{\{\mathbf{x} \in C\}}(\hat{\mathbf{x}}) \right|$$

is decreased by one since $\hat{\mathbf{x}}$ is contained in either C_+ or C_- . Therefore, by repeating this process sufficiently many times, \mathcal{C} will correctly classify $\hat{\mathbf{x}}$. Based on this idea, we provide Algorithm 3 that extracts a polytope-basis cover from a given trained two-layer ReLU network \mathcal{N} .

The result of Algorithm 3 on a network with architecture $2 \xrightarrow{\sigma} 50 \rightarrow 1$, which is trained on the swiss roll dataset, is illustrated in Figure 8. Specifically, the algorithm generates a polytope-basis cover of the dataset consists of 68 polytopes (\mathcal{C}_P and \mathcal{C}_Q consists of 34 polytopes). 14 polytopes in \mathcal{C} is illustrated in 2nd column to 8th column in Figure 8. Proposition C.2

Algorithm 3 Extracting a polytope-basis cover from a trained two-layer ReLU network

Require: a pretrained two-layer ReLU network \mathcal{N} defined in (1), training dataset $\mathcal{D} = \{(x_i, y_i)\}_{i=1}^n$
 Declare the empty collections \mathcal{C}_P and \mathcal{C}_Q .

repeat

Define $o_i := \sum_{C \in \mathcal{C}_P} \mathbb{1}_{\{x_i \in C\}} - \sum_{C \in \mathcal{C}_Q} \mathbb{1}_{\{x_i \in C\}} - \frac{1}{2}$ for all $i \in [n]$.

if \mathcal{C} is not a polytope-basis cover of \mathcal{D} **then**

$\hat{\mathbf{x}} \leftarrow \arg \min_{\text{sgn}(o_i) \neq \text{sgn}(\mathcal{N}(\mathbf{x}_i))} |\mathcal{N}_+(\mathbf{x}_i) + \mathcal{N}_-(\mathbf{x}_i)| \quad \triangleright \hat{\mathbf{x}}$ is not correctly covered by \mathcal{C} , and has the smallest confidence.

$c \leftarrow \frac{1}{2}(\mathcal{N}_+(\hat{\mathbf{x}}) - \mathcal{N}_-(\hat{\mathbf{x}}))$

Add the polytope $C := \{\mathbf{x} \mid \mathcal{N}_-(\mathbf{x}) > -c\}$ in \mathcal{C}_P .

Add the polytope $C := \{\mathbf{x} \mid \mathcal{N}_+(\mathbf{x}) < c\}$ in \mathcal{C}_Q .

$\mathcal{C} \leftarrow \mathcal{C}_P \cup \mathcal{C}_Q$

end if

until \mathcal{C} becomes a polytope-basis cover of \mathcal{D}

Output: \mathcal{C}

\triangleright The polytope-basis cover of \mathcal{D} derived from \mathcal{N} .

guarantees that Algorithm 3 must terminate in finite time, and produces a polytope-basis cover of \mathcal{D} which has the same accuracy with the \mathcal{N} . Therefore, training a two-layer ReLU network to 100% accuracy on the dataset \mathcal{D} , Algorithm 3 allows to derive a polytope-basis cover of the given dataset.

However, there are two drawbacks in this algorithm : 1. generally it induces many polytopes in practice, and 2. the number of faces of each polytope is unknown. For detail comparison with other algorithms, see Section C.4.

C.3. An efficient algorithm to find an optimal polytope-basis cover

In the preceding subsections, we introduced two algorithms in Sections C.1 and C.2 that extract a polytope-basis cover from trained two-layer or three-layer ReLU networks. However, the results obtained from both algorithms, as illustrated in Figure 8 and 4, still exhibit multiple polytopes on the training dataset. As demonstrated for the swiss roll dataset in Figure 1, we have previously shown the existence of a polytope-basis cover comprising only four polytopes (refer to Figure 1 and 2).

In this section, to address the aforementioned issue, we present an efficient algorithm designed to find a polytope-basis cover with a reduced number of polytopes. This algorithm is outlined in Algorithm 4. The key distinction of this algorithm from the previous ones is that it does not derive a polytope cover from a trained network. Instead, it sequentially identifies a convex polytope by training several two-layer ReLU networks defined in (5). Consequently, this algorithm only requires access to the training dataset.

Before we demonstrate the algorithm, we provide modified network and loss functions first. Specifically, we consider the following two types of two-layer ReLU networks. Here, $\lambda_{bias} > 0$ is a hyperparameter that enhances the convergences.

$$\mathcal{T}_+(\mathbf{x}) := \lambda_{bias} + \sum_{k=1}^m v_k \sigma(\mathbf{w}_k^\top \mathbf{x} + b_k), \quad \forall v_k < 0 \quad (10)$$

$$\mathcal{T}_-(\mathbf{x}) := -\lambda_{bias} + \sum_{k=1}^m v_k \sigma(\mathbf{w}_k^\top \mathbf{x} + b_k), \quad \forall v_k > 0 \quad (11)$$

If λ_{bias} has large value, then \mathcal{T}_+ has large output value at initialization, and gradient descent optimization heavily affected from data with 0 labels. The similar situation happens for \mathcal{T}_- , and it helps to find a single polytope that contains whole class data. Practically, it is enough to use $\lambda_{bias} = 5$ to find such polytopes.

The modified loss function is defined by

$$L_{BCE, \lambda}(\Theta) := -\frac{1}{|\mathcal{D}_0|} \sum_{y_i=0} \lambda_0 \cdot \ell(\text{SIG} \circ \mathcal{T}(\mathbf{x}_i), y_i) - \frac{1}{|\mathcal{D}_1|} \sum_{y_i=1} \lambda_1 \cdot \ell(\text{SIG} \circ \mathcal{T}(\mathbf{x}_i), y_i) \quad (12)$$

where $\lambda = (\lambda_0, \lambda_1)$ is the hyperparameter proposed to reinforce to cover a whole data class with specific label. By using a large value of λ_1 , \mathcal{T} is trained to cover whole data points that have label $y_i = 1$. After successfully configured the first

polytope C_1 , we train the second network \mathcal{T}_2 to distinguish data points of another data class, $y_i = 0$, in the obtained polytope C_1 . Repeating this process alternatively, Algorithm 4 generally provides a polytope-basis cover with a small number of polytopes.

Now, we provide a detailed illustration of the algorithm’s functionality with the example displayed in Figure 9. Here we use $\lambda_{bias} = 5$, and $\lambda = (1, 10)$. First, the algorithm trains \mathcal{T}_1 on the entire dataset \mathcal{D} using (12). After fine-tuning through Algorithm 1, we obtain the first polytope C_1 displayed in Figure 9(b). Note that all orange data points (\mathcal{D}_1) are contained in C_1 . Next, the second network \mathcal{T}_2 is trained on $(\mathcal{D}_0 \cap C_1) \cup \mathcal{D}_1$ using (12) with $\lambda = (1, 10)$. \mathcal{T}_2 is aimed to cover all blue data points (\mathcal{D}_0) within C_1 . After training and fine-tuning, we obtain the second polytope C_2 displayed in Figure 9(c). Similarly, we can find the third polytope C_3 by training another network \mathcal{T}_3 on $\mathcal{D}_0 \cup (\mathcal{D}_1 \cap C_2)$, displayed in Figure 9(d) and so on. In the example in Figure 9, a total of four polytopes are obtained ((b) to (e)). Lastly, by Theorem 3.4, we can construct a three-layer ReLU network with architecture $2 \xrightarrow{\sigma} 23 \xrightarrow{\sigma} 4 \rightarrow 1$ that can completely classify this swiss roll dataset, based on the obtained polytope-basis cover. The decision boundary of this network is illustrated in Figure 9(f).

Algorithm 4 The efficient algorithm for finding a polytope-basis cover

Require: training dataset $\mathcal{D} = \mathcal{D}_0 \cup \mathcal{D}_1 = \{(x_i, y_i)\}_{i=1}^n$, hyperparameter $\lambda = (\lambda_0, \lambda_1)$, acc_{th} , λ_{bias} , $width$
 $\mathcal{C}_P \leftarrow \emptyset, \mathcal{C}_Q \leftarrow \emptyset$.
 $m \leftarrow width$
repeat
 repeat
 Initialize \mathcal{T}_+ defined in (10).
 Train \mathcal{T}_+ on the dataset $\mathcal{D} \cap \mathcal{C}_P^c$ by gradient descent, under the modified BCE loss (12).
 Fine tune the trained \mathcal{T}_+ by Algorithm 2.
 if $\mathcal{T}_+(\mathbf{x}) \neq \lambda_{bias}$ for some $\mathbf{x} \in \mathcal{D}_1 \cap \mathcal{C}_P^c$ **then**
 $m \leftarrow m + 1$
 end if
 until $\mathcal{T}_+(\mathbf{x}) = \lambda_{bias}$ for all $\mathbf{x} \in \mathcal{D}_1 \cap \mathcal{C}_P^c$
 $A \leftarrow \{\mathbf{x} \in \mathbb{R}^d \mid \mathcal{T}_+(\mathbf{x}) = \lambda_{bias}\}$ ▷ This is a polytope covering $\mathcal{D}_1 \cap \mathcal{C}_P^c$
 Add A in \mathcal{C}_P
 $m \leftarrow width$
 repeat
 Initialize \mathcal{T}_- defined in (11).
 Train \mathcal{T}_- on $\mathcal{D} \cap \mathcal{C}_Q^c$ by gradient descent, under the modified BCE loss (12).
 Fine tune the trained \mathcal{T}_- by Algorithm 2.
 if $\mathcal{T}_-(\mathbf{x}) \neq -\lambda_{bias}$ for some $\mathbf{x} \in \mathcal{D}_0 \cap \mathcal{C}_Q^c$ **then**
 $m \leftarrow m + 1$
 end if
 until $\mathcal{T}_-(\mathbf{x}) = -\lambda_{bias}$ for all $\mathbf{x} \in \mathcal{D}_0 \cap \mathcal{C}_Q^c$
 $A \leftarrow \{\mathbf{x} \in \mathbb{R}^d \mid \mathcal{T}_-(\mathbf{x}) = -\lambda_{bias}\}$ ▷ This is a polytope covering $\mathcal{D}_0 \cap \mathcal{C}_Q^c$
 Add A in \mathcal{C}_Q
 $\mathcal{C} \leftarrow \mathcal{C}_P \cup \mathcal{C}_Q$
 until \mathcal{C} becomes a polytope-basis cover of \mathcal{D} with accuracy greater than acc_{th}
Output: \mathcal{C}

The key advantage of this algorithm lies in its ability to generate a small number of convex polytopes, in contrast to other algorithms we proposed. As demonstrated in the figure above, it suggests $2 \xrightarrow{\sigma} 23 \xrightarrow{\sigma} 4 \rightarrow 1$ as a feasible architecture of the given swiss roll dataset, which appears to be close to optimal. However, due to its iterative nature of training multiple two-layer networks until achieving a complete polytope-basis cover, it typically requires a longer computation time. A detailed comparison with other algorithms is provided in the subsequent section.

C.4. Comparison of proposed algorithms

Finally, we compare the proposed algorithms: Algorithm 2, 3, and 4. First, we provide theoretical results for the proposed algorithms. The proof involves demonstrating how a polytope-basis cover can be explicitly constructed from the results of

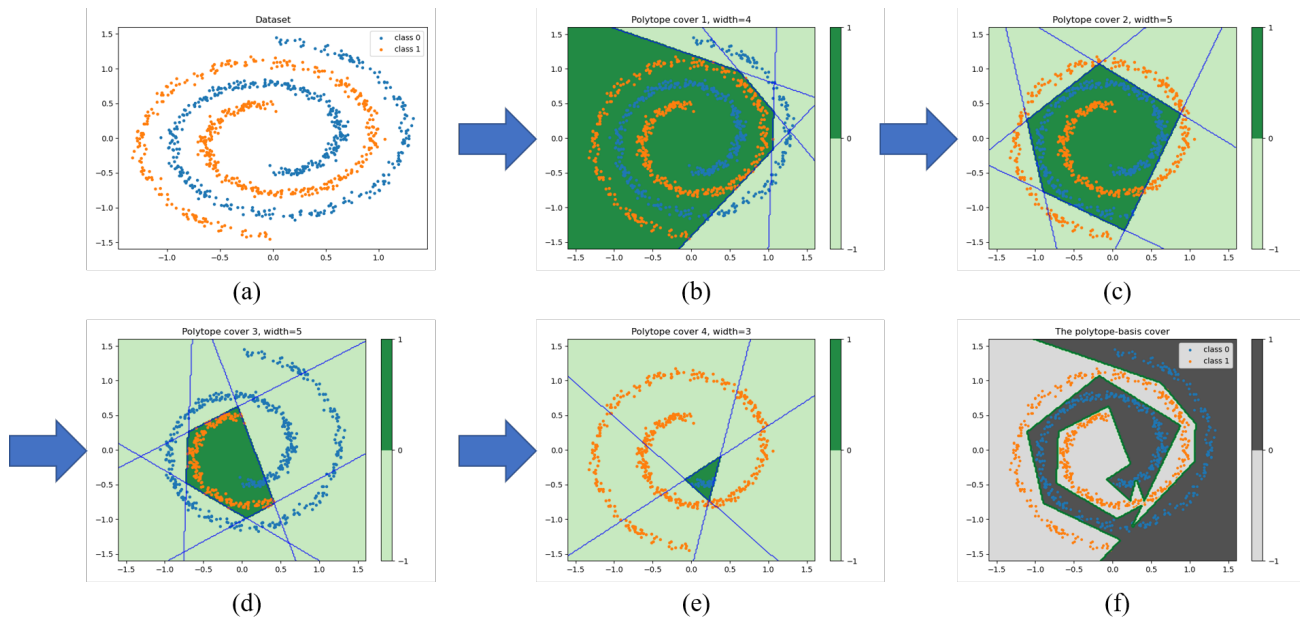


Figure 9. The result of Algorithm 4. For the given dataset (a), the algorithm determines the first polytope C_1 which contains whole orange class (b). In the next step, it obtains the second polytope C_2 which contains the whole blue class inside C_1 . Other polytopes are similarly obtained and described in (c) to (e). Totally, the algorithm produces a polytope-basis cover consisting of four polytopes. Theorem 3.4 shows that $2 \xrightarrow{\sigma} 17 \xrightarrow{\sigma} 4 \rightarrow 1$ is a feasible architecture on this dataset, and the decision boundary of the induced network induced is drawn in (f).

the algorithms. The detailed proof is available in Appendix E.6.

Proposition C.2. *The followings hold.*

1. Let \mathcal{T} be a network produced by repeating Algorithm 1 sufficiently many times. Then, it satisfies both (5) and (7).
2. Algorithm 2 must terminate in finite time, and it produces a polytope-basis cover that has the same accuracy with the compressed network \mathcal{N} .
3. Algorithm 3 must terminate in finite time, and it produces a polytope-basis cover that has the same accuracy with the given network \mathcal{N} .
4. If Algorithm 4 terminates in finite time, then it produces a polytope-basis cover of the training dataset \mathcal{D} .

	Algorithm 2	Algorithm 3	Algorithm 4
Input network	pretrained three-layer (6)	trained two-layer (5)	-
# of obtained polytopes	at most J	large	small
# of obtained faces	known	unknown	known
Theoretical guarantee for termination	yes	yes	no
Time consumption	normal	short	long
Accuracy of the polytope cover	unknown	same with the given network	100% (if it terminates)

Table 3. Comparison of proposed algorithms. These algorithms all generate a polytope-basis cover of the given training dataset, but each of them has its own advantage and disadvantage.

The comparison of proposed algorithms is summarized in Table C.4. Below, we discuss differences of algorithms for each item in Table C.4.

- Input networks.** Algorithm 2 operates on a pre-trained three-layer network outlined in (6). Algorithm 3 necessitates a fully-trained two-layer ReLU network specified by (1). However, Algorithm 4 does not necessitate any pre-existing networks as inputs and generates polytope covers through the training of several two-layer ReLU networks as per (5). It is crucial to note that all algorithms require a training dataset.
- The number of polytopes and faces.** As detailed in Appendix C.2, Algorithm 3 generally yields multiple polytopes to correctly cover all data points present in the dataset. Additionally, it does not calculate the precise number of faces for each polytope. In contrast, Algorithm 2 generates a polytope-basis cover by compressing the given three-layer network. Therefore, if the three-layer network (6) is the sum of J two-layer networks (\mathcal{T}_j), the algorithm is guaranteed to produce a polytope-basis cover consisting of no more than J polytopes. The compressing algorithm and Lemma F.4 provide the exact number of faces for each polytope. Thirdly, Algorithm 4 does not impose any specific lower or upper bounds on the number of polytopes. Similar to Algorithm 2, it also furnishes the exact number of faces for each polytope.

For instance, we recall the example on the swiss roll dataset: Figures 4, 8, and 9 illustrate that the algorithms yield 16, 68, and 4 polytopes, respectively. Note also that the last algorithms suggest a feasible architecture of the dataset by $2 \xrightarrow{\sigma} 17 \xrightarrow{\sigma} 4 \rightarrow 1$, while is sufficiently minimal.
- Theoretical guarantee.** Proposition C.2 guarantees that Algorithm 2 and 3 must terminate in finite time. However, we do not provide theoretically guarantee for Algorithm 4. Even though, in all our experiments, it always terminates in finite time and produces a complete polytope-basis cover for the given dataset.
- Time consumption.** Since Algorithm 3 does not require fine-tuning process, it consumes the shortest time among these algorithms. Algorithm 2 requires only fine-tuning process, so it takes a normal amount of time. However, Algorithm 4 tends to spend relatively more time due to its iterative process of training two-layer networks with fine-tuning until a complete polytope-basis cover is achieved. However, it's essential to note that even for real-world datasets like CIFAR10, the practical execution time is still quite reasonable, typically taking only a few minutes (less than 15 minutes).
- Accuracy of the obtained cover.** The polytope-basis cover generated by Algorithm 3 exhibits the same accuracy as the provided network, as confirmed by Proposition C.2. In the case of Algorithm 2, the fine-tuning process introduces the possibility of a different accuracy level compared to the original network. Consequently, the final accuracy cannot be determined beforehand. Regarding Algorithm 4, its accuracy is guaranteed to be 100% if it terminates within a finite time.

Below, we provide additional experimental results of the proposed algorithms on several synthetic datasets, showcasing visual differences among these algorithms. We consider three synthetic datasets: XOR, two circles, and two moons datasets, depicted in Figure 10. The results of algorithms are shown in Figure 11, 12, 13.

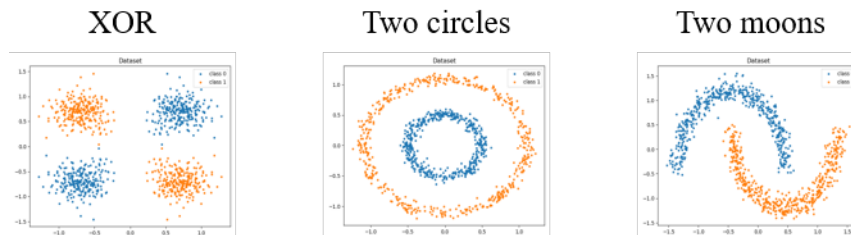


Figure 10. Synthetic datasets - XOR, two circles, and two moons.

It is easily checked that our proposed algorithms generate the polytope-basis cover of the given datasets. In each subfigure, the leftmost column represents the decision boundary and activation boundaries of the final network, and the other columns represent each polytope in the obtained polytope-basis cover. Note that the obtained polytope-basis covers exhibit the

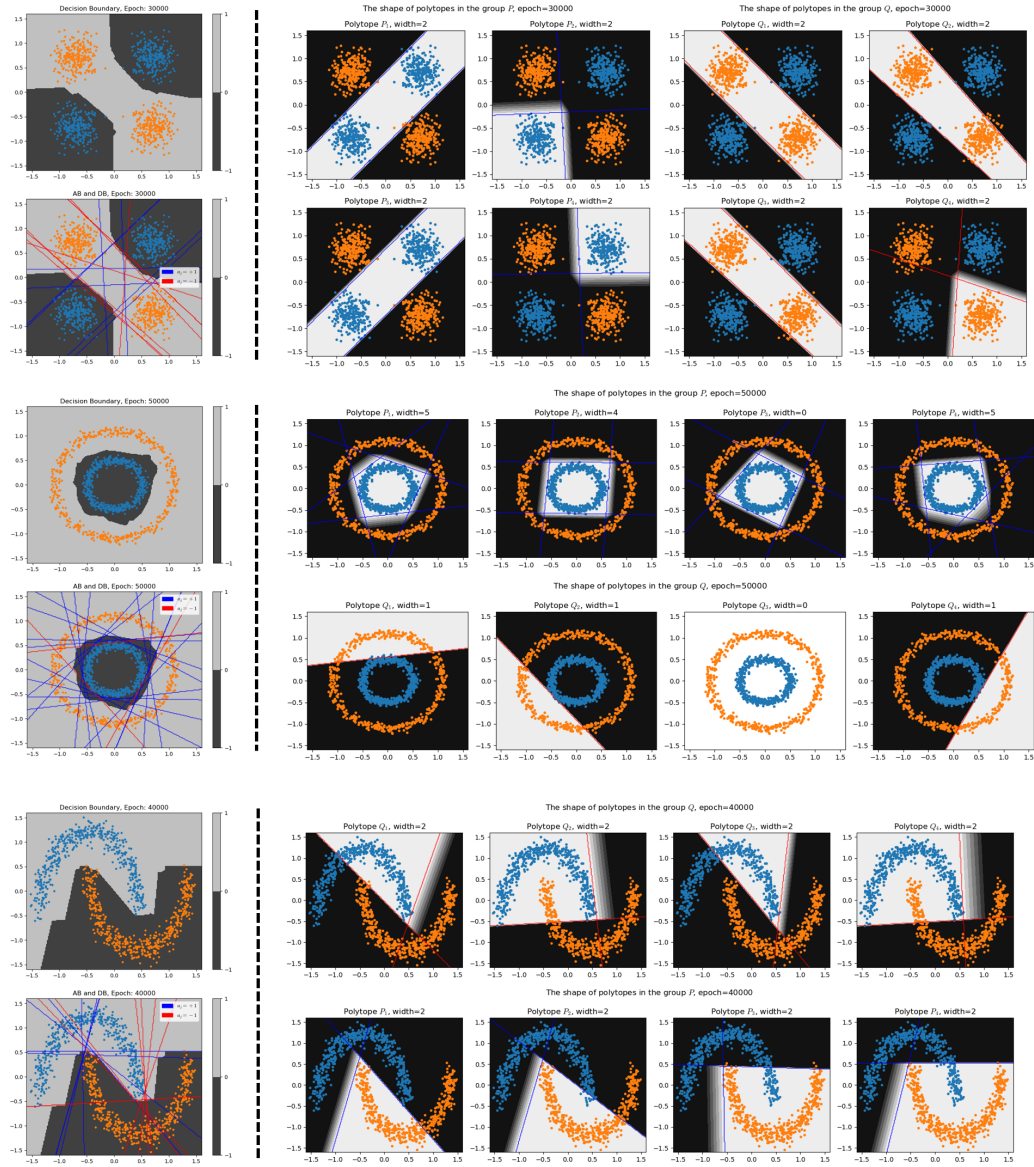


Figure 11. Visualization of Algorithm 2 on synthetic datasets. These polytope-basis covers are derived from trained three-layer ReLU networks.

Defining Neural Network Architecture through Polytope Structures of Dataset

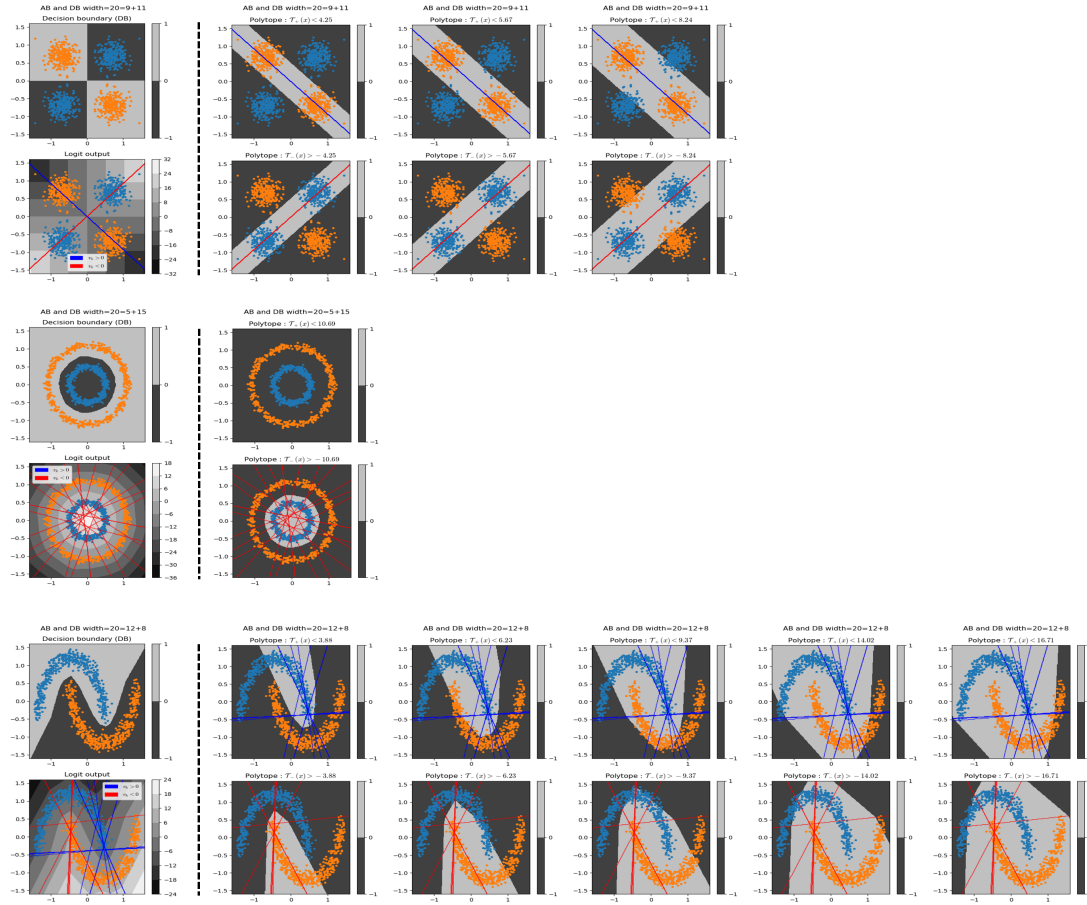


Figure 12. Visualization of Algorithm 3 on synthetic datasets. These polytope-basis covers are derived from trained three-layer ReLU networks.

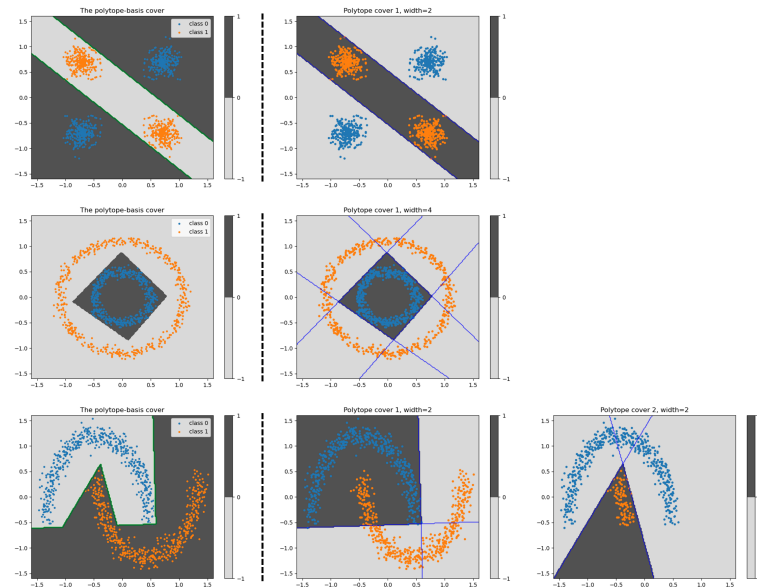


Figure 13. Visualization of Algorithm 4 on synthetic datasets. Empirically, this algorithm provides the smallest number of polytopes and their faces. The obtained polytope-basis covers can be applied to define the minimum architecture of neural networks.

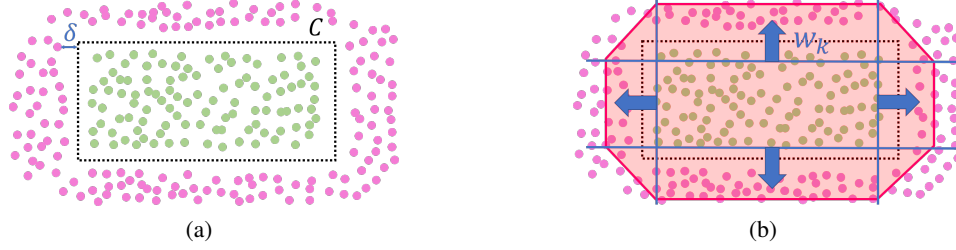


Figure 14. Assumptions for the dataset and the network initialization. (a) Dataset \mathcal{D} and a convex polytope C satisfy the Assumption D.2. (b) One example of network initialization satisfying Assumption D.2. The red line displays the decision boundary ($\{\mathbf{x} \in \mathbb{R}^d \mid \mathcal{N}(\mathbf{x}) = 0\}$).

geometric characteristics of these datasets, and provide the minimal architecture of neural networks that can completely classify the given dataset.

For example, Figure 13 demonstrates that ‘XOR’ and ‘two circles’ datasets have single polytope covers, and ‘two moons’ dataset can be covered by two polytopes. Therefore, the minimal network architecture of these dataset is given by

$$\begin{aligned} \text{XOR} : & \quad 2 \xrightarrow{\sigma} 2 \rightarrow 1 \\ \text{Two circles} : & \quad 2 \xrightarrow{\sigma} 4 \rightarrow 1 \\ \text{Two moons} : & \quad 2 \xrightarrow{\sigma} 4 \xrightarrow{\sigma} 2 \rightarrow 1. \end{aligned}$$

D. Convergence on the proposed networks

In this section, we investigate whether gradient descent can converge to the networks that we proposed in the previous section. Specifically, we focus on the two-layer ReLU networks which are the basic building blocks of the constructions. Let \mathcal{N} be a two-layer ReLU neural network defined in (1), where $\Theta := \{v_0\} \cup \{v_k, \mathbf{w}_k, b_k\}_{k \in [m]}$ denotes the set of parameters of \mathcal{N} . For the given dataset $\mathcal{D} = \{(\mathbf{x}_i, y_i)\}_{i=1}^n$, the mean squared error (MSE) loss and binary cross entropy (BCE) loss are defined by

$$L_{MSE}(\Theta) := \frac{1}{2n} \sum_{i=1}^n \left(\sigma \circ \mathcal{N}(\mathbf{x}_i) - y_i \right)^2, \quad (13)$$

$$L_{BCE}(\Theta) := -\frac{1}{n} \sum_{i=1}^n \ell(\text{SIG} \circ \mathcal{N}(\mathbf{x}_i), y_i) \quad (14)$$

where $\ell(\mathcal{N}, y) := \mathcal{N}y + (1 - \mathcal{N})(1 - y)$. Note that we introduce additional activation function σ, SIG to define both loss functions.

We now employ a notion of ‘polyhedrally separable’ dataset from learning theory (Astorino & Gaudioso, 2002; Manwani & Sastry, 2010), which is a special case of polytope-basis cover; when given dataset can be separated by only one convex polytope as depicted in Figure 14 (a).

Definition D.1. We call that the dataset \mathcal{D} is *polyhedrally separable* by C if there exists a convex polytope C such that $\mathbf{x}_i \in C$ if and only if $y_i = 1$ for all $i \in [n]$.

We further introduce two notations. First, for a convex polytope C composed of m faces, we denote its k -th face by ∂C_k . Similarly, $\partial^2 C_k$ denotes the boundary of ∂C_k , which refers to the ‘edge’ part of C . Second, for a set $A \subset \mathbb{R}^d$, $\#(A) := |\{\mathbf{x}_i \in \mathcal{D} \mid \mathbf{x}_i \in A\}|$ denotes the number of data points $\mathbf{x}_i \in \mathcal{D}$ in A . We further need the following assumption, on the dataset \mathcal{D} and network initialization.

Assumption D.2 (Dataset and initialization assumption). *Suppose the dataset \mathcal{D} is polyhedrally separable by a convex polytope C , which consists of m faces and strictly contains the origin point. Let $\delta > 0$ be the minimum distance between \mathbf{x}_i and ∂C , and l_k be the distance between ∂C_k and the origin point. Then, there exist constants $\rho, R > 0$ such that for any*

$k \in [m]$ and $\delta < r < R$,

$$\#(\mathcal{B}_{2r}(\partial^2 C_k)) \leq \rho \#(\mathcal{B}_{r-\delta}(\partial C_k)). \quad (15)$$

Furthermore, the parameters $\{(\mathbf{w}_k, b_k, v_k)\}_{k \in [m]}$ of a two-layer ReLU network \mathcal{N} defined in (1) are initialized such that \mathbf{w}_k are normal to ∂C_k with outward direction, and satisfying

$$l_k - R < l_k + \frac{v_0}{v_k \|\mathbf{w}_k\|} < -\frac{b_k}{\|\mathbf{w}_k\|} < l_k. \quad (16)$$

The dataset assumption (15) suggests that the data points in the set $\mathcal{B}_r(\partial C)$ for small r are predominantly located in close proximity to the faces of the polytope C , rather than its corners (Figure 14(a)). The network initialization assumption implies that every neuron (\mathbf{w}_k, b_k) of \mathcal{N} is initialized near ∂C_k as described in Figure 14(b). With these assumptions, we can provide a discrete path that strictly decrease the loss value to zero.

Theorem D.3. *Suppose the dataset \mathcal{D} and the two-layer network (1) satisfy Assumption D.2. Then,*

1. *for the MSE loss defined in (13), suppose v_0 is initialized such that*

$$\frac{\rho}{1-\rho} \frac{4m\rho R^2}{\delta^2} < v_0 < 1. \quad (17)$$

Then, with step size $\eta < \min\left\{\frac{2}{\delta}, \frac{2}{mR}, \frac{4\rho m}{(1-\rho)R}\right\}$, there exists a discrete path that the loss value (13) strictly decreases to zero.

2. *For the BCE loss defined in (14), suppose v_0 is initialized such that*

$$0 < v_0 < \log\left(\frac{(1-\rho)\delta}{4\rho R} - 1\right). \quad (18)$$

Then, with step size $\eta < \min\left\{1, \frac{4\rho R}{(1-\rho)\delta^2}\right\}$, there exists a discrete path that the loss value (14) strictly decreases to zero.

The proof of this theorem can be found in Appendix E.7. Theorem D.3 asserts that the loss landscape has no local minima in this initialization region. In other words, this theorem implies that stochastic (noisy) gradient descent is believed to converge to the global minimum, which has zero error on the training dataset \mathcal{D} . Therefore, the initialization conditions described in Assumption D.2, (17), and (18) can be understood as sufficient conditions such that gradient method converges to the global minimum.

E. Proofs

E.1. Proof of Proposition 3.1.

The proof of Proposition 3.1 is divided into two parts. Firstly, we prove the upper bound by constructing the desired neural network. Secondly, we show the lower bound of widths.

E.1.1. THE UPPER BOUND IN PROPOSITION 3.1.

For the given convex polytope \mathcal{X} , let h_1, \dots, h_m be its m hyperplanes enclosing C . Let \mathbf{w}_k be the unit normal vector of the k -th hyperplane h_k oriented inside C , as illustrated in Figure 2(a). Then the equation of the k -th hyperplane h_k is given by $h_k : \{\mathbf{x} \mid \mathbf{w}_k^\top \mathbf{x} + b_k = 0\}$ for some $b_k \in \mathbb{R}$. Let A_k be the intersection of the hyperplane h_k and C , which is a face of the polytope C . Let \mathbf{x} be any point strictly contained in C . Since \mathbf{w}_k is a unit normal vector, $\mathbf{w}_k^\top \mathbf{x} + b_k$ refers the distance between the hyperplane h_k and the point \mathbf{x} . Therefore, the d -dimensional Lebesgue measure of C is computed by

$$\mu_d(C) = \frac{1}{d} \sum_{k=1}^m (\mathbf{w}_k^\top \mathbf{x} + b_k) \cdot \mu_{d-1}(A_k) \quad (19)$$

where μ_{d-1} and μ_d refer the $(d-1)$ and d -dimensional Lebesgue measures, respectively. Note that (19) comes from the volume formula of a convex polytope, which states that the volume is the sum of volume of m pyramids. Then LHS of (19) is constant, which does not depend on the choice of $\mathbf{x} \in \mathbb{R}^d$. Now, we define a two-layer ReLU network \mathcal{T} with the architecture $d \xrightarrow{\sigma} m \rightarrow 1$ by

$$\mathcal{T}(\mathbf{x}) := 1 + M \left(\mu_d(C) - \sum_{k=1}^m \frac{1}{d} \mu_{d-1}(A_k) \cdot \sigma(\mathbf{w}_k^\top \mathbf{x} + b_k) \right) \quad (20)$$

where $M > 0$ is a constant would be determined later. Note that we have $\mathcal{T}(\mathbf{x}) = 1$ for $\mathbf{x} \in C$ from the construction. However, considering the negative sign, it is worth noting that the equation (19) also holds for $\mathbf{x} \notin C$. In particular, for $\mathbf{x} \notin C$, (20) deduces

$$\begin{aligned} \mathcal{T}(\mathbf{x}) &= 1 + M \left(\mu_d(C) - \sum_{k=1}^m \frac{1}{d} \mu_{d-1}(A_k) \cdot \sigma(\mathbf{w}_k^\top \mathbf{x} + b_k) \right) \\ &= 1 + M \left(\mu_d(C) - \sum_{k=1}^m \frac{1}{d} \mu_{d-1}(A_k) \cdot (\mathbf{w}_k^\top \mathbf{x} + b_k) + \sum_{\{k : \mathbf{w}_k^\top \mathbf{x} + b_k < 0\}} \frac{1}{d} \mu_{d-1}(A_k) \cdot (\mathbf{w}_k^\top \mathbf{x} + b_k) \right) \\ &= 1 + M \sum_{\{k : \mathbf{w}_k^\top \mathbf{x} + b_k < 0\}} \frac{1}{d} \mu_{d-1}(A_k) \cdot (\mathbf{w}_k^\top \mathbf{x} + b_k) \\ &< 1. \end{aligned}$$

Therefore, we conclude that

$$\begin{aligned} \mathcal{T}(\mathbf{x}) &= 1 && \text{if } \mathbf{x} \in C, \\ \mathcal{T}(\mathbf{x}) &< 1 && \text{otherwise.} \end{aligned}$$

Lastly, we determine the constant M in \mathcal{T} to satisfy the remained property. For the given $\varepsilon > 0$, consider the closure of complement of the $\frac{\varepsilon}{2}$ -neighborhood of C ; $D := \overline{(\mathcal{B}_{\varepsilon/2}(C))^c}$. Then the previous result shows that

$$\frac{1}{M}(\mathcal{T}(\mathbf{x}) - 1) = \mu_d(C) - \sum_{k=1}^m \frac{1}{d} \mu_{d-1}(A_k) \cdot \sigma(\mathbf{w}_k^\top \mathbf{x} + b_k) \quad (21)$$

is bounded above by 0. Furthermore, (21) is continuous piecewise linear, and has the maximum 0 if and only if $\mathbf{x} \in C$. Since D is closed and (21) is strictly bounded above by 0 on D , (21) has the finite maximum $M' < 0$ on D .

$$\frac{1}{M}(\mathcal{T}(\mathbf{x}) - 1) \leq M' < 0 \quad \text{for } \mathbf{x} \in D.$$

Now, choose M to satisfy $M > -\frac{1}{M'}$. Then if $\mathbf{x} \notin B_\varepsilon(C)$, we have $\mathbf{x} \in D$, thus

$$\begin{aligned} \mathcal{T}(\mathbf{x}) &= 1 + M \left(\mu_d(C) - \sum_{k=1}^m \frac{1}{d} \mu_{d-1}(A_k) \cdot \sigma(\mathbf{w}_k^\top \mathbf{x} + b_k) \right) \\ &\leq 1 + M \cdot M' \\ &< 0. \end{aligned}$$

Therefore, we have constructed a two-layer ReLU network \mathcal{T} with the structure $d \xrightarrow{\sigma} m \rightarrow 1$ such that

$$\begin{aligned} \mathcal{T}(\mathbf{x}) &= 1 && \text{if } \mathbf{x} \in C, \\ \mathcal{T}(\mathbf{x}) &< 1 && \text{if } \mathbf{x} \in C^c, \\ \mathcal{T}(\mathbf{x}) &< 0 && \text{if } \mathbf{x} \notin B_\varepsilon(C). \end{aligned}$$

This completes the proof on the upper bound. Lastly, the minimality of depth comes from the fact that a linear function cannot be a feasible architecture on C . \square

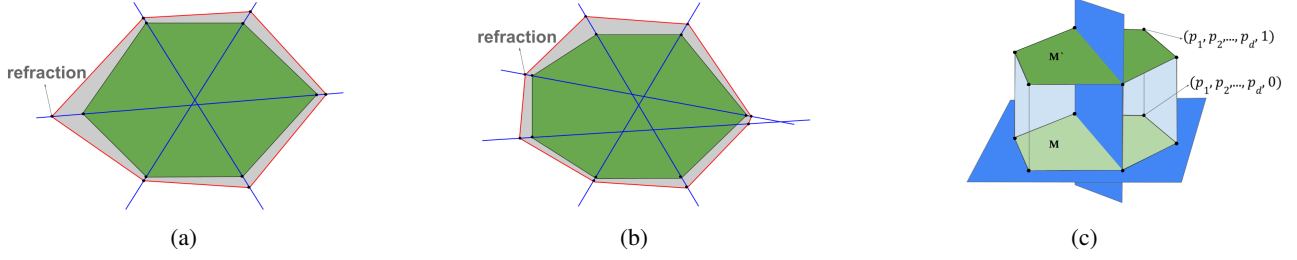


Figure 15. Proof of Proposition 3.1. (a) Given a hexagon which is approximated by 3 hyperplanes given with blue lines and 1 polytope in the second layer given with red hexagon. (b) Given a heptagon which is approximated by 4 hyperplanes given with blue lines and 1 polytope in the second layer given with red heptagon. (c) Hexagon has been extended to the 3-dimensional polytope by incrementing the number of faces by 2 with some potential first layer neurons (blue hyperplanes).

E.1.2. THE LOWER BOUND IN PROPOSITION 3.1.

Before proving the lower bound, we introduce a definition on *refraction points*. Let $\mathcal{N}(\mathbf{x}) := \sigma(v_0 + \sum_{i=1}^{d_1} v_i \sigma(\mathbf{w}_i^\top \mathbf{x} + b_i))$ be a two-layer network with architecture $d \xrightarrow{\sigma} d_1 \xrightarrow{\sigma} 1$. Then the set of refraction point is defined by

$$\{\mathbf{x} \in \mathbb{R}^d \mid \mathcal{N}(\mathbf{x}) = 0 \text{ and } \mathbf{w}_i^\top \mathbf{x} + b_i = 0 \text{ for some } i \in [l].\}$$

In other words, it is the point where the boundary of a linear partition is ‘refracted’.

Lower bound for $d = 2$ using only refraction points for $k = 1$. Assume that we are given a convex m -gon to approximate. Considering the fact that we can approximate the neural network arbitrarily close, we can see that the approximated second layer, i.e. neural network should have at least m refraction points in order to get the shape of polygon. However, if we look from the perspective of first layer neurons, each line has at most 2 intersection with m -gon and it implies that each first layer neuron (or line) can contribute at most 2 meaningful refraction points for the next layer. If we combine above two results, we can obtain that there should be at least $\lceil \frac{m}{2} \rceil$ number of neurons in the first layer, in other words $d_1 \geq \lceil \frac{m}{2} \rceil$. For example, Figure 15(a) and (b) demonstrates the refraction points along with potential first layer hyperplanes (blue lines) and converged polytope at the second layer (red polygon) for hexagon and heptagon, respectively.

Proof of the optimality when $d = 2$ for $k = 1$. First of all, we should note that on \mathbb{R}^2 , any two convex m -gon’s given on the general position (i.e. assume sides are non-parallel mutually) can be approximated by the same neural network (same d_1 value) considering the fact that we can find an approximator for each given error value ϵ . It implies that we can take optimal possible number of neurons in the first layer, which we will denote by $f(m)$ for any given convex m -gon. Let’s prove that $f(m) = \lceil \frac{m}{2} \rceil$ for $m \geq 5$ along with $f(3) = f(4) = 3$. The cases $m = 3, 4$ should be handled separately, because we trivially need at least $d + 1 = 3$ hyperplanes for any shape (Lemma F.1), so we start the base case from $m \geq 5$ for $d = 2$.

According to the Lemma F.1, it is apparent that for any m , the inequality $f(m) \geq 3$ should hold trivially. But if we consider the Figure 15(a), we can observe that one can approximate any hexagon with 3 hyperplanes. Apparently, for any pentagon, quadrilateral, and triangle, we can find a corresponding hexagon to include it as a subfigure and rest of the additional vertices of this hexagon can be shrunked to be almost non-exist. It implies that, same number of hyperplanes approximating hexagon can also approximate the polygons with $m \leq 5$. This final result yields that $f(m) \leq 3$ for $m \leq 6$. If we combine these two findings we can get a nice optimality at the fundamental cases, in other words $f(m) = 3$ for $m \in \{3, 4, 5, 6\}$.

Now, assume the contrary that $f(m) \leq \lceil \frac{m}{2} \rceil - 1$, then it is apparent that there is at least one neuron which contributes to the refraction point of at least 2 vertices (i.e. exactly 2 vertices considering previous discussion). Now, if we remove the chosen neuron and the associated 2 vertices and their edges, then the resulting $(m - 2)$ -gon will be approximated by $f(m) - 1$ number of neurons, which implies that $f(m) - 1 \geq f(m - 2)$. Proceeding with the same argument, we can arrive at the conclusion that $f(5)$ or $f(6) \leq 2$; however, we have already proven that $f(5)$ and $f(6)$ are indeed 3. So, the contradiction at the base case yields the result that $f(m) \geq \lceil \frac{m}{2} \rceil$.

For the base cases $m = 5, 6$, we have already demonstrated that $f(5) = f(6) = 3$. Now, take any m -gon which has been approximated well with $f(m) = \lceil \frac{m}{2} \rceil$ neurons. Let’s add two new vertices to form a new convex polygon with $(m + 2)$ vertices, where the newly added vertices are not adjacent. Then if we add one new neuron which is the line passing through those two points, we can observe that if given $f(m)$ number of neurons approximate m -gon, then $f(m) + 1$ can approximate

$(m+2)$ -gon by triggering 2 new refraction points. This inductive argument $f(m+2) \leq f(m) + 1$ yields the result that if we start from $f(5) = f(6) = 3$, we can reach a conclusion that $f(m) \leq \lceil \frac{m}{2} \rceil$. However, we have already shown $f(m) \geq \lceil \frac{m}{2} \rceil$ in the proof above. Therefore, the result follows immediately that the optimal number of neurons in the first hidden layer to approximate any convex polygon with m vertices is $\lceil \frac{m}{2} \rceil$ for $m \geq 5$ and $f(3) = f(4) = 3$. \square

Lower bound for arbitrary dimension d for $k = 1$. Now we will apply simple induction on the dimensionality to prove the general case for lower bound on the number of first hidden layer neurons. Essentially, we will construct a d -dimensional object for $d \geq 2$ such that, one needs at least $d_1 \geq \lceil \frac{m}{2} \rceil + (d-2)$ number of neurons (hyperplanes) to approximate the convex polytope with l faces. We will proceed with an inductive argument, we have already provided a proof for the base case of $d = 2$ that $d_1 \geq \lceil \frac{m}{2} \rceil$.

Inductive step. Suppose that we have a d -dimensional convex polytope M with v number of vertices and m number of faces such that the following inequality should hold: $d_1 \geq \lceil \frac{m}{2} \rceil + (d-2)$. Let's consider the object on $(d+1)$ -dimensional space by adding new entry at the end of each coordinate, i.e. any point (p_1, p_2, \dots, p_d) on the object will be replaced by the point $(p_1, p_2, \dots, p_d, 0)$. Then consider the new shape M' formed by considering the extension of convex polytope M on $(d+1)$ -dimensional space with all the points from $\{p = (p_1, p_2, \dots, p_d, x) \mid \forall x = [0, 1] \text{ and } (p_1, p_2, \dots, p_d) \in M\}$. Then M' will lie on $(d+1)$ -dimensional space and it will have $2v$ vertices and $(m+2)$ number of faces, of which m will be determined by the extensions of faces of polytope M along with two faces from M and its duplicate M' . We can also observe the inductive incrementing idea through the Figure 15(c), in which polytope M at $d = 2$ with 6 faces has been extended to the 3-dimensional polytope with $6 + 2 = 8$ faces.

If we take a closer look at this construction, we can observe that if we take the intersection of each hyperplane from d_1 neurons designed for the approximation of M' and polytope M , then those intersections will be hyperplane for d -dimensional polytope M . It implies that in order to approximate m faces of new polytope, the intersections themselves should approximate the m faces of M . Furthermore, other than those m faces formed by faces of previous polytope M , we should also consider the other 2 faces, namely M and its duplicate M' . Those two hyperplanes will require additional 2 neurons to trigger new refraction points for their approximation. Therefore, there should be at least $d_1 \geq \lceil \frac{m}{2} \rceil + (d-2) + 2$ number of neurons, in which right-hand-side can be equivalently written as $\lceil \frac{m}{2} \rceil + d = \lceil \frac{m+2}{2} \rceil + (d+1-2)$. So, we were able to prove that to have a neural network of the form $d \xrightarrow{\sigma} d_1 \xrightarrow{\sigma} 1$ to approximate the convex polytopes with m faces arbitrarily close, then universally the value of d_1 should at least $\lceil \frac{m}{2} \rceil + (d-2)$.

The result can be also stated that for all $m \geq 2d+1$ one can find a d -dimensional convex polytope with l faces such that the minimum required number neurons in the first hidden layer is at least $\lceil \frac{m}{2} \rceil + (d-2)$. For $m = 2d-1$ and $l = 2d$, the lower bound becomes $d_1 \geq 2d-1$ as we have already described that $f(3) = f(4) = 3$. The lower bound on m comes from the fact that the construction has an inductive fashion to create a new object from previous one by adding 2 new faces in each step. For the rest of the values of number of faces m , i.e. $m < 2d-1$, one can consider the trivial bound of $d+1$. More strongly, in case of 2-dimensional space, the statement has been proven for all convex polygons that optimal value is indeed $d_1 = \lceil \frac{m}{2} \rceil$.

Generalization to arbitrary dimension d and depth k . In the context of manifold representations shaped as convex polytopes with varying depths, we employ an inductive approach to establish lower bounds. Leveraging prior findings on two-layer neural networks, we derive insights applicable to arbitrary dimensions d . For any given hyperplane in this setting, a maximum of two distinct refraction points can be identified, a premise that underpins our assumption that each second-layer neuron constitutes a polytope comprised of faces, with no more than twice the number of hyperplanes as the first layer. This result has also been used in the proof of Theorem 3.6 and we can observe the trend from the Figure 17(c).

We transform the general case by considering the facets of second or higher-layer neurons as first-layer neurons (hyperplanes), which represent potential refraction points. This transformation allows us to reduce the problem to a two-layer network by decreasing the depth while augmenting the number of hyperplanes in the first layer. More precisely, for a given feasible architecture of the form $d \xrightarrow{\sigma} d_1 \xrightarrow{\sigma} d_2 \xrightarrow{\sigma} \dots \xrightarrow{\sigma} d_k \rightarrow 1$, each of d_2 number of second layer neurons can contribute at most $2d_1$ hyperplanes along with the d_1 hyperplanes in the first layer, which implies total of $d_1 + 2d_1 d_2 = d_1(2d_2 + 1)$ hyperplanes. In other words, we can transform the above network to another network $d \xrightarrow{\sigma} d_1(2d_2 + 1) \xrightarrow{\sigma} d_3 \xrightarrow{\sigma} \dots \xrightarrow{\sigma} d_k \rightarrow 1$ by reducing the depth by 1. By applying the similar process as above, we assert that initial architecture can be effectively transformed into a more robust architecture, $d \xrightarrow{\sigma} d_1(2d_2 + 1)(2d_3 + 1) \dots (2d_k + 1) \xrightarrow{\sigma} 1$.

Consequently, we can generalize lower bounds for convex polytope representations of varying depths, drawing on the

insights gained from our two-layer formulation. The ultimate result yields a powerful lower bound as

$$d_1 \cdot \prod_{j=2}^k (2d_j + 1) \geq \begin{cases} \lceil \frac{m}{2} \rceil + (d-2), & \text{if } m \geq 2d+1, \\ 2d-1, & \text{if } m = 2d-1, 2d, \\ d+1, & \text{if } m < 2d-1. \end{cases}$$

Moreover, the above result is particularly optimal for the case of convex polygons in two dimensions, where $d = 2$ and $k = 1$, as previously discussed. \square

E.2. Proof of Theorem 3.4

By Proposition 3.1, for each set $A \in \mathcal{C} = \{P_1, \dots, P_{n_P}, Q_1, \dots, Q_{n_Q}\}$, we can construct a two-layer ReLU network \mathcal{T}_A with the architecture $d \xrightarrow{\sigma} m_A \xrightarrow{\sigma} 1$ such that $\mathcal{T}_A(\mathbf{x}) = 1$ for $\mathbf{x} \in A$ and $\mathcal{T}_A(\mathbf{x}) = 0$ for $\mathbf{x} \notin B_\varepsilon(A)$, where m_A denotes the number of faces of A . Let $a_i := \mathcal{T}_{P_i}$ for $i \in [n_P]$ and $b_j := \mathcal{T}_{Q_j}$ for $j \in [n_Q]$. Define the output layer by

$$\mathcal{N}(\mathbf{x}) = \sum_{i=1}^{n_P} a_i - \sum_{j=1}^{n_Q} b_j - \frac{1}{2}.$$

Then, we obtain the desired network \mathcal{N} which has the architecture $d \xrightarrow{\sigma} m \xrightarrow{\sigma} (n_P + n_Q) \rightarrow 1$. \square

E.3. Proof of Theorem 3.5

Let X_1, X_2, \dots, X_k be the k facets of \mathcal{X} . For each facet X_i , we can construct a two-layer ReLU network \mathcal{T}_i such that $\mathcal{T}_i(\mathbf{x}) = 1$ for $\mathbf{x} \in X_i$ and $\mathcal{T}_i(\mathbf{x}) < 0$ for $\mathbf{x} \notin B_\varepsilon(X_i)$ by Lemma F.1. Then Theorem 3.4 gives a neural network \mathcal{N} with the architecture $d \xrightarrow{\sigma} d_1 \xrightarrow{\sigma} k \rightarrow$ with $d_1 = k(d+1)$, therefore, it is a feasible architecture on \mathcal{X} . The remaining goal is to reduce the width of the first layer d_1 .

From the construction, we recall that $d_1 \leq k(d+1)$ comes from the fact where each simplex X_i is covered by a d -simplex which has $(d+1)$ hyperplanes. Now consider two j -simplices in \mathbb{R}^d . If $2j+2 \leq d+1$, then we can connect all points of the two j -simplices in \mathbb{R}^d , and it becomes a $(2j+2)$ -simplex Δ^{2j+2} . Now construct a d -simplex Δ^{d+1} by choosing $(d+1) - (2j+2)$ points in $B_\varepsilon(\Delta^{2j+2})$, whose base is this $(2j+2)$ -simplex. Then, by adding two distinguishing hyperplanes at last, we totally consume $(d+3)$ hyperplanes to separate two j -simplices.

Now we apply this argument to each pair of two simplices. The above argument shows that two j -simplices separately covered by $2(d+1)$ hyperplanes can be re-covered by $(d+3)$ hyperplanes if $j \leq \lfloor \frac{d-1}{2} \rfloor$, which reduces $(d-1)$ number of hyperplanes. In other words, we can save $(d-1)$ hyperplanes for each pair of two j -simplices whenever $j \leq \lfloor \frac{d-1}{2} \rfloor$. This provides one improved upper bound of d_1 :

$$d_1 \leq k(d+1) - (d-1) \left\lfloor \frac{1}{2} \sum_{j=0}^{\lfloor \frac{d-1}{2} \rfloor} k_j \right\rfloor. \quad (22)$$

Now, we consider another pairing. For $0 \leq j \leq J$, \mathcal{X} has k_j j -simplex facets. Since each j -simplex has $(j+1)$ points, in particular, a d -simplex consists of $(d+1)$ -points. Therefore, all points in $\lfloor \frac{d+1}{j+1} \rfloor$ many j -simplices can be contained in one d -simplex. In this case, these j -simplices can be covered by adding $\lfloor \frac{d+1}{j+1} \rfloor$ hyperplanes more. Thus if we have k_j many j -simplices, then the required number of hyperplanes to separately encapsulate the j -simplices is less than or equal to

$$\begin{aligned} & \# \text{ (the number of } d\text{-simplices)} \cdot \# \text{ (the required number of hyperplanes in each } d\text{-simplex)} \\ &= \left(\left\lfloor \frac{k_j}{\lfloor \frac{d+1}{j+1} \rfloor} \right\rfloor + 1 \right) \cdot \left(d+1 + \left\lfloor \frac{d+1}{j+1} \right\rfloor \right) \end{aligned}$$

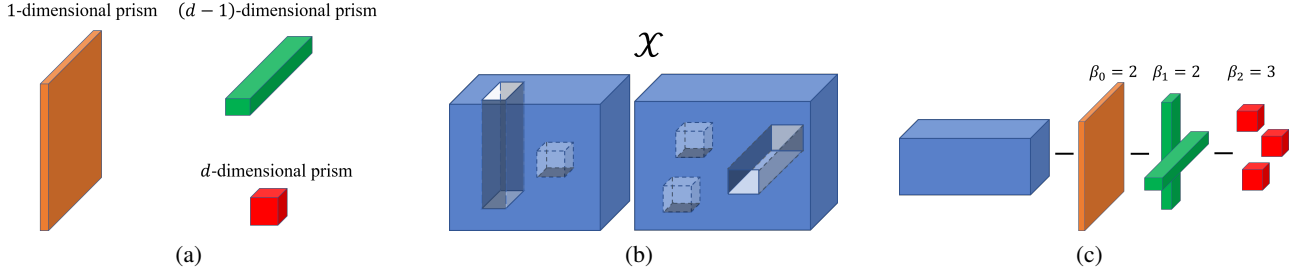


Figure 16. The Proof of upper bounds in Theorem 3.6. (a) Some examples of prismatic polytopes. (b) \mathcal{X} is a topological space satisfying the assumption in Theorem 3.6. (c) The removed prismatic polytopes from \mathcal{X} are displayed. Theorem 3.6 demonstrates that $3 \xrightarrow{\sigma} 34 \xrightarrow{\sigma} 7 \rightarrow 1$ is a feasible architecture on \mathcal{X} .

$$\begin{aligned}
 &\leq \left(k_j \frac{j+1}{d-j} + 1 \right) \cdot \left(d+1 + \frac{d+1}{j+1} \right) \\
 &< (d+1) \left(\frac{j+2}{j+1} \right) \left(k_j \frac{j+1}{d-j} + 1 \right) \\
 &= (d+1) \left(k_j \frac{j+2}{d-j} + \frac{j+2}{j+1} \right)
 \end{aligned} \tag{23}$$

where the inequality is reduced from the property of the floor function: $a-1 < \lfloor a \rfloor \leq a < \lfloor a \rfloor + 1$ for any $a \in \mathbb{R}$. Then another upper bound of d_1 is obtained by applying (23) for all $j \leq J$. However, further note that (23) is greater than the known upper bound $k(d+1)$ if $J > \frac{d}{2}$; the sharing of covering simplex is impossible in this case. Therefore, the upper bound of d_1 is given by

$$\begin{aligned}
 d_1 &\leq (d+1) \sum_{j \leq \frac{d}{2}} \left(k_j \frac{j+2}{d-j} + \frac{j+2}{j+1} \right) + (d+1) \sum_{j > \frac{d}{2}} k_j \\
 &= (d+1) \left[\sum_{j \leq \frac{d}{2}} \left(k_j \frac{j+2}{d-j} + \frac{j+2}{j+1} \right) + \sum_{j > \frac{d}{2}} k_j \right]
 \end{aligned} \tag{24}$$

To sum up, from (22) and (24), we get the desired result

$$d_1 \leq \min \left\{ k(d+1) - (d-1) \left[\frac{1}{2} \sum_{j=0}^{\lfloor \frac{d-1}{2} \rfloor} k_j \right], (d+1) \left[\sum_{j \leq \frac{d}{2}} \left(k_j \frac{j+2}{d-j} + \frac{j+2}{j+1} \right) + \sum_{j > \frac{d}{2}} k_j \right] \right\}.$$

□

E.4. Proof of Theorem 3.6.

The proof consists of two parts: we prove the upper bound first, and second, we show the lower bound.

E.4.1. THE UPPER BOUND IN THEOREM 3.6.

We establish a terminology about the shape of prismatic polytopes. A prism in \mathbb{R}^3 consists of a ‘base’ and ‘height’ dimensions, and we generalize it to high dimensional prisms. We define a **k -dimensional prismatic polytope** in \mathbb{R}^d as a topological space homeomorphic to $K \times \mathbb{R}^{d-k}$, where \times denotes the Cartesian product and $K \subset \mathbb{R}^k$ is a compact set which is the ‘base’ of the prism. Roughly speaking, an 1-dimensional prismatic polytope is a thick ‘hyperplane’ in \mathbb{R}^d , $(d-1)$ -dimensional prismatic polytope is a long ‘rod,’ and a d -dimensional prismatic polytope is just a convex polytope (Figure 16(a)). Then, for $k = 1, 2, \dots, d$, removing a k -dimensional prism from \mathcal{X} generates a k -dimensional hole, which increases the $(k-1)$ -th Betti number β_{k-1} .

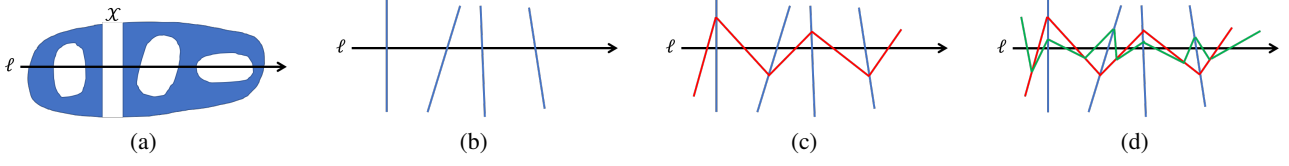


Figure 17. Proof of lower bounds in Theorem 3.6. (a) Consider a topological space \mathcal{X} whose holes intersect with a straight line ℓ . (b) d_1 neurons in the first hidden layer of \mathcal{N} (blue color) have at most d_1 intersection points with ℓ . (c) A neuron in the second layer (red color) has at most $(d_1 + 1)$ intersection points with ℓ . (d) Similarly, a neuron in the third layer (green color) has at most $d_2(d_1 + 1) + 1$ intersection points with ℓ .

Now, we prove the theorem. Since \mathcal{X} can be described as the union and difference of $\sum_{k=0}^{d-1} \beta_k$ convex polytopes, applying Theorem 3.4 provides

$$d \xrightarrow{\sigma} d_1 \xrightarrow{\sigma} \left(\sum_{k=0}^{d-1} \beta_k \right) \rightarrow 1$$

is an upper bound of a feasible architecture, where

$$\begin{aligned} d_1 &\leq m + m \cdot \left(\sum_{k=0}^{d-1} \beta_k - 1 \right) \\ &= m \left(\sum_{k=0}^{d-1} \beta_k \right). \end{aligned}$$

For $1 \leq k < d$, β_k means the number of k -dimensional holes in \mathcal{X} , which was made by punching out a k -dimensional prismatic polytope. Since k -dimensional prisms have $2k$ faces that penetrate \mathcal{X} , we can reduce $2(d - k - 1)$ number of hyperplanes that cover the hole. When $k = 0$, it is easy to check that $2(\beta_0 - 1)$ hyperplanes are required to separate β_0 connected components. For example, Figure 16(c) shows this process for a topological space given in Figure 16(b). Then, the required total number of hyperplanes is bounded by

$$d_1 \leq m + 2(\beta_0 - 1) + \sum_{k=1}^{d-1} (m - 2(d - k - 1)) \beta_k$$

which completes the proof. \square

E.4.2. THE LOWER BOUND IN THEOREM 3.6.

Suppose the given architecture $d \xrightarrow{\sigma} d_1 \xrightarrow{\sigma} d_2 \xrightarrow{\sigma} \dots \xrightarrow{\sigma} d_k \rightarrow 1$ is a universally feasible architecture on any topological space \mathcal{X} satisfying the assumptions stated in Theorem 3.6. Then, it is enough to consider the ‘worst’ case of dataset to prove a lower bound. We will use the same idea in the proof of Proposition F.2. Specifically, for the given Betti numbers β_k , we consider a topological space \mathcal{X} such that every ‘hole’ intersects with a straight line, say ℓ . Since each hole intersects with ℓ at least two points, we conclude that \mathcal{N} has at least $2 \sum_{k=0}^d \beta_k$ piecewise linear regions on ℓ (Figure 17(a)).

Now we introduce one terminology: from the piecewise linearity of deep ReLU networks, we define a *linear partition region* to be a maximum connected component where the network is affine on. Note also that the boundary of each linear partition region is non-differentiable points of \mathcal{N} in \mathbb{R}^d , which are vanished points of some hidden layers.

We establish the proof by computing the upper bounds of number of linear partition regions on the straight line ℓ made by \mathcal{N} . For d_1 neurons in the first hidden layer, the set of vanishing points are d_1 hyperplanes in \mathbb{R}^d , thus it can intersect with ℓ at most d_1 times (Figure 17(b)). Then, consider the vanishing points of the second hidden layer. These points form a bent hyperplane in \mathbb{R}^d , which is refracted on the intersection with a vanishing hyperplane of the first layer (Figure 17(c)). Therefore, a vanishing hyperplane of the second hidden layer can intersect with ℓ at most $(d_1 + 1)$ times for each neuron. This concludes that the number of vanishing hyperplanes of the second hidden layers can intersect with ℓ at most $d_2(d_1 + 1)$ times. By the same argument, after the third layer, the number of maximum partitions on ℓ is bounded by

$d_3(d_2(d_1 + 1) + 1) + 1$ (Figure 17(d)), and so on. Then, for the given architecture $d \xrightarrow{\sigma} d_1 \xrightarrow{\sigma} d_2 \xrightarrow{\sigma} \cdots \xrightarrow{\sigma} d_k \rightarrow 1$, the number of linear partition regions on ℓ is bounded by

$$\begin{aligned} & 1 + d_k + d_k d_{k-1} + d_k d_{k-1} d_{k-2} + \cdots + d_k \cdots d_1 \\ &= 1 + \sum_{i=1}^k \prod_{j=i}^k d_j. \end{aligned}$$

Therefore, to be a feasible architecture on \mathcal{X} , we get

$$1 + \sum_{i=1}^k \prod_{j=i}^k d_j \geq 2 \sum_{k=0}^d \beta_k - 1,$$

which completes the proof. \square

E.5. Proof of Theorem 3.7

Recall that \mathcal{T}_j satisfies that $\sigma(\mathcal{T}_j(\mathbf{x}_i)) = 0$ or 1 for all $\mathbf{x}_i \in \mathcal{D}, j \in [J]$. From (5) and Lemma F.4, we know that $C_j := \{\mathbf{x} \mid \mathcal{T}_j(\mathbf{x}) = 1\}$ is a convex polytope for each $j \in [J]$. Then, we get

$$\begin{aligned} \mathcal{N}(\mathbf{x}) &= \frac{1}{2} + \sum_{j=1}^J a_j \sigma(\mathcal{T}_j(\mathbf{x})) \\ &= \frac{1}{2} + \sum_{j=1}^J a_j \mathbb{1}_{\{\mathbf{x} \in C_j\}}(\mathbf{x}). \end{aligned}$$

Now, we define $\mathcal{C}_P := \{C_j \in \mathcal{C} \mid a_j = +1\}$ and $\mathcal{C}_Q := \{C_j \in \mathcal{C} \mid a_j = -1\}$. Then, we get

$$\mathcal{N}(\mathbf{x}_i) > 0 \quad \Leftrightarrow \quad \sum_{C \in \mathcal{C}_P} \mathbb{1}_{\{\mathbf{x}_i \in C\}} \geq \sum_{C \in \mathcal{C}_Q} \mathbb{1}_{\{\mathbf{x}_i \in C\}}$$

for all $i \in [n]$. Therefore, Definition 3.2 establishes that \mathcal{C} is a polytope-basis cover of \mathcal{D} , ensuring its accuracy matches that of \mathcal{N} . \square

E.6. Proof of Proposition C.2

Here we present proofs for each statement.

1. Firstly, we establish the validity of (5), ensuring $v_{jk} < 0$. This condition holds at initialization as the network adheres to (8). Throughout the algorithm, consisting of neuron removal and neuron scaling, neither action compromises (5). Proposition F.5 assures the persistence of (8) under gradient flow. Consequently, (5) remains satisfied throughout.

Secondly, we scrutinize the condition (7). Suppose there exists $\mathbf{x}_i \in \mathcal{D}$ such that $0 < \mathcal{T}(\mathbf{x}_i) < 1$. From Definition 5, it implies that

$$-1 < \mathcal{T}(\mathbf{x}_i) - 1 = \sum_{k \in [m]} v_k \sigma(\mathbf{w}_k^\top \mathbf{x}_i + b_k) < 0$$

Recall that all v_k are negative, by the preceded proof, and ReLU is positive homogeneous. Therefore, by scaling neurons (v_k, \mathbf{w}_k, b_k) by $(\lambda_{scale} v_k, \lambda_{scale} \mathbf{w}_k, \lambda_{scale} b_k)$ such that $\mathbf{w}_k^\top \mathbf{x}_i + b_k > 0$, the network output changes from

$$\mathcal{T}(\mathbf{x}_i) - 1 \quad \rightarrow \quad \lambda_{scale}^2 (\mathcal{T}(\mathbf{x}_i) - 1).$$

Therefore, by repeating this scaling sufficiently many times, given $\lambda_{scale} > 1$, $(\mathcal{T}(\mathbf{x}_i) - 1)$ decreases beyond -1 . This process applies to all such \mathbf{x}_i in the dataset, eventually leading to $\sigma(\mathcal{T}(\mathbf{x}_i)) = 0$ or 1 for all $\mathbf{x}_i \in \mathcal{D}$.

2. In Algorithm 2, first for loop must terminate after $Epochs$ repetition. Then, the following repeat loop makes all \mathcal{T}_j to satisfy $\sigma(\mathcal{T}_j(\mathbf{x}_i))$ is either 0 or 1, for all $\mathbf{x}_i \in \mathcal{D}$. However, by the previous proof, we know Algorithm 1 provides a network satisfying both (5) and (7) in finite time. Therefore, this algorithm is guaranteed to terminate in finite time. Lastly, since each \mathcal{T}_j has binary output 0 or 1, convex polytopes defined by $C_j := \{\mathcal{T}_j > 0\}$ forms a polytope-basis cover, which has the same accuracy with the produced network \mathcal{N} .
3. To prove finite-time termination of Algorithm 3, it is enough to show that the **repeat** loop in the algorithm must terminate in finite time. Specifically, we prove the following two statements: 1. the incorrectly covered data $\hat{\mathbf{x}}$ is correctly covered after one process in the **repeat** loop by adding two polytopes, and 2. these added polytopes do not hurt other correctly covered data.

First, let \mathcal{C} be a (constructing) polytope-basis cover and let $\hat{\mathbf{x}}$ be an incorrectly covered data by \mathcal{C} . Then, it means the sign of $\mathcal{N}_+(\hat{\mathbf{x}}) - \mathcal{N}_-(\hat{\mathbf{x}})$ and the sign of $\hat{o}_i := \sum_{c \in \mathcal{C}_P} \mathbb{1}_{\{\hat{\mathbf{x}} \in C\}} - \sum_{c \in \mathcal{C}_Q} \mathbb{1}_{\{\hat{\mathbf{x}} \in C\}} + \frac{1}{2}$. Let c be the value between $\mathcal{N}_-(\hat{\mathbf{x}})$ and $\mathcal{N}_+(\hat{\mathbf{x}})$, and define two convex polytopes

$$\begin{aligned} C_+ &:= \{\mathbf{x} \mid \mathcal{N}_+(\mathbf{x}) < c\} \\ C_- &:= \{\mathbf{x} \mid \mathcal{N}_-(\mathbf{x}) > -c\}. \end{aligned}$$

Then, by the definition, $\hat{\mathbf{x}}$ is only contained in either C_+ or C_- , determined by the sign of $\mathcal{N}(\hat{\mathbf{x}})$. Therefore, adding these two polytopes to the polytope-basis cover \mathcal{C} , by $C_- \in \mathcal{C}_P$ and $C_+ \in \mathcal{C}_Q$, $\hat{\mathbf{x}}$ is now correctly classified by the cover \mathcal{C} .

Second, we claim that adding above two polytopes do not disrupt other correctly covered data. Recall the approximation of convex functions discussed in Appendix C.2. Let $f : \mathbb{R}^d \rightarrow \mathbb{R}$ be a convex function, and let $P := \{p_0, p_1, \dots, p_{J+1}\}$ be a finite partition of real number by

$$-\infty = p_0 \leq p_1 \leq p_2 \leq \dots \leq p_J \leq p_{J+1} = +\infty$$

Then, f can be approximated by

$$f(\mathbf{x}) \approx p_1 + \sum_{j=1}^J (p_{j+1} - p_j) \mathbb{1}_{\{f(\mathbf{x}) < p_j\}}.$$

This approximation can be understood as quantization of the function f by values in P . Then, elementary analysis (Rudin et al., 1976) shows that refinement of the partition P only increases the accuracy of the above approximation. I.e., as polytopes added in the constructing polytope-basis cover \mathcal{C} , the number of incorrectly covered data by \mathcal{C} strictly decreases. Since there is finite data points in the training dataset \mathcal{D} , Algorithm 3 must terminate in finite time. More precisely, the **repeat** loop in the algorithm must be halted in $n = |\mathcal{D}|$ times.

4. Let $\mathcal{C} = \{C_1, C_2, C_3, \dots, C_J\}$ be the output of Algorithm 4. Then, from its construction described in the algorithm, it implies that

$$\begin{aligned} C_1 &\text{ contains all points in } \mathcal{D}_0. \\ C_2 &\text{ contains all points in } \mathcal{D}_1 \cap C_1. \\ C_3 &\text{ contains all points in } \mathcal{D}_0 \cap C_2. \\ &\vdots \\ C_{J-1} &\text{ contains all points in } \mathcal{D}_{\frac{1+(-1)^{J-1}}{2}} \cap C_{J-2}. \\ C_J &\text{ contains all points in } \mathcal{D}_{\frac{1+(-1)^J}{2}} \cap C_J, \text{ and does not contain the another class.} \end{aligned}$$

Now, define

$$\mathcal{N}(\mathbf{x}) := -\frac{1}{2} + \sum_{j=1}^J (-1)^j \sigma(\mathcal{T}(\mathbf{x})). \quad (25)$$

Then, \mathcal{N} is a three-layer ReLU network of the form (6). Furthermore, $\mathcal{T}_j(\mathbf{x}_i)$ is either 0 or 1 for all $i \in [n]$ and $j \in [J]$, satisfying the condition (7). Therefore, Theorem 3.7 verifies that $\mathcal{C} := \{C_j\}_{j \in [J]}$ becomes a polytope-basis cover of the dataset. \square

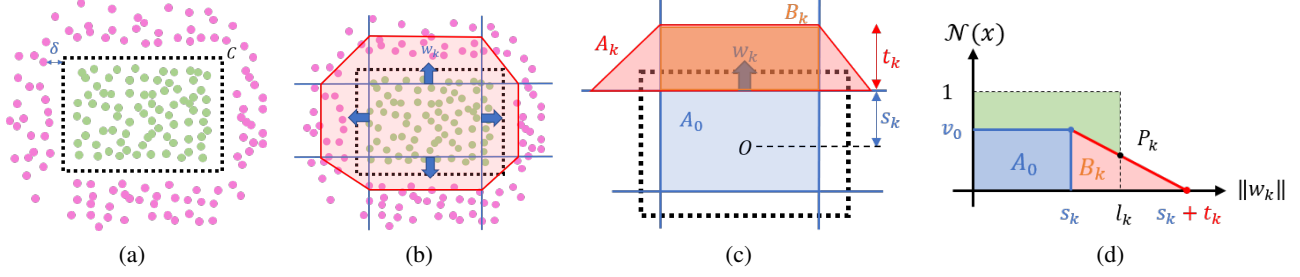


Figure 18. Proof of Theorem D.3. (a) The given dataset \mathcal{D} is polyhedrally separable by a black dashed rectangle C . (b) Initialization of a two-layer ReLU network \mathcal{N} . (c) For $k \in [m]$, sets A_k and B_k defined in (26) and (27) are illustrated. (d) A sideview of the function \mathcal{N} with respect to $\|\mathbf{w}_k\|$. s_k and t_k are defined in (28) and (29). Note that the intersection point P_k is invariant after the update of parameters.

E.7. Proof of Theorem D.3.

E.7.1. PROOF FOR THE MSE LOSS (13).

The proof is divided into several steps. First, for $k \in [m]$, we define the following sets:

$$A_k := \{\mathbf{x} \in \mathbb{R}^d \mid \mathbf{w}_k^\top \mathbf{x} + b_k > 0\} \quad (26)$$

$$B_k := \{\mathbf{x} \in \mathbb{R}^d \mid \mathbf{w}_k^\top \mathbf{x} + b_k > 0 \text{ and } \mathbf{w}_j^\top \mathbf{x} + b_j > 0 \text{ for } j \neq k\} \quad (27)$$

I.e., A_k is the region where k -th neuron is alive, and B_k is the region where only k -th neuron is alive (see Figure 18(b,c)). Similarly, we define

$$A_0 := \{\mathbf{x} \in \mathbb{R}^d \mid \mathbf{w}_k^\top \mathbf{x} + b_k < 0\}$$

which is the region where all neurons are dead, except the last bias term v_0 . Now, we define the following values for every $k \in [m]$:

$$l_k := \text{the distance between } O \text{ and } \partial C_k,$$

$$s_k := -\frac{b_k}{\|\mathbf{w}_k\|}, \quad (28)$$

$$t_k := -\frac{v_0}{v_k \|\mathbf{w}_k\|}, \quad (29)$$

$$t := \max_{k \in [m]} \{t_k, \delta\}.$$

Then, the network initialization condition (16) gives

$$\begin{aligned} 0 < t_k < R, \\ 0 < s_k < l_k < s_k + t_k. \end{aligned}$$

In other words, s_k is the distance between the origin point O and the hyperplane $\{\mathbf{w}_k^\top \mathbf{x} + b_k = 0\}$. t_k is the length of ‘height’ of the region B_k as depicted in Figure 18(c). To be familiar for these notations, we demonstrate the output \mathcal{N} in Figure 18(d) with respect to $\|\mathbf{w}_k\|$.

It is clear that $\mathcal{N}(\mathbf{x}) = v_0$ if $\mathbf{x} \in A_0$, and it linearly decreases to zero for $\mathbf{x} \in B_k$. When $\mathbf{x}_i \in B_k$ satisfies $\mathbf{x}_i^\top \frac{\mathbf{w}_k}{\|\mathbf{w}_k\|} = s_k + t_k$, $\mathcal{N}(\mathbf{x}_i) = 0$. Now we are ready to prove the theorem.

For the previously defined sets A_k and B_k , the MSE loss (13) is computed by

$$\begin{aligned} L_{MSE} &= \frac{1}{2n} \sum_{i=1}^n (\mathcal{N}(\mathbf{x}_i) - y_i)^2 \\ &= \frac{1}{2n} \sum_{\mathbf{x}_i \in A_0} (\mathcal{N}(\mathbf{x}_i) - y_i)^2 + \frac{1}{2n} \sum_{\mathbf{x}_i \in \cup_k B_k} (\mathcal{N}(\mathbf{x}_i) - y_i)^2 + \frac{1}{2n} \sum_{\mathbf{x}_i \in \cup_k (A_k \setminus B_k)} (\mathcal{N}(\mathbf{x}_i) - y_i)^2 \end{aligned}$$

$$=: L_1 + L_2 + L_3. \quad (30)$$

Note that we omitted Θ notation, the set of all learnable parameters. We will observe the change of these loss values with respect to one update of parameters. We add prime ($'$) for the updated parameter. For the given step size η , we explicitly provide the update of parameters by

$$\begin{aligned} v_0 &\rightarrow v'_0 := v_0 + \Delta v_0, \\ s_k &\rightarrow s'_k := s_k + \Delta s_k, \\ t_k &\rightarrow t'_k := t_k + \Delta t_k \end{aligned}$$

for all $k \in [m]$, where

$$\Delta v_0 := \begin{cases} 0 & \text{if } \#(\cup_{k \in [l]} A_k) > 0, \\ -\frac{1}{2}(v_0 - 1)t\eta, & \text{otherwise,} \end{cases} \quad (31)$$

$$\Delta s_k := \begin{cases} \frac{\eta t_k^2}{v_0 + \eta t_k} \cdot \frac{l_k - s_k}{t_k + t_k - s_k} & \text{if } \#(A_k) > 0, \\ 0 & \text{otherwise,} \end{cases} \quad (32)$$

$$\Delta t_k := \begin{cases} \Delta s_k - \frac{\eta t_k^2}{v_0 + \eta t_k} & \text{if } \#(A_k) > 0, \\ \frac{t_k \Delta v_0 - \eta t_k^2}{v_0 + \eta t_k} & \text{otherwise.} \end{cases} \quad (33)$$

Specifically, v_0 is updated if and only if $\cup_{k \in [l]} A_k$ contains a data point, where s_k and t_k are updated exclusively. The given update terms are proposed to have some invariant quantity. In Figure 18(d), we set P_k to be the output value of \mathcal{N} at l_k , and update equations in (31)~(33) are determined to keep this value P_k . Furthermore, it satisfies that the change of the slope is exactly $-\eta$, i.e.,

$$\begin{aligned} \Delta \left(-\frac{v_0}{t_k} \right) &:= -\frac{v_0 + \Delta v_0}{t_k + \Delta t_k - \Delta s_k} + \frac{v_0}{t_k} \\ &= -\eta. \end{aligned}$$

Note also that $v_0 < 1$ and $s_k < l_k$ are increasing, where $t_k > 0$ is decreasing.

In the subsequent steps, we examine the change of each loss value. The main idea of the proof is computing lower bounds on the reduction of the loss value resulting from one-step update given by (31)~(33). It is divided into four steps.

STEP 1. First, we consider when $\#(\cup_{k \in [l]} A_k) = 0$. In this case, since $L_2 = L_3 = 0$ from the definition (30), it is enough to investigate the change of L_1 . Recall that

$$L_1 := \frac{1}{2n} \#(A_0) (v_0 - 1)^2.$$

By one-step update of parameters, it becomes $L_1 \rightarrow L'_1 := L_1 + \Delta L_1$. Then,

$$\begin{aligned} \Delta L_1 &= L'_1 - L_1 \\ &= \frac{1}{2n} \sum_{\mathbf{x}_i \in A_0} (v_0 + \Delta v_0 - 1)^2 - \frac{1}{2n} \sum_{\mathbf{x}_i \in A_0} (v_0 - 1)^2 \\ &= \frac{1}{2n} \cdot (2v_0 - 2 + \Delta v_0) \Delta v_0 \cdot \#(A_0) \\ &= -\frac{\#(A_0)}{n} (1 - v_0) \Delta v_0 + \frac{\#(A_0)}{2n} (\Delta v_0)^2 \\ &= -\frac{\#(A_0)}{2n} (1 - v_0)^2 (t\eta - \frac{1}{4} t^2 \eta^2) \\ &< -\frac{\#(A_0)}{2n} (1 - v_0)^2 \cdot \frac{1}{2} t\eta. \end{aligned}$$

Note that we use $\eta < \frac{2}{t} < \frac{2}{\delta}$ on the last inequality. Then, we get

$$L'_1 = L_1 + \Delta L_1$$

$$\begin{aligned}
 &= \left(1 + \frac{\Delta L_1}{L_1}\right) L_1 \\
 &< \left(1 - \frac{\frac{1}{2n} \#(A_0)(1-v_0)^2 \cdot \frac{1}{2} t \eta}{\frac{1}{2n} \#(A_0)(1-v_0)^2}\right) L_1 \\
 &= \left(1 - \frac{1}{2} t \eta\right) L_1 \\
 &\leq \left(1 - \frac{1}{2} \delta \eta\right) L_1
 \end{aligned} \tag{34}$$

which states that L_1 strictly decreases after the update.

STEP 2. Now, we consider when $\#(\cup_{k \in [l]} A_k) > 0$. We investigate the second term in (30), defined by

$$L_2 := \frac{1}{2n} \sum_{k \in [l]} \sum_{\mathbf{x}_i \in B_k} (\mathcal{N}(\mathbf{x}_i) - y_i)^2.$$

Recall that the update of parameters given in (31)~(33) are chosen to keep P_k value and increasing the absolute value of the slope $-\frac{v_0}{t_k}$ by η . Therefore, for any $\mathbf{x}_i \in B_k$, it $\mathcal{N}(\mathbf{x}_i)$ increases (or decreases) if and only if $\mathbf{x}_i \in B_k \cap C$ (or $\mathbf{x}_i \in B_k \setminus C$). Therefore, $|\mathcal{N}(\mathbf{x}_i) - y_i|$ always strictly decreases after the update, which implies that

$$\Delta L_2 := L'_2 - L_2 < 0. \tag{35}$$

STEP 3. We observe the last term in (30) when $\#(\cup_{k \in [m]} A_k) > 0$, which is the most technical part in this proof. Recall that

$$L_3 := \frac{1}{2n} \sum_{\mathbf{x}_i \in \cup_k (A_k \setminus B_k)} (\mathcal{N}(\mathbf{x}_i) - y_i)^2.$$

The goal of this step is showing that the absolute change of L_3 is less than it of L_2 , i.e., $|\Delta L_3| < \Delta L_2$. The idea is based on the sparsity of the data distribution in $\mathcal{B}_r(\partial^2 C)$; near the neighborhood of ‘edge’ parts of the polytope C .

Note that for each $k \in [m]$, obviously we have $(A_k \setminus B_k) \subset \mathcal{B}_t(\partial^2 C_k)$ from the linearity of \mathcal{N} (see Figure 18(c) and (d)). It is also worth noting that if $t_k \leq \delta$, then $L_3 = 0$ because there is no \mathbf{x}_i in $\cup_{k \in [m]} (A_k \setminus B_k)$, and we have nothing to do. Thus we mostly consider $t_k > \delta$ cases.

Let \mathcal{N}' be the network after the one-step update from \mathcal{N} . The difference of output is $\Delta \mathcal{N}(\mathbf{x}) := \mathcal{N}'(\mathbf{x}) - \mathcal{N}(\mathbf{x})$. Recall that parameters v_0, s_k, t_k follow the updated rule (31) ~ (33) such that network have a constant output on $\partial C_k \cap B_k$ (Figure 18(c) and (d)). This implies that both networks \mathcal{N} and \mathcal{N}' have fixed outputs for $\partial C_k \cap B_k$, and then the affine space connecting those fixed points also has the fixed output which comes from the piecewise linearity of \mathcal{N} .

STEP 3-1 First, we compute an upper bound of $|\Delta L_3|$. Since $\mathcal{N}(\mathbf{x})$ is piecewise linear, we consider the input space partition in $A_k \setminus B_k$ where \mathcal{N} is linear on. Observing the ‘corner’ parts of the polytope C (see Figure 18(c) and (d)), each partition is intersection of some neurons of \mathcal{N} . Choose one partition $P \subset A_k \setminus B_k$, and let $J_P \subset [m]$ be the index set of P that w_j is activated on P if and only if $j \in J_P$, or namely, $P = \bigcap_{j \in J_P} A_j$. Then obviously, the partition P is contained in a ball with radius $\max_{j \in J_P} t_j \leq t < R$. On the contrary, any partition P is contained in t_k -radius ball from ∂_k for some k . Using this, we can disjointly separate the partitions to \mathcal{Q}_k such that

1. $Q_k \subset (A_k \setminus B_k)$
2. Every $P \in \cup_{k \in [m]} (A_k \setminus B_k)$ is exactly contained in one of Q_k .
3. Every $P \in Q_k$ can be bounded by a ball with radius t_k .

Note that \mathcal{Q}_k is a collection of partitions, which can be empty. Using this, we decompose L_3 by the following way. This is just rearranging the terms in L_3 .

$$L_3 = \frac{1}{2} \sum_{\mathbf{x}_i \in \cup_{k \in [m]} (A_k \setminus B_k)} (\mathcal{N}(\mathbf{x}_i) - y_i)^2$$

$$\begin{aligned}
 &= \frac{1}{2} \sum_{k \in [m]} \sum_{\mathbf{x}_i \in \mathcal{Q}_k} (\mathcal{N}(\mathbf{x}_i) - y_i)^2 \\
 &=: \frac{1}{2} \sum_{k \in [m]} L_{3,k}.
 \end{aligned}$$

Now, we bound the change of network output $\Delta \mathcal{N}(\mathbf{x}_i)$ for $\mathbf{x}_i \in P \in \mathcal{Q}_k$.

$$\begin{aligned}
 |\Delta \mathcal{N}(\mathbf{x}_i)| &= |\mathcal{N}(\mathbf{x}_i) - \mathcal{N}'(\mathbf{x}_i)| \\
 &\leq \left| \sum_{j \in J_P} \Delta \left(-\frac{v_0}{t_j} \right) t_k \right| \\
 &= \sum_{j \in J_P} \eta R \\
 &\leq l R \eta.
 \end{aligned}$$

Above inequalities come from the fact that, the change of linear value is bounded by product of the change of slope and the maximum diameter of the set. Finally, for a $k \in [m]$, we compute an upper bound of the loss variation of $L_{3,k}$.

$$\begin{aligned}
 |\Delta L_{3,k}| &= \left| \frac{1}{2n} \sum_{\mathbf{x}_i \in (A_k \setminus B_k)} (\mathcal{N}(\mathbf{x}_i) + \Delta \mathcal{N}(\mathbf{x}_i) - y_i)^2 - \frac{1}{2n} \sum_{\mathbf{x}_i \in (A_k \setminus B_k)} (\mathcal{N}(\mathbf{x}_i) - y_i)^2 \right| \\
 &= \left| \frac{1}{n} \sum_{\mathbf{x}_i \in (A_k \setminus B_k)} \left(\mathcal{N}(\mathbf{x}_i) - y_i + \frac{1}{2} \Delta \mathcal{N}(\mathbf{x}_i) \right) \cdot \Delta \mathcal{N}(\mathbf{x}_i) \right| \\
 &\leq \frac{1}{n} \sum_{\mathbf{x}_i \in (A_k \setminus B_k)} \left(|\mathcal{N}(\mathbf{x}_i) - y_i| \cdot |\Delta \mathcal{N}(\mathbf{x}_i)| + \frac{1}{2} |\Delta \mathcal{N}(\mathbf{x}_i)|^2 \right) \\
 &\leq \frac{1}{n} \sum_{\mathbf{x}_i \in (A_k \setminus B_k)} \left(1 \cdot |\Delta \mathcal{N}(\mathbf{x}_i)| + \frac{1}{2} |\Delta \mathcal{N}(\mathbf{x}_i)|^2 \right) \\
 &\leq \frac{1}{n} \#(\mathcal{B}_{t_k}(\partial^2 C_k)) \cdot (m R \eta + \frac{1}{2} m^2 R^2 \eta^2) \\
 &\leq \frac{2}{n} \#(\mathcal{B}_{t_k}(\partial^2 C_k)) \cdot m R \eta \\
 &\leq \frac{2m R \eta}{n} \cdot \rho \#(\mathcal{B}_{t_k}(\partial C_k)).
 \end{aligned} \tag{36}$$

Note that we used $\eta < \frac{2}{mR}$ to bound the quadratic term η^2 .

STEP 3-2. Now, we compute a similar bound for ΔL_2 . It can be decomposed to the sum on each B_k .

$$\begin{aligned}
 L_2 &= \frac{1}{2n} \sum_{k \in [m]} \sum_{\mathbf{x}_i \in B_k} (\mathcal{N}(\mathbf{x}_i) - y_i)^2 \\
 &=: \sum_{k \in [m]} L_{2,k}.
 \end{aligned}$$

We use the fact that each data point \mathbf{x}_i is far from ∂C at least δ . From the definition, we get $\Delta \mathcal{N}(\mathbf{x}_i) > \delta \eta$. Note that if $t_k < 2\delta$, then $L_{3,k}$ strictly decreases and we have nothing to do. Otherwise, when $t_k > 2\delta$, we have $R > 2\delta$ and there is data far from δ distance from ∂B_k . For such data point \mathbf{x}_i , we get

$$\mathcal{N}(\mathbf{x}_i) - 0 = v_0 - \frac{v_0}{t_k} (t_k - \delta)$$

$$\begin{aligned}
 &= v_0 \frac{\delta}{t_k} \\
 &> \frac{v_0 \delta}{R}
 \end{aligned}$$

and

$$\begin{aligned}
 1 - \mathcal{N}(\mathbf{x}_i) &= 1 - \left(v_0 - \frac{v_0}{t_k}(t_k - \delta) \right) \\
 &= 1 - \frac{v_0}{t_k} \delta \\
 &> 1 - \frac{1}{2} v_0 \\
 &> \frac{1}{2} v_0 \\
 &> \frac{v_0 \delta}{R}.
 \end{aligned}$$

Therefore, we have shown that

$$\min_{s_k + \delta \leq \|\mathbf{x}_i\| \leq s_k + t_k - \delta} |\mathcal{N}(\mathbf{x}_i) - y_i| \geq \frac{v_0 \delta}{R}.$$

Now we induce the lower bound of $\Delta L_{2,k}$.

$$\begin{aligned}
 \Delta L_{2,k} &= \frac{1}{2n} \sum_{\mathbf{x}_i \in B_k} ((\mathcal{N}(\mathbf{x}_i) + \Delta \mathcal{N}(\mathbf{x}_i) - y_i)^2 - (\mathcal{N}(\mathbf{x}_i) - y_i)^2) \\
 &= \frac{1}{n} \sum_{\mathbf{x}_i \in B_k} \left(\mathcal{N}(\mathbf{x}_i) - y_i + \frac{1}{2} \Delta \mathcal{N}(\mathbf{x}_i) \right) \cdot \Delta \mathcal{N}(\mathbf{x}_i) \\
 &= \frac{1}{n} \sum_{\mathbf{x}_i \in B_k} \left(-|\mathcal{N}(\mathbf{x}_i) - y_i| \cdot |\Delta \mathcal{N}(\mathbf{x}_i)| + \frac{1}{2} |\Delta \mathcal{N}(\mathbf{x}_i)|^2 \right) \\
 &\leq \frac{1}{n} \sum_{\mathbf{x}_i \in B_k} \left(-\min_{\delta \leq \|\mathbf{x}_i\| - s_k \leq t_k - \delta} |\mathcal{N}(\mathbf{x}_i) - y_i| \cdot \eta \delta + \frac{1}{2} R^2 \eta^2 \right) \\
 &\leq -\frac{1}{n} \#(\mathcal{B}_{\frac{t_k}{2} - \delta}(\partial C_k) - \mathcal{B}_{t_k}(\partial^2 C_k)) \cdot \left(\frac{v_0 \delta}{R} \cdot \delta \eta - \frac{1}{2} R^2 \eta^2 \right) \\
 &\leq -\frac{1}{n} (1 - \rho) \#(\mathcal{B}_{t_k}(\partial C_k)) \cdot \left(\frac{v_0 \delta^2 \eta}{R} - \frac{1}{2} R^2 \eta^2 \right) \\
 &< \frac{1}{n} \frac{(1 - \rho) v_0 \delta^2 \eta}{2R} \#(\mathcal{B}_{t_k}(\partial C_k)). \tag{37}
 \end{aligned}$$

Note that Assumption D.2 on dataset \mathcal{D} is used to induce this inequality. Now, we compare (37) and (36) with initialization condition (17) for v_0 . Then, we finally get

$$\begin{aligned}
 |\Delta L_{3,k}| &\leq \frac{2lR\eta\rho}{n} \#(\mathcal{B}_{t_k}(\partial C_k)) \\
 &< \frac{(1 - \rho)v_0\delta^2}{2nR} \eta \cdot \#(\mathcal{B}_{t_k}(\partial C_k)) \\
 &< -\Delta L_{2,k}
 \end{aligned}$$

for every $k \in [m]$. By summing up, we conclude $|\Delta L_3| < -\Delta L_2$ or,

$$\Delta L_2 + \Delta L_3 < 0. \tag{38}$$

STEP 4. Finally, we combine all results in the previous steps. When $\#(\cup_{k \in [m]} A_k) > 0$, only L_2 and L_3 are changed, then one step update gives

$$\begin{aligned} L' &= L + \Delta L \\ &= L_1 + L_2 + L_3 + \Delta L_1 + \Delta L_2 + \Delta L_3 \\ &< L_1 + L_2 + L_3 \end{aligned}$$

from (35) and (38). Furthermore, since $s_k < l_k$ increases and $t_k > 0$ decreases, the updated parameters satisfy the assumption (16) again. Using mathematical induction, we can repeat above steps until $\#(\cup_{k \in [m]} A_k) = 0$. After achieving $\#(\cup_{k \in [m]} A_k) = 0$, we get $L_2 = L_3 = 0$ from their definition (30). Then, the remained loss L_1 exponentially decreases to zero because

$$\begin{aligned} L' &= L_1 + \Delta L_1 \\ &\leq \left(1 - \frac{1}{2}\delta\eta\right) L_1 \\ &\leq \left(1 - \frac{1}{2}\delta\eta\right) L \end{aligned}$$

from (34). This completes the proof. \square

E.7.2. PROOF FOR THE BCE LOSS (14).

The proof idea is similar with the previous proof. We use the same definitions for A_k, B_k, s_k, t_k, l_k , and other notations. The BCE loss (14) is rearranged by

$$\begin{aligned} L_{BCE} &= -\frac{1}{n} \sum_{i=1}^n (y_i \log \text{SIG} \circ \mathcal{N}(\mathbf{x}_i) + (1 - y_i) \log(1 - \text{SIG} \circ \mathcal{N}(\mathbf{x}_i))) \\ &= -\frac{1}{n} \sum_{\mathbf{x}_i \in A_0} \log \text{SIG} \circ \mathcal{N}(\mathbf{x}_i) \\ &\quad - \frac{1}{n} \sum_{k \in [m]} \sum_{\mathbf{x}_i \in B_k} (y_i \log \text{SIG} \circ \mathcal{N}(\mathbf{x}_i) + (1 - y_i) \log(1 - \text{SIG} \circ \mathcal{N}(\mathbf{x}_i))) \\ &\quad - \frac{1}{n} \sum_{k \in [m]} \sum_{\mathbf{x}_i \in (A_k \setminus B_k)} (y_i \log \text{SIG} \circ \mathcal{N}(\mathbf{x}_i) + (1 - y_i) \log(1 - \text{SIG} \circ \mathcal{N}(\mathbf{x}_i))) \\ &=: L_1 + L_2 + L_3. \end{aligned} \tag{39}$$

Before we start, we compute the derivative and its bound of some functions. For $\zeta \in \mathbb{R}$, define

$$\begin{aligned} f(\zeta) &:= \log \text{SIG}(\zeta), \\ g(\zeta) &:= \log(1 - \text{SIG}(\zeta)). \end{aligned}$$

Then their derivatives are given by

$$\begin{aligned} \frac{d}{d\zeta} f(\zeta) &:= 1 - \text{SIG}(\zeta), \\ \frac{d}{d\zeta} g(\zeta) &:= -\text{SIG}(\zeta). \end{aligned}$$

From the mean value theorem (MVT), we get

$$f(\zeta + \Delta\zeta) = f(\zeta) + f'(\zeta)\Delta\zeta + \frac{1}{2}f''(\tilde{\zeta})(\Delta\zeta)^2$$

$$\geq f(\zeta) + (1 - \text{SIG}(\zeta))\Delta\zeta - \frac{1}{2}(\Delta\zeta)^2$$

and

$$\begin{aligned} f(\zeta + \Delta\zeta) - f(\zeta) &= (1 - \text{SIG}(\tilde{\zeta}))\Delta\zeta \\ &\leq \Delta\zeta. \end{aligned}$$

Now we define the update of parameters. For $k \in [l]$, the update of v_0 is given by

$$\Delta v_0 := \begin{cases} 0 & \text{if } \#(\cup_{k \in [l]} A_k) > 0, \\ (1 - \text{SIG}(v_0))\eta. & \text{otherwise} \end{cases} \quad (40)$$

For Δs_k and Δt_k , we adopt the same update defined in (32) and (33). Namely, the update of parameters preserves the value of \mathcal{N} on l_k and the change of slope is set to $-\eta$. We repeat the analogous arguments in the previous proof.

STEP 1. Firstly, we consider the first loss term L_1 in (39) when $\#(\cup_{k \in [m]} A_k) = 0$. It is changed by

$$\begin{aligned} \Delta L_1 &= L'_1 - L_1 \\ &= -\frac{1}{n} \sum_{\mathbf{x}_i \in A_0} \log \text{SIG}(v_0 + \Delta v_0) + \frac{1}{n} \sum_{\mathbf{x}_i \in A_0} \log \text{SIG}(v_0) \\ &= -\frac{\#(A_0)}{n} (f(v_0 + \Delta v_0) - f(v_0)) \\ &\leq -\frac{\#(A_0)}{n} \left((1 - \text{SIG}(v_0))\Delta v_0 - \frac{1}{2}(\Delta v_0)^2 \right) \\ &= -\frac{\#(A_0)}{n} \left((1 - \text{SIG}(v_0))^2 \eta - \frac{1}{2}(1 - \text{SIG}(v_0))^2 \eta^2 \right) \\ &< -\frac{\#(A_0)}{n} \frac{1}{2} (1 - \text{SIG}(v_0))^2 \eta. \end{aligned}$$

Therefore, L_1 strictly decreases. Note that we used $\eta < 1$ to bound the η^2 term.

STEP 2. Secondly, we consider when $\#(\cup_{k \in [m]} A_k) > 0$. As discussed in the previous subsection, $\mathcal{N}(\mathbf{x}_i)$ strictly increases (or decreases) if and only if $y_i = 1$ (or 0, respectively) because the slope $-\frac{v_0}{t_k}$ changes $-\eta$. This shows that $\Delta L_2 < 0$.

STEP 3. Thirdly, we observe ΔL_2 and $|\Delta L_3|$ when $\#(\cup_{k \in [m]} A_k) > 0$. We compute a bound of ΔL_3 first. For any $k \in [m]$,

$$\begin{aligned} |\Delta L_3| &= \frac{1}{n} \left| \sum_{\mathbf{x}_i \in (A_k \setminus B_k)} y_i (f(\mathcal{N}(\mathbf{x}_i) + \Delta \mathcal{N}(\mathbf{x}_i)) - f(\mathcal{N}(\mathbf{x}_i))) \right. \\ &\quad \left. + (1 - y_i) (g(\mathcal{N}(\mathbf{x}_i) + \Delta \mathcal{N}(\mathbf{x}_i)) - g(\mathcal{N}(\mathbf{x}_i))) \right| \\ &\leq \frac{1}{n} \sum_{\mathbf{x}_i \in (A_k \setminus B_k)} \left| (f(\mathcal{N}(\mathbf{x}_i) + \Delta \mathcal{N}(\mathbf{x}_i)) - f(\mathcal{N}(\mathbf{x}_i))) \right| + \left| (g(\mathcal{N}(\mathbf{x}_i) + \Delta \mathcal{N}(\mathbf{x}_i)) - g(\mathcal{N}(\mathbf{x}_i))) \right| \\ &< \frac{1}{n} \sum_{\mathbf{x}_i \in (A_k \setminus B_k)} 2|\Delta \mathcal{N}(\mathbf{x}_i)| \\ &< \frac{2}{n} \#(\mathcal{B}_{t_k}(\partial^2 C_k)) \cdot \max_{\mathbf{x}_i \in (A_k \setminus B_k)} |\Delta \mathcal{N}(\mathbf{x}_i)| \\ &< \frac{2R\eta}{n} \#(\mathcal{B}_{t_k}(\partial^2 C_k)). \end{aligned}$$

We obtain a similar bound for $\Delta L_{2,k}$. Let $V_0 := \log\left(\frac{(1-\rho)\delta}{4\rho R} - 1\right)$ be the upper bound of initialization of v_0 . Note also that

$\text{SIG}(V_0) = 1 - \frac{4\rho R}{(1-\rho)\delta}$ and $\eta < \frac{1-\text{SIG}(v_0)}{\delta}$. Then,

$$\begin{aligned}
 \Delta L_{2,k} &= -\frac{1}{n} \sum_{\mathbf{x}_i \in B_k} \left(y_i (f(\mathcal{N}(\mathbf{x}_i) + \Delta\mathcal{N}(\mathbf{x}_i)) - f(\mathcal{N}(\mathbf{x}_i))) \right. \\
 &\quad \left. + (1 - y_i) (g(\mathcal{N}(\mathbf{x}_i) + \Delta\mathcal{N}(\mathbf{x}_i)) - g(\mathcal{N}(\mathbf{x}_i))) \right) \\
 &= -\frac{1}{n} \sum_{\mathbf{x}_i \in B_k, y_i=1} \left((f(\mathcal{N}(\mathbf{x}_i) + \Delta\mathcal{N}(\mathbf{x}_i)) - f(\mathcal{N}(\mathbf{x}_i))) \right. \\
 &\quad \left. - \frac{1}{n} \sum_{\mathbf{x}_i \in B_k, y_i=0} (g(\mathcal{N}(\mathbf{x}_i) + \Delta\mathcal{N}(\mathbf{x}_i)) - g(\mathcal{N}(\mathbf{x}_i))) \right) \\
 &< -\frac{1}{n} \sum_{\mathbf{x}_i \in B_k, y_i=1} \left((1 - \text{SIG} \circ \mathcal{N}(\mathbf{x}_i)) \Delta\mathcal{N}(\mathbf{x}_i) - \frac{1}{2} (\Delta\mathcal{N}(\mathbf{x}_i))^2 \right) \\
 &\quad - \frac{1}{n} \sum_{\mathbf{x}_i \in B_k, y_i=0} \left(-\text{SIG} \circ \mathcal{N}(\mathbf{x}_i) \cdot \Delta\mathcal{N}(\mathbf{x}_i) - \frac{1}{2} (\Delta\mathcal{N}(\mathbf{x}_i))^2 \right) \\
 &< -\frac{1}{n} \sum_{s_k - l_k + \delta < h_i < -\delta} \left((1 - \text{SIG} \circ \mathcal{N}(\mathbf{x}_i)) \Delta\mathcal{N}(\mathbf{x}_i) - \frac{1}{2} (\Delta\mathcal{N}(\mathbf{x}_i))^2 \right) \\
 &\quad - \frac{1}{n} \sum_{\delta < h_i < s_k + t_k - \delta} \left(-\text{SIG} \circ \mathcal{N}(\mathbf{x}_i) \cdot \Delta\mathcal{N}(\mathbf{x}_i) - \frac{1}{2} (\Delta\mathcal{N}(\mathbf{x}_i))^2 \right) \\
 &< -\frac{1}{n} \sum_{s_k - l_k + \delta < h_i < -\delta} \left((1 - \text{SIG}(V_0)) \delta \eta - \frac{1}{2} \delta^2 \eta^2 \right) \\
 &\quad - \frac{1}{n} \sum_{\delta < h_i < s_k + t_k - \delta} \left(\text{SIG}(0) \cdot \delta \eta - \frac{1}{2} \delta^2 \eta^2 \right) \\
 &< -\frac{1}{n} \# \left(\mathcal{B}_{\frac{t_k}{2} - \delta}(\partial C_k) - \mathcal{B}_{t_k}(\partial C_k) \right) \cdot \left((1 - \text{SIG}(V_0)) \delta \eta - \frac{1}{2} \delta^2 \eta^2 \right) \\
 &< -\frac{1}{n} (1 - \rho) \# (\mathcal{B}_{t_k}(\partial C_k)) \cdot \frac{1}{2} (1 - \text{SIG}(V_0)) \delta \eta.
 \end{aligned}$$

Therefore,

$$\begin{aligned}
 |\Delta L_{3,k}| &< \frac{2R\eta}{n} \rho \# (\mathcal{B}_{t_k}(\partial C_k)) \\
 &< \frac{1}{n} (1 - \rho) \# (\mathcal{B}_{t_k}(\partial C_k)) \cdot \frac{1}{2} (1 - \text{SIG}(V_0)) \delta \eta \\
 &< -L_{2,k}
 \end{aligned}$$

and we get $\Delta L_2 + \Delta L_3 < 0$.

STEP 4. Finally, we combine results in the previous steps. When $\#(\cup_{k \in [m]} A_k) > 0$, v_0 is bounded by V_0 and we get $\Delta L_2 + \Delta L_3 < 0$ from **STEP 3**. After update, since $s_k < l_k$ increases and $t_k > 0$ decreases, the updated parameters satisfy Assumption **D.2** again. It is repeated with strictly decreasing loss until reaching $\#(\cup_{k \in [m]} A_k) = 0$. After that, v_0 begins to strictly increase, which strictly decreases all L_1 , L_2 , and L_3 . Further, the update equation (40) provides v_0 goes to infinity. Therefore, $\mathcal{N}(\mathbf{x}_i) \rightarrow \infty$ if and only if it label $y_i = 1$, concludes L_{BCE} converges to zero.

This completes the whole proof of Theorem **D.3**. □

F. Additional Propositions and Lemmas

Lemma F.1. *Let $0 \leq m \leq d$ be integers, and Δ^m be an m -simplex in \mathbb{R}^d . For a given $\varepsilon > 0$, there exists a two-layer ReLU network $\mathcal{T} : \mathbb{R}^d \rightarrow \mathbb{R}$ with the architecture $d \xrightarrow{\sigma} (d+1) \rightarrow 1$ such that*

$$\begin{aligned} \mathcal{T}(\mathbf{x}) &= 1 && \text{if } \mathbf{x} \in \Delta^m, \\ \mathcal{T}(\mathbf{x}) &\leq 1 && \text{if } \mathbf{x} \in B_\varepsilon(\Delta^m), \\ \mathcal{T}(\mathbf{x}) &< 0 && \text{if } \mathbf{x} \notin B_\varepsilon(\Delta^m). \end{aligned}$$

Furthermore, the minimal width of such two-layer ReLU networks with the architecture $d \xrightarrow{\sigma} d_1 \rightarrow 1$ is exactly $d_1 = d + 1$.

Proof. We prove the existence part first. For the given m -simplex Δ^m , pick $(d - m)$ distinct points in $B_\varepsilon(\Delta^m)$. By connecting all these points with the points of Δ^m , we obtain a d -simplex contained in $B_\varepsilon(\Delta^m)$, which is a convex polytope. By Proposition 3.1, there exists a neural network $\mathcal{T} : \mathbb{R}^d \rightarrow \mathbb{R}$ with the architecture $d \xrightarrow{\sigma} d_1 \rightarrow 1$ that satisfies the desired properties.

Now, we prove the minimality part. For every $\varepsilon > 0$, suppose there exists a two-layer ReLU network $\mathcal{T}(\mathbf{x}) := \sum_{i=1}^{d_1} v_i \sigma(\mathbf{w}_i^\top \mathbf{x} + b_i) + v_0$ with $d_1 \leq d$ such that $\mathcal{T}(\mathbf{x}) = 1$ for $\mathbf{x} \in \Delta^m$ and $\mathcal{T}(\mathbf{x}) < 0$ for $\mathbf{x} \notin B_\varepsilon(\Delta^m)$. First, we claim that the set of weight vectors $\{\mathbf{w}_1, \dots, \mathbf{w}_{d_1}\}$ spans \mathbb{R}^d . If the set cannot span \mathbb{R}^d , then there exists a nonzero vector $\mathbf{u} \in \mathbb{R}^d - \text{span} \langle \mathbf{w}_1, \dots, \mathbf{w}_{d_1} \rangle$. Then, from $\mathcal{T}(\mathbf{x}) = 1$ for $\mathbf{x} \in \Delta^m$, we get

$$\begin{aligned} \mathcal{T}(\mathbf{x} + t\mathbf{u}) &= \sum_{i=1}^{d_1} v_i \sigma(\mathbf{w}_i^\top (\mathbf{x} + t\mathbf{u}) + b_i) + v_0 \\ &= \sum_{i=1}^{d_1} v_i \sigma(\mathbf{w}_i^\top \mathbf{x} + b_i) + v_0 \\ &= \mathcal{T}(\mathbf{x}) \\ &= 1 \end{aligned}$$

for any $t \in \mathbb{R}$. This contradicts to the condition $\mathcal{T}(\mathbf{x}) < 0$ for $\mathbf{x} \notin B_\varepsilon(\Delta^m)$. Therefore, the set of weight vectors must span \mathbb{R}^d .

From the above claim, we further deduce that $d_1 \geq d$. Since we start with the assumption $d_1 \leq d$, thus $d_1 = d$. Then, we conclude that the set of weight vectors $\{\mathbf{w}_1, \dots, \mathbf{w}_{d_1}\}$ is a basis of \mathbb{R}^d . Now, we focus on the sign of v_0 . Suppose $v_0 \geq 0$. Define

$$A := \bigcap_{i=1}^{d_1} \{\mathbf{x} \mid \mathbf{w}_i^\top \mathbf{x} + b_i < 0\},$$

which is an unbounded set since the set $\{\mathbf{w}_i\}$ is linearly independent. Then for $\mathbf{x} \in A$, we get $\mathcal{T}(\mathbf{x}) = v_0 \geq 0$. This contradicts to the assumption $\mathcal{T}(\mathbf{x}) < 0$ for all $\mathbf{x} \notin B_\varepsilon(\Delta^m)$. Therefore, $v_0 < 0$.

Lastly, we consider the sign of v_i . Since $\mathcal{T}(\mathbf{x}) = 1 > 0$ for $\mathbf{x} \in \Delta^m$ and $v_0 < 0$, there exists some positive $v_i > 0$, say, $v_1 > 0$. Similar to the above argument, we define

$$B := \{\mathbf{x} \mid v_1 \mathbf{w}_1^\top \mathbf{x} + b_1 + v_0 > 0\} \bigcap_{i=2}^{d_1} \{\mathbf{x} \mid \mathbf{w}_i^\top \mathbf{x} + b_i < 0\},$$

which is also nonempty and unbounded. Then, for $\mathbf{x} \in B$, we have

$$\begin{aligned} \mathcal{T}(\mathbf{x}) &= \sum_{i=1}^{d_1} v_i \sigma(\mathbf{w}_i^\top \mathbf{x} + b_i) + v_0 \\ &= v_1 \mathbf{w}_1^\top \mathbf{x} + b_1 + v_0 \\ &> 0. \end{aligned}$$

Since B is unbounded, this implies that $\mathcal{T}(\mathbf{x}) > 0$ over the unbounded subset in \mathbb{R}^d , which contradicts to the condition $\mathcal{T}(\mathbf{x}) < 0$ for all $\mathbf{x} \notin \mathcal{B}_\varepsilon(\Delta^m)$. This completes the whole proof, which shows that the minimum width of two-layer ReLU network is exactly $d + 1$. \square

Proposition F.2. *Let $\mathcal{X} \subset \mathbb{R}^d$ be a topological space and \mathcal{A} be a neural network architecture that is a feasible architecture on \mathcal{X} . Then, there exists a topological space \mathcal{X}' which is homeomorphic to \mathcal{X} , but \mathcal{A} is not a feasible architecture on \mathcal{X}' .*

Proof. We use the similar technique introduced in (Telgarsky, 2015). Before we start, recall that a network \mathcal{N} with the architecture \mathcal{A} is a piecewise linear function on \mathbb{R}^d . Thus \mathbb{R}^d can be partitioned into finitely many regions, where \mathcal{N} is linear on each region. Let M be the maximum number of such regions, that networks with the architecture \mathcal{A} can partition. I.e., any network with the architecture \mathcal{A} has linear regions at most M partitions in \mathbb{R}^d .

Now, we consider a contractible topological space \mathcal{Y} which has zig-zag shape as described in Figure 19(b), where the number of sawtooths is greater than $M + 2$. We define another topological space $\mathcal{X}' := \mathcal{X} \# \mathcal{Y}$, where $\#$ denotes the connected sum. Note that we can glue \mathcal{Y} to \mathcal{X} preserving the number of sawtooths in \mathcal{Y} , because \mathcal{X} is bounded. Then \mathcal{X}' is homeomorphic to \mathcal{X} since \mathcal{Y} is contractible.

Finally, we prove the proposition using contradiction. Suppose there exists a deep ReLU network \mathcal{N}' with the same architecture \mathcal{A} , which can approximate $\mathbb{1}_{\{\mathcal{X}'\}}$ under the given error bound $\varepsilon > 0$. Then, by the \mathcal{Y} part in \mathcal{X}' , there exists a straight line ℓ that intersects \mathcal{X}' more than $M + 3$ times. Therefore, to approximate $\mathbb{1}_{\{\mathcal{X}'\}}$ sufficiently close, \mathcal{N}' must have at least $M + 1$ linear regions on ℓ . However, \mathcal{N}' can have at most M linear regions in \mathbb{R}^d from the definition of M . This contradiction completes the proof. \square

Theorem F.3. *Let $d_x, d_y \in \mathbb{N}$ and $p \geq 1$. Then, the set of three-layer ReLU networks is dense in $L^p(\mathbb{R}^{d_x}, [0, 1]^{d_y})$. Furthermore, let $f : \mathbb{R}^{d_x} \rightarrow [0, 1]^{d_y}$ be a compactly supported function whose Lipschitz constant is L . Then, for any $\varepsilon > 0$, there exists a three-layer ReLU network \mathcal{N} with the architecture*

$$d_x \xrightarrow{\sigma} (2nd_x d_y) \xrightarrow{\sigma} (nd_y) \rightarrow d_y$$

such that $\|\mathcal{N} - f\|_{L^p(\mathbb{R}^{d_x})} < \varepsilon$. Here, $n = \varepsilon^{-d_x} (1 + (\sqrt{d_x}L)^p)^{d_x/p} = O(\varepsilon^{-d_x})$.

Proof. First we recall a result in real analysis: the set of compactly supported continuous functions is dense in $L^p(\mathbb{R}^{d_x})$ for $p \geq 1$ (Rudin et al., 1976, Theorem 3.14). Therefore, it is enough to prove the second statement; which claims that any compactly supported Lipschitz function can be universally approximated by three-layer ReLU networks.

We consider $d_y = 1$ case first. Let $f \in \mathbb{R}^{d_x} \rightarrow [0, 1]$ be Lipschitz, and let L be its Lipschitz constant. Without loss of generality, suppose the support of f is contained in $[0, 1]^{d_x}$. Let $\delta > 0$ be the small number which will be determined. Now we partition $[0, 1]^{d_x}$ by regular d_x -dimensional cubes with length δ . Now, consider estimating the definite integral uses a Riemann sum over cubes. The total number of cubes are $n := (\frac{1}{\delta})^{d_x}$, and we number these cubes by C_1, C_2, \dots, C_n . For each cube C_i , by Proposition 3.1, we can define a two-layer ReLU network \mathcal{T}_i with the architecture $d_x \xrightarrow{\sigma} 2d_x \rightarrow 1$ such that $\mathcal{T}_i(\mathbf{x}) = 1$ in C_i and $\mathcal{T}_i(\mathbf{x}) = 0$ for $\mathbf{x} \notin B_r(C_i)$ with $r := \frac{1}{2d_x} \frac{\delta^{p+1}}{1+\delta^p}$. Then for any $\mathbf{x}_i \in C_i$, we get

$$\begin{aligned} \int_{B_r(C_i)} |f - f(\mathbf{x}_i)\mathcal{T}_i|^p d\mu &= \int_{C_i} |f - f(\mathbf{x}_i)\mathcal{T}_i|^p d\mu + \int_{B_r(C_i) \setminus C_i} |f - f(\mathbf{x}_i)\mathcal{T}_i|^p d\mu \\ &\leq \int_{C_i} (\sqrt{d_x}L\delta)^p d\mu + \int_{B_r(C_i) \setminus C_i} 1^p d\mu \\ &\leq (\sqrt{d_x}L\delta)^p \cdot \delta^{d_x} + [(\delta + 2r)^{d_x} - \delta^{d_x}] \\ &= (\sqrt{d_x}L)^p \cdot \delta^{d_x+p} + \left[\left(1 + \frac{2r}{\delta}\right)^{d_x} - 1 \right] \delta^{d_x} \\ &< [(\sqrt{d_x}L)^p + 1] \delta^{d_x+p}. \end{aligned}$$

Note that we use two inequalities, $|f(\mathbf{x}) - f(\mathbf{x}_i)| \leq L\sqrt{d_x}\delta$ for $\mathbf{x} \in C_i$ and $(1+a)^k < \frac{1}{1-ak}$ for $0 < a < \frac{1}{k}$. Then, the above equation implies the L^p distance between f and $f(\mathbf{x}_i)\mathcal{T}_i$ in C_i is bounded by the above value. Now we define a

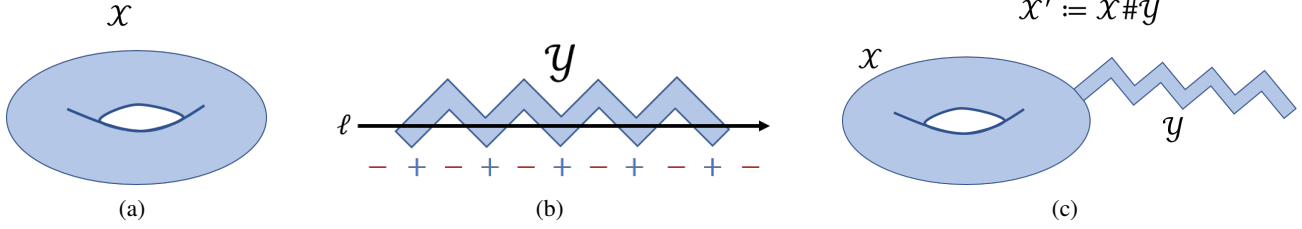


Figure 19. Proof of Proposition F.2. (a) \mathcal{X} is a given topological space, and \mathcal{A} is a feasible architecture on \mathcal{X} . (b) \mathcal{Y} is a zig-zag shaped long band, which is a contractible space. There exists a straight line ℓ such that \mathcal{Y} and ℓ has sufficiently many intersection points, so that \mathcal{A} cannot approximate \mathcal{Y} . (c) \mathcal{X}' is the connected sum of \mathcal{X} and \mathcal{Y} , which is homeomorphic with \mathcal{X} . However, \mathcal{A} is not a feasible architecture on \mathcal{X}' .

three-layer neural network \mathcal{N} by

$$\mathcal{N}(\mathbf{x}) := \sum_{i=1}^n f(\mathbf{x}_i) \mathcal{T}_i(\mathbf{x}),$$

which is a Riemann sum over the n cubes partitions. Then \mathcal{N} has the architecture $d_x \xrightarrow{\sigma} (2nd_x) \xrightarrow{\sigma} n \rightarrow 1$ and satisfies

$$\begin{aligned} \int_{\mathbb{R}^{d_x}} |f - \mathcal{N}|^p d\mu &= \int_{B_r([0,1]^{d_x})} |f - \mathcal{N}|^p d\mu \\ &< \sum_{i=1}^n \int_{B_r(C_i)} |f - f(\mathbf{x}_i) \mathcal{T}_i|^p d\mu \\ &\leq \left[(\sqrt{d_x} L)^p + 1 \right] n \delta^{d_x+p}. \\ &= \left[(\sqrt{d_x} L)^p + 1 \right] \delta^p. \end{aligned}$$

Therefore, take $\delta < \varepsilon (1 + (\sqrt{d_x} L)^p)^{-\frac{1}{p}}$ for given ε , we conclude that $\|f - \mathcal{N}\|_{L^p([0,1]^{d_x})} < \varepsilon$. From this choice of δ , we get

$$n = \delta^{-d_x} > \varepsilon^{-d_x} \left(1 + (\sqrt{d_x} L)^p \right)^{d_x/p} = O(\varepsilon^{-d_x}).$$

If $d_y > 1$, we can obtain the desired network by concatenating d_y networks, thus the architecture is

$$d_x \xrightarrow{\sigma} (2nd_x d_y) \xrightarrow{\sigma} (nd_y) \rightarrow d_y.$$

□

Lemma F.4. Let \mathcal{T} be a two-layer ReLU network defined in (5). Then, the classification region $R := \{\mathbf{x} \in \mathbb{R}^d \mid \mathcal{T}(\mathbf{x}) > 0\}$ is a convex polytope. Specifically, if the subset $S := \{\mathbf{x} \in \mathbb{R}^d \mid \mathcal{T}(\mathbf{x}) = 1\}$ is nonempty, then it is a convex polytope with m faces.

Proof. First, we prove that \mathcal{T} is a concave function. Note that σ is convex thus $v_k \sigma(\mathbf{w}_k^\top \mathbf{x} + b_k)$ is a concave function with respect to input \mathbf{x} , and the sum of concave functions is again concave (we use all $v_k < 0$ here). Therefore, \mathcal{T} is a concave function, and the region $R := \{\mathbf{x} \mid \mathcal{T}(\mathbf{x}) > 0\}$ is convex. The piecewise linearity of \mathcal{T} implies that R forms a convex polytope.

Now we consider the subset $S := \{\mathbf{x} \mid \mathcal{T}(\mathbf{x}) = 1\}$. Since all $v_k < 0$, $\mathbf{x} \in S$ if and only if $\mathbf{w}_k^\top \mathbf{x} + b_k \leq 0$ for all $k \in [m]$. Then, S is a convex polytope with m faces by Definition 2.1. □

Proposition F.5 (Theorem 2.1 in (Du et al., 2018), two-layer version). *Let $\mathcal{N}(\mathbf{x}) := v_0 + \sum_{k=1}^l v_k \sigma(\mathbf{w}_k^\top \mathbf{x} + b_k)$ be a two-layer ReLU network, and $L = \frac{1}{n} \sum_{i=1}^n \ell(\mathcal{N}(\mathbf{x}_i), y_i)$ be the loss function. Then, on the gradient flow, for all $k \in [l]$, the quantity*

$$v_k^2 - \|\mathbf{w}_k\|^2 - b_k^2 \quad (41)$$

is invariant.

Proof. The proof is written in (Du et al., 2018), and we provide here for completeness. The gradient of each component is computed by

$$\begin{aligned} \frac{\partial L}{\partial v_k} &= \frac{1}{n} \sum_{i=1}^n \frac{\partial \ell}{\partial \mathcal{N}(\mathbf{x}_i)} \cdot \sigma(\mathbf{w}_k^\top \mathbf{x}_i + b_k), \\ \frac{\partial L}{\partial \mathbf{w}_k} &= \frac{1}{n} \sum_{i=1}^n \frac{\partial \ell}{\partial \mathcal{N}(\mathbf{x}_i)} \cdot v_k \mathbb{1}_{\{\mathbf{w}_k^\top \mathbf{x}_i + b_k > 0\}} \mathbf{x}_i, \\ \frac{\partial L}{\partial b_k} &= \frac{1}{n} \sum_{i=1}^n \frac{\partial \ell}{\partial \mathcal{N}(\mathbf{x}_i)} \cdot v_k \mathbb{1}_{\{\mathbf{w}_k^\top \mathbf{x}_i + b_k > 0\}}. \end{aligned}$$

Then, it is easy to check that

$$v_k \frac{\partial L}{\partial v_k} = \mathbf{w}_k^\top \left(\frac{\partial L}{\partial \mathbf{w}_k} \right) + b_k \cdot \frac{\partial L}{\partial b_k}.$$

Now, we differentiate (41). It gives

$$\begin{aligned} \frac{d}{dt} (v_k^2 - \|\mathbf{w}_k\|^2 - b_k^2) &= 2v_k \frac{dv_k}{dt} - 2\mathbf{w}_k^\top \left(\frac{d\mathbf{w}_k}{dt} \right) - 2b_k \frac{db_k}{dt} \\ &= 2 \left(-v_k \frac{\partial L}{\partial v_k} + \mathbf{w}_k^\top \left(\frac{\partial L}{\partial \mathbf{w}_k} \right) + b_k \frac{\partial L}{\partial b_k} \right) \\ &= 0 \end{aligned}$$

for all t . Therefore, (41) is constant. □